



PONTIFICIA
**UNIVERSIDAD
CATÓLICA**
DEL PERÚ

th
TECHNISCHE UNIVERSITÄT
ILMENAU

Pontificia Universidad Católica del Perú

Escuela de Posgrado

Tesis de Maestría

Synthesis of silver nanoparticles
in hydrogels

Para obtener el grado de:

Master of Science (M. Sc.)

en Ingeniería y Ciencia de los Materiales

Presentado por: Kristina Schelestow

Fecha y Lugar de Nacimiento: 11/01/1991 Pawlodar, Alemania

Tutor Responsable (TU Ilmenau): Dr. Edda Rädlein

Professor Responsable (TU Ilmenau): Dr. Bernd Halbedel

Professor Responsable (PUCP): Dr. Juan Carlos Rueda Sánchez

Fecha y Lugar: 30/09/2016, Lima

TECHNISCHE UNIVERSITÄT ILMENAU

Department of Electrical Engineering and Information Technology

Master Thesis

Submitted by: Kristina Schelestow

Date of birth: 11.01.1991

Major: **Materials Science and Engineering
(Double Degree)**

Registration number: 54903

Responsible professor: Edda Rädlein

Responsible professor at PUCP: Juan Carlos Rueda Sanchez

Chairperson of the examination committee: Edda Rädlein

2nd examiner: Juan Carlos Rueda Sanchez

Topic: Synthesis of silver nanoparticles in hydrogels

Issued on: 01.10.2015

Submission date: 30.09.2016

Univ.-Prof. Dr. rer. nat. habil. P. Schaaf
Chairman of the Examination Board

Edda Rädlein
Responsible professor

Acknowledgments

At first I would like to express my deep gratitude to Prof. Juan Carlos Rueda and Prof. Edda Rädlein, my thesis supervisors, for their guidance, constant encouragement and useful critiques of this research work. My grateful thanks are also extended to Dr. Ulrike Brokmann for her advice and assistance during my work in Ilmenau.

I would also like to thank the following persons and institutions for enabling me to use their equipment and know-how as well as for their kindly support:

- Andrés Guerra (Physics Department, Pontifical Catholic University of Peru) for his assistance with UV/Vis measurements,
- Dr. Thomas Kups, Diana Rossberg (Group for Materials for Electrical Engineering and Electronics, Technische Universität Ilmenau) and Mathias May for their support in SEM imaging,
- Dr. Hartmut Komber (Leibniz-Institute of Polymer Research Dresden (IPF)) as well as Prof. Siegfried Stapf and Dr. Carlos Mattea (Group Technical Physics/ Polymer Physics, Technische Universität Ilmenau) for nuclear magnetic resonance measurements and their evaluation,
- Dr. Ronald Schade and Juliane Zirm (Institute for Bioprocessing and Analytical Measurement Techniques (iba) Heiligenstadt) for their help in doing the antibacterial analysis,
- Dr. Gerd Teichert and Dr. Susanne Schiermeyer (Group for Materials for Electrical Engineering and Electronics, Technische Universität Ilmenau) for their support with XRF measurements,
- Michael Fischer and Dr. Heike Bartsch (Electronics Technology Group, Technische Universität Ilmenau) for their help with layer fabrication and characterization,
- Dagmar Raab and the staff of Group for Inorganic-Nonmetallic Materials (Technische Universität Ilmenau) for their support during my work there and
- Dr. Bernd Halbedel and Dr. Rolf Grieseler (Technische Universität Ilmenau) for their supervision of the Double Degree Programm.

Finally, I wish to thank my parents and friends for their support and encouragement throughout my study.

Abstract

The present work is concerned with the fabrication of a novel hydrogel-silver hybrid material, the characterization regarding its structural and antibacterial properties and the investigation of its interaction with glass surfaces.

Hydrogels based on N-isopropylacrylamide, a functionalized macromonomer of 2-oxazolines and N,N'-methylene bisacrylamide as a cross-linker were synthesized via radical polymerization using ammonium persulfate and N,N,N',N'-tetramethylene diamine as an initiator system. By complexation with silver cations from a silver nitrate solution and a subsequent reduction with sodium borohydride, silver nanoparticles inside the polymer network were formed.

Bulk hydrogels of different compositions were characterized concerning their structure and their water absorptive capacity. The formation of silver nanoparticles as well as its influencing factors were analysed and could be confirmed quantitatively. The antibacterial activity of the developed composite material in its powder form was determined via count test applying it to *Staphylococcus aureus*. The number of bacteria could be reduced to approximately 0.1 % compared to the reference value without silver nanoparticles. Thus, the hydrogel-silver hybrid can be appraised as suitable for biomedical applications.

Finally, different hydrogel layers were produced on photosensitive glass FS21 and evaluated regarding their applicability for microsystems technology.

Contents

Acknowledgments	III
Abstract	IV
Acronyms	VIII
1 Introduction	1
2 Fundamentals	2
2.1 2-Oxazolines	2
2.1.1 Synthesis of 2-Oxazolines	3
2.1.2 Polymerization of 2-oxazolines	4
2.1.3 Properties and applications of poly-2-oxazolines	6
2.2 N-isopropylacrylamide	7
2.2.1 Synthesis of N-isopropylacrylamide	7
2.2.2 Polymerization mechanism of N-isopropylacrylamide	8
2.2.3 Properties and applications of poly(N-isopropylacrylamide)	9
2.3 Macromonomers	10
2.3.1 Synthesis of macromonomers	10
2.3.2 Synthesis of graft copolymers and hydrogels by macromonomer method	11
2.4 Hydrogels	11
2.4.1 Methods of hydrogel synthesis	12
2.4.2 General characteristics and applications of hydrogels	13
2.4.3 Stimuli-responsive hydrogels	14
2.4.4 Nanocomposite hydrogels	15
2.4.5 Hydrogel thin films	18
2.5 Silver nanoparticles	22
2.5.1 Fabrication of silver nanoparticles	22
2.5.2 Antimicrobial effect	24
2.6 Photosensitive glass	25
2.6.1 Functional principle	26
2.6.2 Properties and application of photosensitive glass	27
2.7 Basic principles of characterization methods used in present work	28
2.7.1 Nuclear magnetic resonance spectroscopy	28
2.7.2 UV/Vis spectroscopy	29
2.7.3 Fourier transformed infrared spectroscopy	30
2.7.4 Scanning electron microscopy	30
2.7.5 X-ray fluorescence spectroscopy	30

2.7.6	Fluorescence microscopy	31
2.7.7	Atomic force microscopy	31
2.7.8	Profilometry	31
3	Experimental Part	33
3.1	Materials	33
3.1.1	Equipment	33
3.1.2	Reagents	33
3.2	Preparation methods	35
3.2.1	Macromonomer synthesis	35
3.2.2	Synthesis of hydrogels	36
3.2.3	Synthesis of silver nanoparticles in hydrogels	36
3.2.4	Coating of glass substrates	37
3.3	Characterization of bulk hydrogels	39
3.3.1	Nuclear magnetic resonance spectroscopy	39
3.3.2	Measurement of water absorption	39
3.3.3	Determination of reaction yield	39
3.3.4	Measurement of transition temperature	40
3.3.5	UV/Vis spectroscopy	40
3.3.6	Fourier transform infrared spectroscopy	40
3.3.7	Scanning electron microscope imaging	41
3.3.8	X-ray fluorescence spectroscopy	41
3.3.9	Examination of antibacterial activity towards <i>Staphylococcus aureus</i>	41
3.4	Characterization of glass substrates	42
3.4.1	Atomic force microscopy	42
3.4.2	Profilometry	42
3.4.3	Scanning electron microscopy	42
4	Results and discussion	43
4.1	Materials syntheses	43
4.1.1	Macromonomer synthesis	43
4.1.2	Hydrogel synthesis	50
4.1.3	Synthesis of silver nanoparticles in hydrogels	55
4.2	Characterization of hydrogels	57
4.2.1	Nuclear magnetic resonance spectroscopy of hydrogels	57
4.2.2	Measurement of water absorption	61
4.2.3	Measurement of transition temperature T_{tr}	62
4.2.4	UV/Vis spectroscopy	63
4.2.5	Fourier transform infrared spectroscopy	65
4.2.6	Scanning electron microscope analysis	66
4.2.7	X-ray fluorescence spectroscopy	70
4.2.8	Antibacterial tests	71
4.3	Characterization of glass surfaces	73
4.3.1	Visual control	73
4.3.2	Atomic force microscopy	75
4.3.3	Profilometry	80

4.3.4	Scanning electron microscope imaging of glass surfaces	82
4.4	Discussion	83
5	Conclusions and Perspectives	86
	Bibliography	88
A	Appendix	95
A.1	Calculations	95
A.1.1	Calculations for macromonomer synthesis	95
A.1.2	Calculation of water absorption	96
A.1.3	Calculation of reaction yield	96
A.2	Photographic images	98
	Declaration of Authorship	104



Acronyms

Ag	silver
Ag-NPs	silver nanoparticles
AgNO₃	silver nitrate
AIBN	azobisisobutyronitrile
AiMM	acid groups in the macromonomer
APS	ammonium persulfate
APTES	3-aminopropyltriethoxysilane
CaH₂	calcium hydride
CMS	chloromethylstyrene
CSD	chemical solution deposition
DNA	deoxyribonucleic acid
EDAX	energy-dispersive X-ray spectroscopy microanalysis
FOxa	2-methoxycarbonylethyl-2-oxazoline
FTIR	Fourier transformed infrared spectroscopy
H₂O	water
HCl	hydrochloric acid
HG	hydrogel
IMS	iodomethylstyrene
KBr	potassium bromide
KOH	potassium hydroxide
KPS	potassium persulfate
LCST	lower critical solution temperature
MBA	N,N'-methylene bisacrylamide
MeOxa	2-methyl-2-oxazoline
MM	macromonomer
NaBH₄	sodium borohydride
NaCl	sodium chloride
NaI	sodium iodide
NaOH	sodium hydroxide
NASI	N-acryloxysuccinimide
NiPAAm	N-Isopropylacrylamide
NMR	nuclear magnetic resonance spectroscopy
NPs	nanoparticles

polyNiPAAm	poly(N-isopropylacrylamide)
ROS	reactive oxygen species
SEM	scanning electron microscope
TEM	transmission electron microscope
TEMED	N,N,N',N'-tetramethylene diamine
T_{tr}	transition temperature
UCST	upper critical solution temperature



1 Introduction

Hydrogels are three-dimensional water absorbent, but water-insoluble polymer networks. They are mainly based on at least two different monomer types: a monomer containing hydrophilic functional groups, which cause the absorption of water, and a cross-linking monomer with two or more double bonds, which induces strong crosslinks between polymer network chains and thus insolubility and mechanical stability. The versatile application spectrum ranges from cosmetic and sanitary products (due to water storage) to sensor devices (owing to dimensional change) or biomedical appliances (by reason of the biocompatibility). Further monomers or macromonomers can be used to add, to modify or to improve particular properties such as a higher water absorption or an additional pH- or temperature sensitivity. By synthesis of silver nanoparticles inside the hydrogel network an additional antimicrobial effect can be achieved. A novel hydrogel-silver hybrid is reported to show a high antibacterial activity towards common bacteria such as *E. coli* and is of special interest for medical devices such as catheters or implants.

At the same time the application of hydrogels is not limited to the bulk material. Particularly in microsystems technology and microfluidics hydrogel thin films can be used as multifunctional surfaces. However, the interaction between the film and the substrate material must not be ignored.

The present thesis is aiming at the synthesis and the characterization of hydrogels containing silver nanoparticles for biomedical applications.

The hydrogels were produced via radical polymerisation of N-isopropylacrylamide and a macromonomer of 2-oxazolines (functionalized with acidic groups) using N,N'-methylene bisacrylamide as a cross-linker as well as ammonium persulfate and N,N,N,N'-tetramethylene diamine as an initiator system. Silver nanoparticles were formed inside the hydrogel network by complexation with silver cations from a silver nitrate solution and a subsequent reduction with sodium borohydride.

After the characterization of the bulk composite material and the evaluation of its antibacterial properties, hydrogel-silver hybrid was investigated as a coating material regarding its interaction with glass substrates. Therefore photosensitive glass FS21, a lithium aluminosilicate glass doped with small amounts of cerium oxide and silver oxide, was used as a substrate.

2 Fundamentals

Sections 2.1, 2.2 and 2.3 of this chapter discuss materials used for hydrogel synthesis as well as their main properties. Sections 2.4 and 2.5 give a theoretical overview of hydrogels (including hydrogel layers) and silver nanoparticles, the main subject of this thesis. Photosensitive glasses, which were used as substrates for hydrogel layers, are described in Section 2.6. Finally Section 2.7 gives a short summary about characterization methods used for evaluation of produced hydrogels.

2.1 2-Oxazolines

Oxazolines are heterocyclic compounds with a five-membered ring containing one oxygen atom, one nitrogen atom and one double bond in the ring [1]. The oxygen and nitrogen atoms are in the 1,3-position to each other, where the oxygen atom is assigned to position 1 and the nitrogen atom to position 3. Depending on the location of the double bond in the heterocyclic ring, there are three types of isomeric oxazolines: 2-oxazolines, 3-oxazolines and 4-oxazolines as can be seen in Figure 2.1 [1,2].

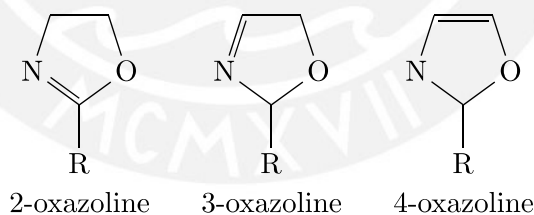


Figure 2.1: Three different types of oxazolines

A multiplicity of different oxazolines can be obtained by varying substituent R, which affects the reactivity and the physical properties of this substance [3].

Their chemical structure and the consequential tendency to ring-opening polymerization allow a copolymerization of different 2-oxazolines to polymers with tunable hydrophilicity [2]. Copolymerized with N-Isopropylacrylamide (NiPAAm), the oxazolines can potentially be used in biomaterials or for thermoresponsive applications [4].

2.1.1 Synthesis of 2-Oxazolines

The synthesis of 2-oxazoline is in general carried out via cyclisation of amide or amine compounds by condensation reaction [2,3]. There are many known methods to obtain 2-oxazolines, some of them are described below, for more detailed information see [2].

Reaction of nitriles with aminoalcohols

Witte and Seeliger described a condensation reaction of aliphatic and aromatic nitriles with 2-aminoalcohol to 2-oxazoline in the presence of cadmium acetate and elimination of ammonia [2, 5]. Figure 2.2 shows the entire reaction. Instead of cadmium acetate an other moderate Lewis acid like zinc acetate can be used as a catalyst [2].

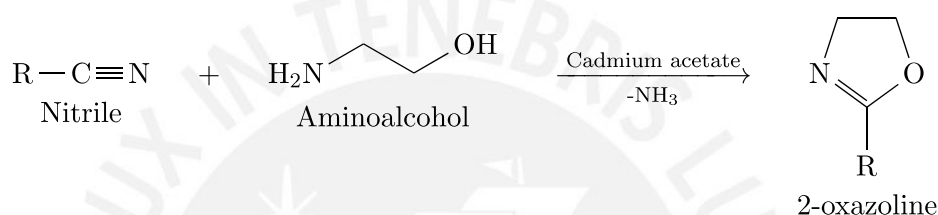


Figure 2.2: 2-oxazoline synthesis by reaction of nitrile and aminoalcohol [2,5]

Cyclization of haloamides

The method shown in Figure 2.3 allows to obtain unsubstituted 2-oxazolines. Haloamides can be synthesised from 2-haloethylamine and carboxylic acid derivatives, e.g. acid halides. For the cyclization reaction a strong base such as potassium hydroxide (KOH) or sodium hydroxide (NaOH) is used to dehydrohalogenate haloamide [2].

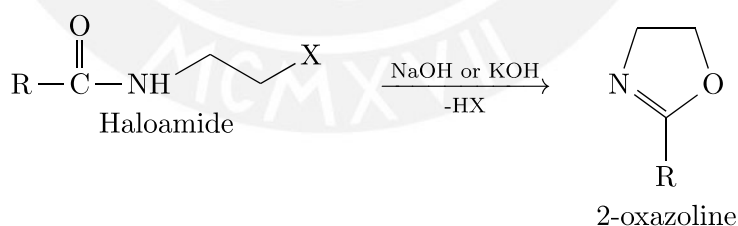


Figure 2.3: 2-oxazoline synthesis by cyclization of haloamide [2]

Cyclization of hydroxyamides

In this method hydroxyamides are dehydrated by triphenylphosphine and diethyl azodicarboxylate at 0°C. Solid acids are used as a catalyst [6]. The entire reaction can be seen in Figure 2.4.

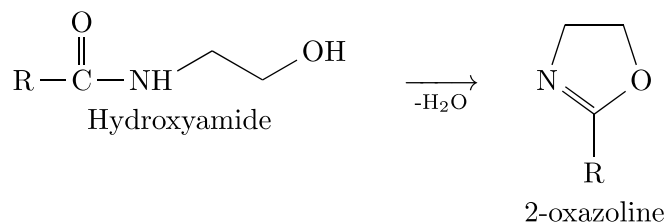


Figure 2.4: 2-oxazoline synthesis by cyclization of hydroxyamide [2, 6]

2.1.2 Polymerization of 2-oxazolines

2-oxazolines are polymerized via living cationic ring-opening reaction (see Figure 2.5). The polymerization is called living because it does not interrupt by chain transfer or termination and runs until the monomers are consumed. Cationic species are used as an initiator [1, 2].

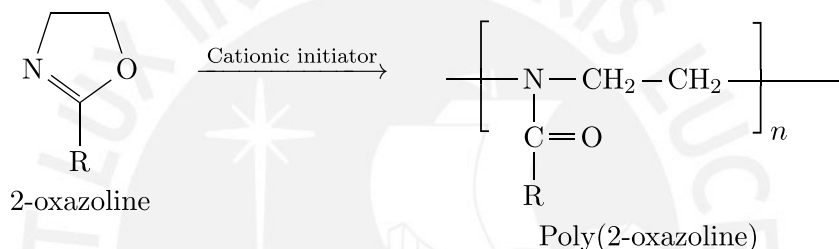


Figure 2.5: Polymerization of 2-oxazolines [2]

Depending on the nucleophilicity of the counter ion (generated from initiator) related to the monomer the polymerization mechanism can be ionic or covalent.

Polymerization mechanism

Ionic type The ionic mechanism occurs when the nucleophilicity of the counter ion is less than the nucleophilicity of the 2-oxazoline monomer [2]. The polymerization proceeds as follows:

An initiator and a monomer form a counterion and a propagating 2-oxazoline species **1**, which is stable due to lower nucleophilicity of the counterion [2, 7]. This step is shown in Figure 2.6.

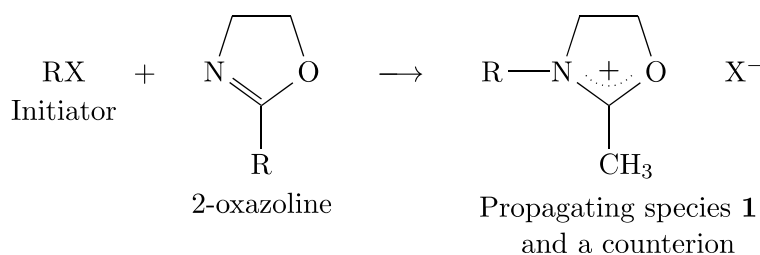


Figure 2.6: Initiation mechanism of ionic polymerization [2, 7]

In the propagation species **1** is attacked by a nitrogen atom from a further monomer at the fifth carbon atom. As a result a C-O bond breaks and a new bond between the fifth carbon atom of **1** and a nitrogen atom from a monomer is formed (see Figure 2.7).

The resulted poly-2-oxazoline contains N-acetylamine groups.

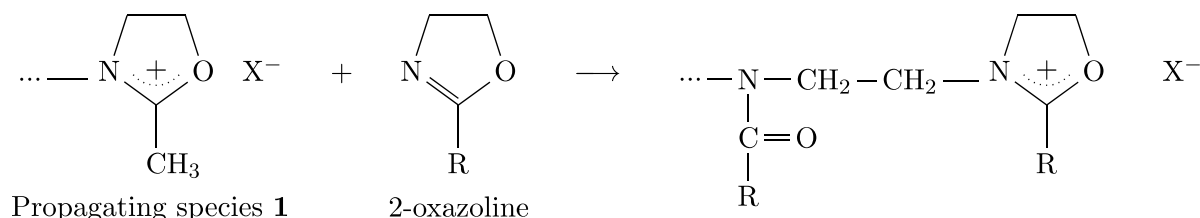


Figure 2.7: Propagation phase of ionic polymerization [2, 7]

Covalent type The covalent mechanism occurs when the nucleophilicity of the counterion is higher than the nucleophilicity of the 2-oxazoline monomer [2].

An initiator and a monomer form a counterion and a propagating 2-oxazoline species **1**, which is unstable due to higher nucleophilicity of the counterion, which attacks **1** at the fifth carbon atom, breaks a C-O bond and opens the ring. As a result a covalent propagation species **2** is formed (see Figure 2.8).

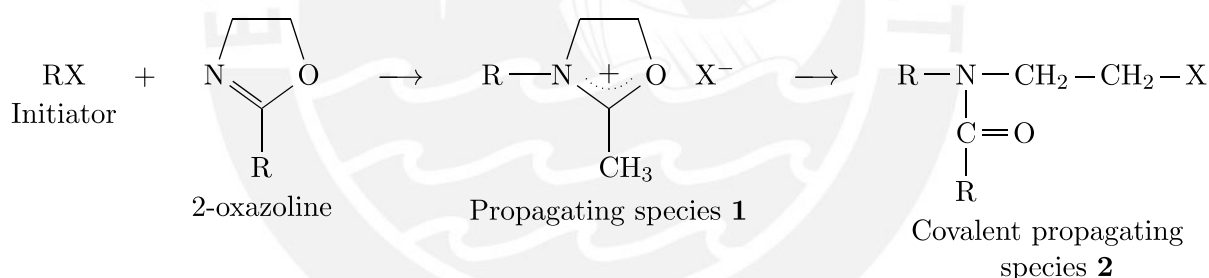


Figure 2.8: Initiation mechanism of covalent polymerization [2, 7]

In the propagation (see Figure 2.9) a nitrogen atom from the further oxazoline monomer attacks **2** at a carbon atom next to the previous counterion that opens the ring of the monomer and creates the poly-2-oxazoline.

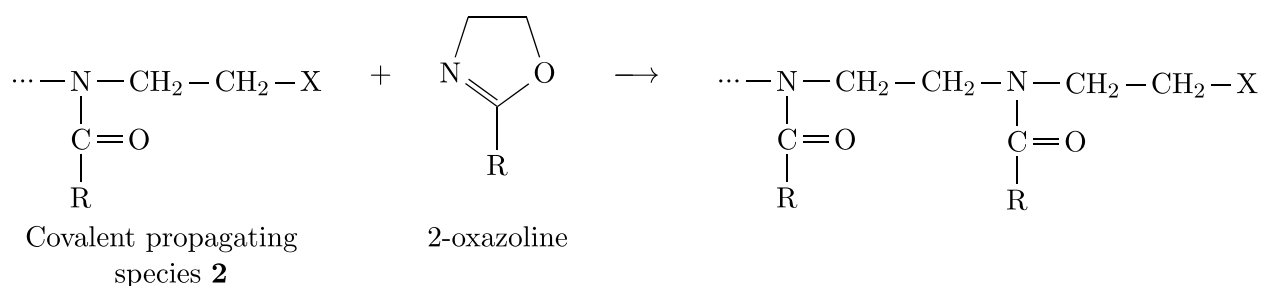


Figure 2.9: Propagation of covalent polymerization [2, 7]

Different 2-oxazoline monomers and their reactivity

The reactivity of 2-oxazoline monomer depends on the substituent type: electron accepting species reduce the reaction velocity and electron donating species increase it [2]. Some important monomers and counter ions are listed in Figure 2.10.

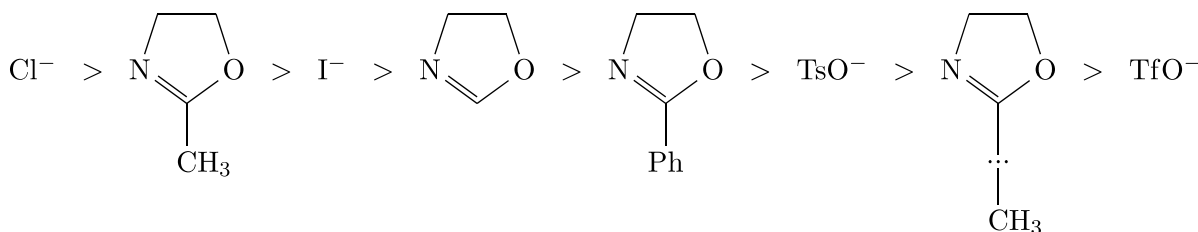


Figure 2.10: Monomers and counterions in order of nucleophilicity: chlorid ion, 2-methyl-2-oxazoline, iodid ion, unsubstituted 2-oxazoline, 2-phenyl-2-oxazoline, tosylate, 2-oxazoline with aliphatic substituent, triflate [2]

Initiators

For the polymerization of 2-oxazoline different cationic initiators such as Lewis acids, strong protonic acids and their esters as well as alkyl halides can be used [2].

Solvents

Solvents used for the polymerization of 2-oxazolines are chosen by considering various aspects: The polarity of the solvent should correlate with the polarity of the used 2-oxazoline monomer, thus: Oxazolines with a low molecular weight and polar substituents such as methyl, ethyl or phenyl can be dissolved in polar solvents like acetonitril or benzonitril. Oxazoline monomers with a high molecular weight due to a non-polar substituent can be dissolved in non-polar solvents like toluene [7].

Further the effect of solvent on the polymerization should be taken into account. Litt and Lewis reported about interference mechanism of some solvents, e.g. carboxylic acids, in the polymerization due to which the molecular weight of the reaction product decreases or the polymerization stops completely [8].

2.1.3 Properties and applications of poly-2-oxazolines

Versatile properties such as amphiphilic behavior, lower toxicity or ability to undergo living cationic ring-opening polymerisation enable a multiplicity of possible applications [2].

- **Nonionic polymer surfactants**

While 2-methyl- and 2-ethyl-2-oxazoline are hydrophilic, oxazolines with longer substituents are hydrophobic. Block copolymers containing hydrophilic and hydrophobic

oxazoline monomers show wetting behavior similar to peptides and can be used to produce nonionic surfactants [2, 9].

- **Polymer composites**

Poly(*N*-acetylenimine) is miscible with many common polymers such as polyamide (Nylon 6), poly(vinyl alcohol), poly(vinyl chloride), poly(styrene), etc. and can be used for manufacturing of various blends [2].

- **Hydrogel synthesis**

Oxazolines can be used as monomers for hydrogel synthesis. Carbonyl oxygen may interact with water molecules and form a hydrogen bond [2].

- **Biomaterials**

Poly(*N*-acetylenimine) shows low toxicity, is non-irritating to skin or eyes and can be applied in biomaterials [2].

2.2 *N*-isopropylacrylamide

Acrylamide is a monomer with two functional groups: an amid group and a carbon double bond which enables polymerization reactions.

NiPAAm is an *N*-substituted acrylamide with an isopropyl group at the nitrogen atom. It is an important monomer for synthesis of temperature-responsive polymers or stimuli-sensitive hydrogels [4, 10–12] and is widely researched for sensor and biomedical applications [13–16].

2.2.1 Synthesis of *N*-isopropylacrylamide

There are several ways to synthesize NiPAAm. The most common and industrially used method (see Figure 2.11) is a Ritter-reaction of acryl nitrile and isopropanol in acid environment [17, 18].

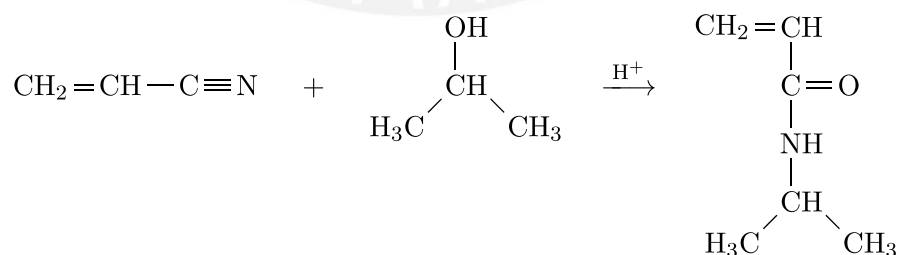


Figure 2.11: Ritter-reaction of acryl nitrile and isopropanol [17, 18]

Other possible synthesis reactions are less significant due to more expensive reactants and lower reaction yields.

2.2.2 Polymerization mechanism of *N*-isopropylacrylamide

The polymerization of NiPAAm is usually held in organic or aqueous solutions initiated by free radicals, e.g. azobisisobutyronitrile (AIBN), or redox initiation systems, e.g. potassium persulfate (KPS) or ammonium persulfate (APS) with *N,N,N',N'*-tetramethylene diamine (TEMED) [4, 12, 16, 19].

The homopolymerisation of NiPAAm monomer units leads to formation of water soluble and linear poly(*N*-isopropylacrylamide) (polyNiPAAm) (see Figure 2.12).

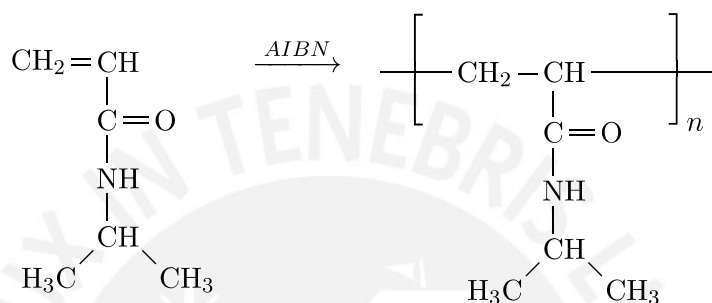


Figure 2.12: Linear polymerization of *N*-isopropylacrylamide

PolyNiPAAm shows inverse solubility upon heating due to a macromolecular transition from a hydrophilic to a hydrophobic structure [20]. This range of temperature is known as the lower critical solution temperature (LCST) and lies between approx. 30 °C and 35 °C [21]. This effect occurs owing to thermodynamic dependent influence of two contrary functional groups in NiPAAm: a polar hydrophilic amid group and a non-polar hydrophobic isopropyl group. The LCST can be increased by using more hydrophilic comonomers and decreased with more hydrophobic comonomers.

Using a difunctional comonomer with two double bonds enables a three-dimensional crosslinking between NiPAAm units and leads to gelation (see Figure 2.13).

Crosslinking prevents solubility of the gel, but enables absorption of water: below a certain transition temperature the hydrogel absorbs water until its saturation value and releases it above this temperature. The process is reversible, the transition temperature can also be changed by additional hydrophilic or hydrophobic comonomers.

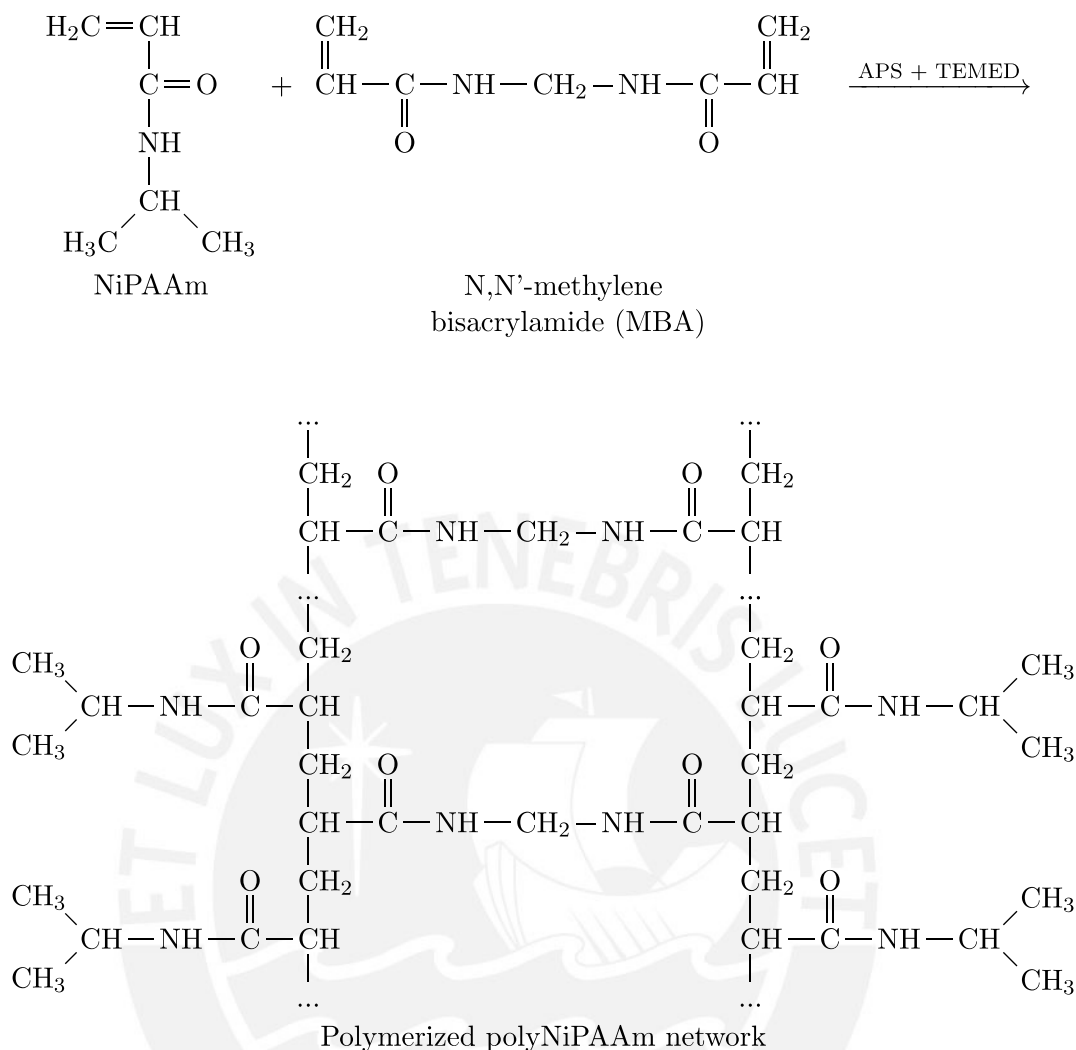


Figure 2.13: Three dimensional polymerization of *N*-isopropylacrylamide

2.2.3 Properties and applications of poly(*N*-isopropylacrylamide)

With regard to applications of polyNiPAAm there shall first be distinguished between polymerized non-crosslinked linear water-soluble NiPAAm (with or without any further comonomers) and crosslinked water-insoluble, but water-absorbent, hydrogels containing NiPAAm (and at least a further crosslinking agent).

Due to temperature-dependent solubility of polyNiPAAm in water, aqueous polyNiPAAm solutions have a variable viscosity, which can be changed by temperature or presence of hydrophilic or hydrophobic comonomers. Thus, polyNiPAAm is used as a thickening agent, a general viscosity-controlling agent or a viscosity modifier [12, 22].

The precipitation of polyNiPAAm at higher temperature is utilised in immunoassay technology [23], where polyNiPAAm chains are polymerized with *N*-acryloxysuccinimide (NASI) to allow conjugation of enzymes and antibodies to polyNiPAAm [24]. Heating at temperature

above LCST enables separation of unbound species and isolation of desired substances. Crosslinked polyNiPAAm gels are insoluble in water because of strong bounds between main and side chains. But due to hydrophilic functional groups they are able to absorb considerable amounts of water inside their polymer network. Owing to this ability of water absorption they are also called hydrogels. More detailed description of properties and application of hydrogels can be found in Section 2.4.

2.3 Macromonomers

A macromonomer is a large molecule created by polymerization of smaller submolecules and which may act as a monomer due to reactive carbon double bond end group in further polymerization reactions [25].

The Macromonomer method is a useful technique for preparing copolymers with defined structure and composition [26].

2.3.1 Synthesis of macromonomers

As polymers, macromonomers can be synthesized by conventional methods by polymerization of main-chain monomers and terminal functional group on the end of the polymer chain [26]. Macromonomers with functional groups on both chain ends are also possible and are termed telechelic [26].

Most common macromonomer synthesis methods are shown below.

Macromonomer synthesis by ionic polymerization

Anionic and cationic polymerization are living polymerization methods and allow synthesis of graft copolymers with controlled chain length. General reaction schemes are presented in Figure 2.14 [26].

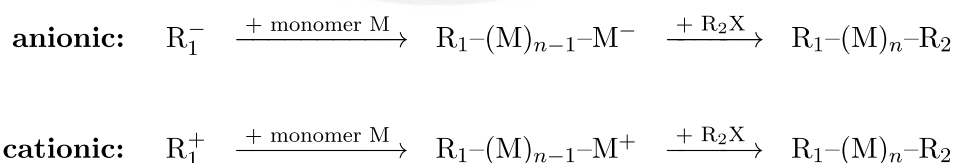


Figure 2.14: Macromonomer synthesis via anionic and cationic polymerization [26]

Both of them can be subdivided into two main types: the initiating and the end-capping methods. In the initiating method functional initiator are used, whereupon functional groups persist unreacted after the polymerization reaction of the monomer. In the end-capping method functional monomers are used to terminate the polymerization reaction by simultaneous integration into the polymer chain as an end group. Styrene is a common applied

monomer in anionic polymerization, acryl cations can be applied in cationic polymerization of e.g. tetrahydrofuran [26].

Macromonomer synthesis by radical polymerization

In comparison with living polymerization methods, polymers created by radical polymerization show wider molecular weight distribution. This method is nonetheless often applied due to its practical simplicity [26].

The general method consists of two steps: the radical chain transfer polymerization and the transformation of the functional end group. Chain-transfer agents should be suitable to the respective monomer. A typical example of radical polymerization is synthesis of poly(methyl methacrylate) macromonomer using thioglycolic acid as a chain-transfer agent [26].

2.3.2 Synthesis of graft copolymers and hydrogels by macromonomer method

As mentioned previously the macromonomer method can be used to produce graft copolymers with well-defined molecular weight distribution. Graft copolymers are macromolecules with one polymer type in the main chain and another in the side chains. In the macromonomer method side chains, which contain a C=C double bond on the one end, are prepared first. The main chain is connected afterwards through addition or condensation with the second polymer type with polymerizable end group [27].

Hydrogels can be made of cross-linked water-soluble polymers or block or graft copolymers with hydrophilic and hydrophobic functional groups, whereupon hydrogels out of block and graft copolymers are distinguished by better mechanical properties. Graft copolymers soluble in water normally have a hydrophilic main chain and hydrophobic side chains. The swelling degree depends on number and size of the side chains compared to the main chain. Coexistence of hydrophobic and hydrophilic parts leads to amphiphilic behavior [28].

2.4 Hydrogels

Hydrogels are three-dimensional polymer networks with ability to absorb water (see Figure 2.15) due to hydrophilic functional groups in polymer network, but not to be dissolved because of strong crosslinks between them [29, 30].

Versatile properties (see Section 2.4.2) have made them interesting materials in several fields, e.g. for biomedical applications, agriculture or sensor technology.

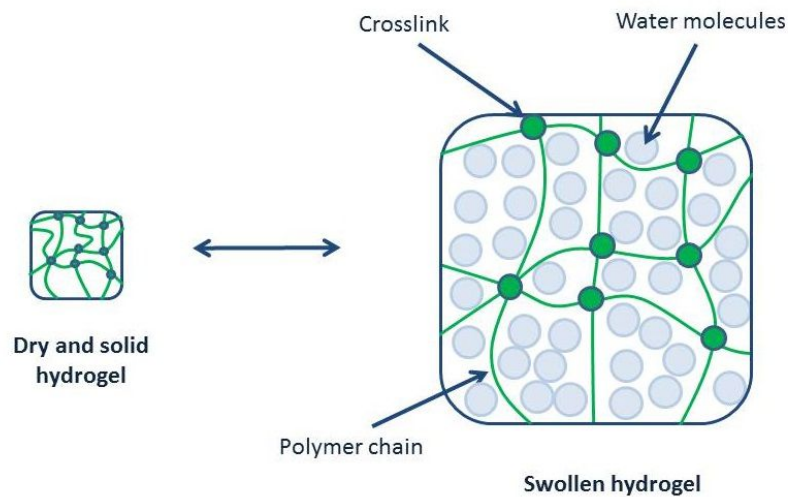


Figure 2.15: Schematic representation of a hydrogel network

2.4.1 Methods of hydrogel synthesis

Numerous methods to synthesize a hydrogel can generally be classified into two main areas: modifying an existing polymer or polymerization of monomer units [30].

Hydrogel synthesis by modification

Hydrogels can be proceeded by modification or functionalization of existing natural or synthetic polymers.

Gelatine is an animal hydrogel produced by partial hydrolysis of collagen fibers. Microstructurally it is based on macromolecular amino acid threads which are twisted to a triple-helical structure stabilized by hydrogen bonding [31]. It swells in water and dissolves at temperatures above 50 °C. Cooling to lower temperatures effectuates a reversible gel formation that can be dissolved by heating anew [31]. Moreover there is a considerable amount of hydrogels synthesized by modifying natural polymers such as collagen, starch, cellulose or sugar [29]. A well-known example of synthetic hydrogel proceeded by modification is polyvinyl alcohol derived from polyvinyl acetate by hydrolysis. Polyvinyl alcohol hydrogels are widely used in daily soft contact lenses [29].

Hydrogel synthesis from monomers

Free radical polymerization is the most common synthesis method to obtain the hydrogel by assembling hydrophilic monomers [29]. Carbon double bonds in monomer units enable the polymerization. The reaction is initiated by a redox pair producing radicals which attack carbon double bond and create further radicals. Combination reactions propagate a chain formation. To form a three dimensional structure, a crosslinking monomer unit with

two or more carbon double bonds is necessary. The connection of single chains provided by this crosslinking agent leads to gelation [29]. Initiator systems are not compulsory. The polymerization can also be initiated thermally, by light, radiation or electron beams [29]. Depending on monomers and desired properties various polymerization techniques can be applied. Most common is solution polymerization using a solvent. Emulsion and suspension polymerization are applied to obtain hydrogel particles [29].

In the present work, hydrogels were synthesized from NiPAAm, N,N'-methylene bisacrylamide (MBA) and a self-synthesized macromonomer containing 2-carboxyethyl-2-oxazolines and 2-methyl-2-oxazolines as monomers. APS and TEMED were used as redox initiator system.

2.4.2 General characteristics and applications of hydrogels

The properties of the hydrogels are closely related to their structure, resulting in a variety of applications. The most important are listed below:

- **Water storage**

Hydrophilic units and free spaces between crosslinked chains enable water absorption and makes them suitable for applications in sanitary products such as diapers or sanitary towels. The ability to release water in dry environment to achieve an equilibrium state is important for applications in the agricultural sector.

- **Permeability for small molecules**

Three dimensional network with free spaces between crosslinked molecules allows permeability of molecules that are smaller than this spaces. Such a capability is connected with a number of crosslinks in molecular structure and allows on the one hand permeation of e.g. oxygen which is important for biomedical applications and on the other hand sorting of molecules in chromatography [29, 30].

- **Biocompatibility**

Inert and non-toxic basic structure, compatibility with aqueous solvents, permeability to oxygen and soft consistency minimize irritation of biological tissue and enable biomedical applications e.g. in soft contact lenses or in implants [29].

- **Flexibility**

Mechanical properties are strongly influenced by its water content, which is connected with hydrophilicity and a number of crosslinks in the molecular structure. But all of them are flexible in swollen state and brittle in dry state [30]. Due to their flexibility in swollen state hydrogels can be produced in several shapes.

- **Optical transparency**

For their application in contact lenses optical transparency of hydrogels is very important. Just as other properties it can be controlled by chemical structure and water content. Further optical applications are optical sensors [30].

2.4.3 Stimuli-responsive hydrogels

Stimulus-responsive hydrogels or also referred to as smart hydrogels reacts with structural change to environmental stimuli such as temperature, pH, electrical current, etc. The stimulus responsive behavior enables new applications areas. Hydrogels with thermosensitive NiPAAm, for example, are widely studied for drug delivery applications [10,11].

Thermosensitive hydrogels

Thermosensitive materials can be divided into two main types: upper critical solution temperature (UCST) and lower critical solution temperature (LCST) materials [20].

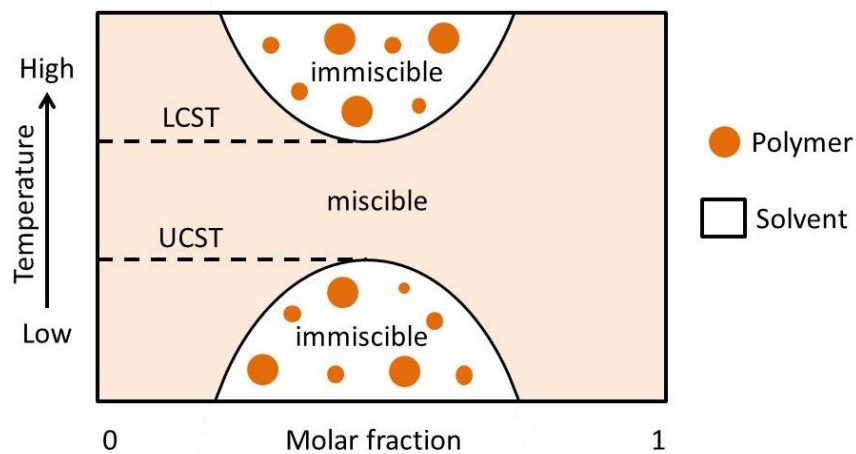


Figure 2.16: Schematic representation of temperature dependent solubility of LCST and UCST materials (according to [32])

UCST materials gelate due to reversible formation of intermolecular hydrogel bonds induced by temperature change from hot to cool state. This behavior is typical for gelatine [20]. Heating above a material characteristic temperature LCST materials undergo a phase change from hydrophilic to hydrophobic state driven by an entropy change [20]. This behavior is typical for NiPAAm, which change its solubility in water depending on temperature. Due to this effect hydrogels containing NiPAAm are able to change the amount of absorbed water. Further examples for LCST systems are cellulose derivatives [20].

NiPAAm is soluble below 32°C [21] and precipitates above this temperature due to reversible formation of hydrogen bonds between water molecules and -NH and C=O groups in NiPAAm. The LCST can be increased by polymerisation with hydrophilic monomers and decreased by using hydrophobic monomers. Thus, LCST near body temperature can be achieved for biomedical applications.

pH-sensitive hydrogels

Environmental changes from acidic to basic state cause swelling or shrinkage in pH-sensitive hydrogels. Generally these are hydrogels that contain weak acidic or basic groups (or both), which are easy to ionize [14]. Most common pH-sensitive hydrogels comprise carboxyl groups or tertiary amines [14, 33].

Depending on surrounding conditions following reactions are possible: In basic environment acidic groups are deprotonated and the hydrogel swells due to repulsive effect of new-formed COO^- ions inside the gel. In acidic ambient the present COO^- groups protonate. This leads to decrease of electrostatic repulsion and consequently shrinkage of the hydrogel (see Figure 2.17). The phase transition is associated with the apparent acid dissociation constant pK_a of the ionisable group [14, 34].

Hydrogels with basic tertiary amines show a contrary behavior: In acidic ambient tertiary amine protonate, which leads to formation of electrical charges and swelling due to osmotic pressure (see Figure 2.17). Basic environment induces deprotonation and thus shrinkage of the gel [14, 33].

A smart combination of basic and acidic ionizable group enables an amphiphilic behavior of hydrogels [14].

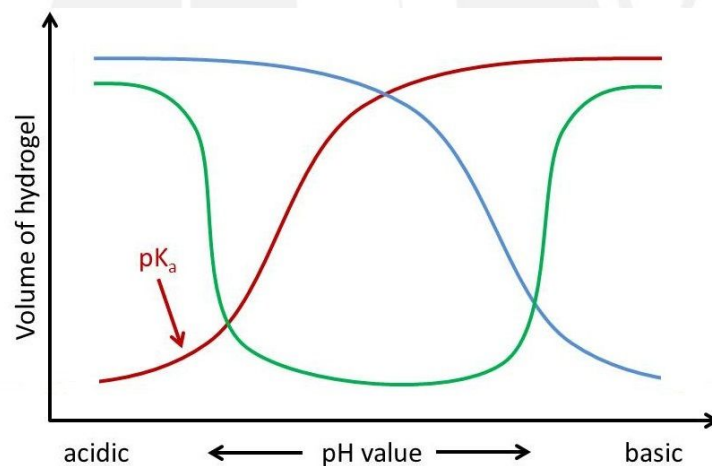


Figure 2.17: Phase transition behavior of hydrogels containing acidic (red), basic (blue) and both types of ionizable groups (green) (according to [14])

2.4.4 Nanocomposite hydrogels

Nanocomposite polymer hydrogel is a three dimensional cross-linked polymer network with nanostructures and ability to absorb water. The cross-linking between polymer chains is covalent and permanent, the interaction with water molecules non-covalent and temporary, depending on environmental conditions [35].

Nanostructures can be used as a crosslinking agent between polymer chains or a filler material trapped between them. Hydrogel serves as a matrix, nanostructures lead to improved or

novel properties [35]. Two main techniques are distinguished: hydrogel polymerization using ready-made nanostructures or synthesis of nanostructures inside the hydrogel.

Various systems and their applications are shown below.

Hydrogel-silicate nanocomposites

Silicate nanostructures such as Laponite (silicate discs with 30 nm diameter and 1 nm thickness) can be used as cross-linking members in the polymer matrix to improve mechanical stability of the hydrogel (see Figure 2.18).

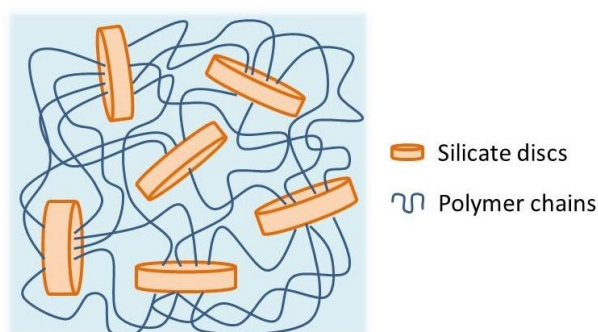


Figure 2.18: Schematic representation of a hydrogel-silicate nanocomposite (according to [36])

Frequently used polymer systems are poly(ethylene dioxide), poly(vinyl alcohol) and poly(acryl amide). The cross-links between Laponite and poly(ethylene dioxide) are physical (adsorption of polymer chains on Laponite surface) and reversible. Poly(acryl amide)-based hydrogels are responsive on environmental changes such as temperature or pH. The crosslinking between Laponite and this polymer is chemical. Depending on desired properties other silicates such as montmorillonite, mica or zeolite can be used [35].

Hydrogel- magnetic nanoparticles composites

Hydrogels with magnetic nanoparticles allow to combine thermosensitive and magnetoresponsive properties. The hydrogel matrix is generally poly(acryl amide)-based, but other synthetical and natural polymers can be applied. Used nanoparticles are cobalt, nickel, iron or iron oxides. Possible applications are e.g. in the medical sector: High-frequency magnetic field heats magnetic nanoparticles and the hydrogel matrix. The local temperature increase leads to controlled drug release [37]. Further application areas are sensor technology or nanoparticle synthesis, where hydrogel matrix serves as a mould for particle production [35].

Hydrogel- metal nanoparticles composites

Using nanoparticle inside (see Figure 2.19) hydrogel networks enhance properties like electrical conductivity, antimicrobial effect or optical stimulation. Poly(N-isopropylacrylamide) hydrogel represents the hydrogel matrix in most cases [35].

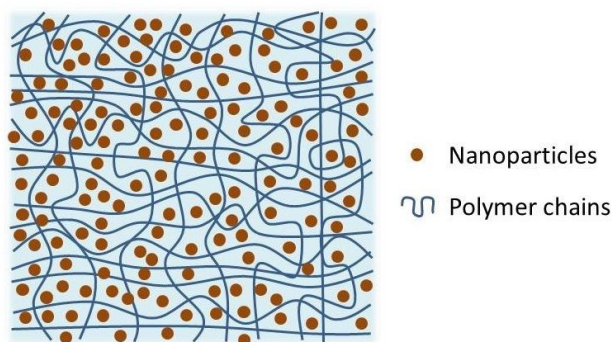


Figure 2.19: Schematic structure of a hydrogel-nanoparticles composite (according to [16])

Hydrogels with gold nanoparticles Gold nanoparticles (Au-NPs) from gold reactive thiol groups form covalent bonds to polyNiPAAm hydrogel. Au-NPs provides electrical conductivity which can be changed with temperature due to expansion or shrinkage of hydrogel matrix and therewith connected interparticle distance [38].

Hydrogels with silver nanoparticles Besides the electrical conductivity hydrogels containing silver nanoparticles (Ag-NPs) show an antibacterial effect as well [15, 16]. Carboxylic groups are generally used to attach silver cations to a hydrogel network [16]. Reducing agents convert them to nanoparticles [39]. Carboxylic groups are not inevitable, even though the number of carboxylic groups increases considerable the silver content in hydrogel. The cross-linking intensity influences free space between polymer chains and affects the particle size: hydrogels with more cross-links have smaller capacities and generate thereby composites with smaller particles [16]. Various systems can be used for hydrogel synthesis, hydrogel complexation with silver cations and reduction to Ag-NPs. Some of them are listed below.

Thomas et al. used acrylamide and acrylic acid as monomers, MBA as crosslinking agent and KPS as initiator for synthesis of a hydrogel matrix. Ag-NPs of 24-30 nm size were obtained by complexation with silver nitrate (AgNO_3) and reduction with trisodium citrate. Silver content and antibacterial activity was related to content of acid groups. Thus, antibacterial activity depends on size and amount of nanoparticles. 20 mg/30 mL was determined as the most suitable concentration of AgNO_3 solution to gain optimal antibacterial effects [40].

Bajpai et al. synthesized the hydrogel matrix out of NiPAAm as a monomer, MBA as a cross-linking agent and KPS as an initiator. Silver nitrate was used for complexion with silver cations, sodium borohydride (NaBH_4) for reduction to nanoparticles (NPs). The attachment of silver nanoparticles to C=O groups (of amide) was determined with Fourier transformed infrared spectroscopy (FTIR) characterization. The NP-size was measured with transmission electron microscope (TEM) and was about 20 nm. Antibacterial effects against *E. coli* was proved qualitative [15].

Mohan et al. used a hydrogel matrix based on NiPAAm and sodium acrylate as monomers, MBA as a cross-linking agent and APS and TEMED as an initiator system. For synthesis of Ag-NPs AgNO_3 and NaBH_4 were used. Content of MBA as a cross-linker was crucial for the obtained size of NPs. Minimal achieved diameter of nanoparticles was about 3 nm. Hydrogel-Ag-NPs composite was observed to have much less swelling capacity in comparison with hydrogel without silver nanoparticles. Antibacterial activity was studied using *E. coli*. Hydrogels with smaller particles were more effective against the bacteria due to higher mobility and diffusion tendency [16].

Present work uses hydrogel with NiPAAm and self-synthesized macromonomer based on oxazolines with acid groups in side chains. MBA was used as a cross-linking agent and APS and TEMED as an initiator system. AgNO_3 and NaBH_4 were used for NP-synthesis. Amounts of cross-linker and acid groups were varied to observe their effect on Ag-NPs size, amount and antibacterial activity.

2.4.5 Hydrogel thin films

Rising progress in micro- and nanotechnology redounds to growing interest in thin film material systems. Hydrogels are not excepted from this trend [34]. Especially their stimuli-responsive behavior makes them an interesting material for miniaturized devices such as sensors or actuators [14, 34].

Effects of thin film confinement

Beside numerous advantageous properties of bulk hydrogels it is crucial to consider the thin film confinement effect. This means the greatly changed behavior of the film compared with the bulk material due to the attachment to the surface [34].

Particularly the swelling behavior was found to be much lower [41]. The volumetric expansion is limited in lateral direction and is only possible vertically to the substrat plane that leads to a factitious anisotropic behavior [34].

The prevented expansion leads to mechanical stress inside the layer and might lead to delamination as soon as the adhesion gets overcome by the mechanical stress. Wrinkling or

bending of the surface is possible as well [34,42]. However, this effect can also be purposeful used in devices with membranes or cantilevers [43].

Adhesion between glass substrate and hydrogel thin film

One of the upmost requirements for a good adhesion between a solid surface and a liquid layer is a sufficient wetting [44]. Wetting is the ability of a liquid to adhere on a solid surface [45]. The equilibrium state between adhesive and cohesive forces determines the state of wetting that can be described by a contact angle between the liquid-vapor and the solid-liquid interfaces (see Figure 2.20) [44,46]. The contact angle and the wettability itself is associated with polar or non-polar (or rather hydrophilic or hydrophobic) character of the surface and the liquid [47].

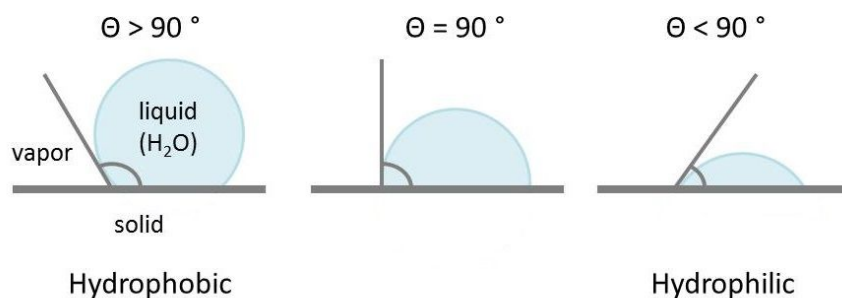


Figure 2.20: Characterization of wetting behavior by measuring the contact angle (according to [48])

Glass surfaces are generally hydrophilic due to many oxygen and hydrogen atoms on their surface, which form hydrogen bonds with water [49]. A purely applied polymer layer, which is non-polar or hydrophobic, does not adhere sufficiently. For this reason surface active agents are applied to reduce the surface tension of the liquid and to improve the adhesion to the surface [50].

Silanes are used as coupling agents to link mineral (glass) and organic (polymer) components chemically. Hydroxyl group on the glass surface and alkoxy groups of silane react forming a covalent -Si-O-Si- bond [51]. Organofunctional silanes contain both the inorganic and the organic functional group, e.g. the amine group [50].

3-aminopropyltriethoxysilane (APTES) is a frequently used aminosilane for silanization. In the present work it was used as a coupling agent between glass substrates and polymeric hydrogel layer.

Hydrogel thin film coating process

Hydrogel thin film coating is classified as a chemical solution deposition (CSD) process and can be largely compared with photoresists from microsystems technology. Most important CSD techniques are dip and spin coating.

Dip coating is a common used technique for layer fabrication on glasses where the substrate is dipped into a solution which is desired to be deposited as a coating (see Figure 2.21). After pulling the substrate out of the solution a thin liquid film remains. The contained solvent evaporates in the atmosphere so that only a solid layer remains on a substrate [52, 53].

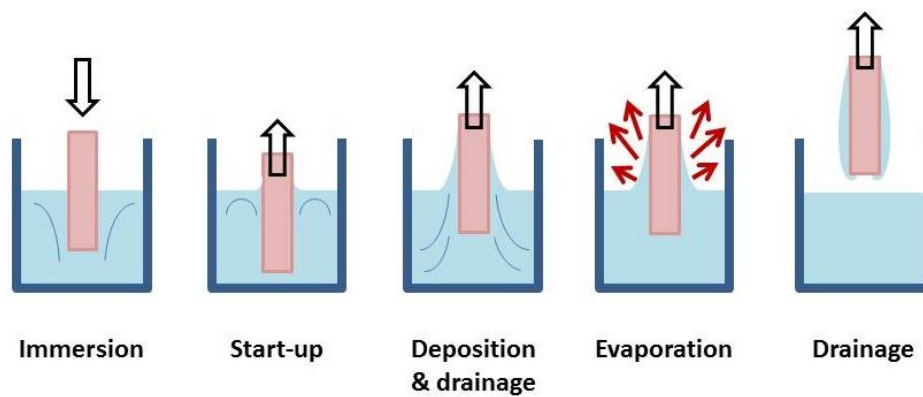


Figure 2.21: Dip coating process (according to [53])

The layer thickness depends on many factors such as temperature, atmospheric pressure, humidity, pulling speed and solution viscosity and can be described by Landau-Levich equation [52, 54].

$$d = 0.946 \frac{(\eta v)^{2/3}}{\gamma^{1/6} \sqrt{\rho g}} \sim v^{2/3} \quad (2.1)$$

with

d = Layer thickness

η = Fluid viscosity

v = Relative velocity

γ = Fluid surface tension

ρ = Fluid density

g = Acceleration of gravity

Compared with other deposition techniques the main advantage of dip coating is a constant deposition on substrates with large and complex geometries.

Spin coating is widely used in semiconductor industry for deposition of thin photoresist films [53]. In this technique the substrate is placed on a rotating plate and a small amount of coating solution is dropped in its center (see Figure 2.22). Due to centrifugal force the coating material is spread uniformly on the rotating substrate.

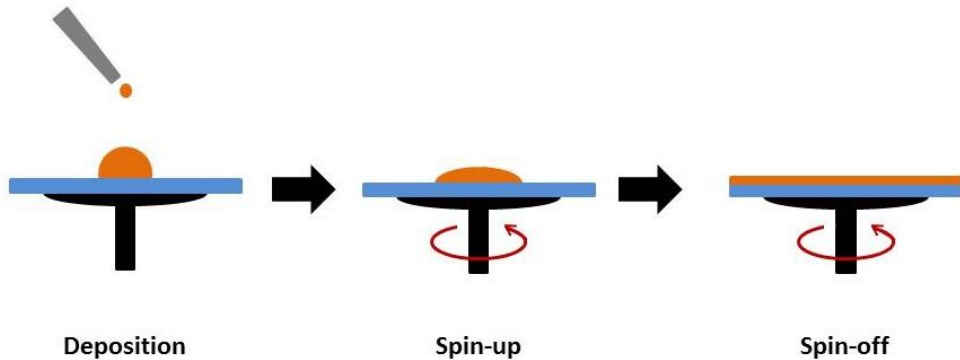


Figure 2.22: Spin coating process (according to [55])

The layer thickness is mainly influenced by rotation speed and solution viscosity and can be described by following equation [53, 56].

$$d = \frac{d_0}{\sqrt{\frac{1+4\rho\omega^2 d_0^2 t}{3\eta}}} \sim \omega^{2/3} \quad (2.2)$$

with

- d = Layer thickness
- d_0 = Initial layer thickness
- ρ = Fluid density
- ω = Angular velocity
- η = Fluid viscosity
- t = Time

Thus, the higher the rotation speed, the thinner the layer. Most important advantages of spin coating are fast processing, small required volume of coating solution and one-side layers. The substrate geometry however is limited to plane surfaces.

As distinguished from comparatively simple photoresist coating the hydrogel solution is normally less stable due to thermally driven polymerization and has to be prepared carefully in a defined time before use. The polymerization and cross linking can be achieved

(depending on used hydrogel solution) due to free-radical initiators, plasma, high-energy irradiation or thermally [34]. Selective polymerization techniques (e.g. initiated by ultraviolet irradiation or electron beam) allow microstructuring of hydrogel thin films comparable to photoresists [34].

In present work the hydrogel solution was applied to silanized glass surfaces using dip coating.

2.5 Silver nanoparticles

Nanoparticles are defined as particles between 1 nm and 100 nm in size [57]. Due to their large surface-to-volume-ratio they often show changed, increased or even different properties compared to ordinary bulk material [58].

Silver was historically common used for hygienic and healing purposes, but almost fell into oblivion with intense use of antibiotics and other anti-infection media [58,59]. Appearance of multiresistant germs, however, puts the excessive use of antibiotics nowadays into question and demands alternative solutions.

Compared to bulk silver, silver nanoparticles show a higher antimicrobial effect due to their larger surface-to-volume-ratio [58]. Recent developments in micro- and nanotechnology not even allow a precise fabrication of particles of certain size or shape, but also give an understanding of the antimicrobial mechanism [58,60,61].

Of course the application of silver nanoparticles is not just limited to medical and antimicrobial sector. Optical (e.g. plasmonic devices [62,63]), electrical (e.g. conductive adhesives [64,65]) or chemical (e.g. catalysts [66,67]) application are also common.

2.5.1 Fabrication of silver nanoparticles

There is a huge amount of methods to fabricate nanoparticles and silver nanoparticles in particular. Nonetheless almost all of them can be classified into one of the three following types: physical (top-down), chemical (bottom-up) or biological methods [58].

Physical top-down methods use materials in their bulk form and comminute them to the nanoscale [58,68]. Mechanical milling is the most known technique, but also lithography and laser ablation can be used [69–71]. For fabrication of silver nanoparticles top-down methods are not negligible, but less considerable.

Chemical bottom-up techniques imply the use of dissolved silver salts generating silver ions which are reduced to elemental silver by chemical agents (see Figure 2.23).

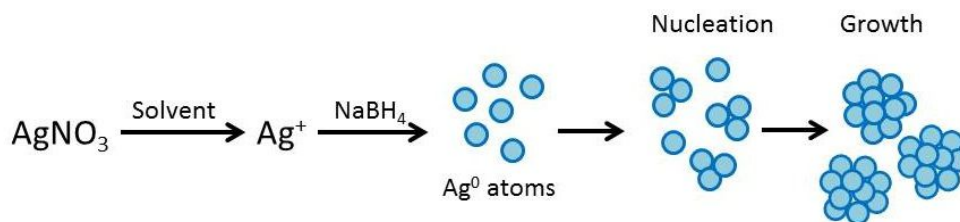


Figure 2.23: Mechanism of chemical bottom-up synthesis of silver nanoparticles from AgNO_3 salt [72]

The most widely used silver salt is AgNO_3 due to its low cost and chemical stability [59]. Water is commonly used as a solvent, but also ethanol, dimethylformamide, ethylene glycol, toluene, chloroform etc. are possible [59]. Reducing agents such as sodium borohydride or citrate provide free electrons and reduce silver ions forming nanoparticles [59].

The formation of nanoparticles is self-assembled and can be influenced by stabilizing agents. Stabilizing agents are used to avoid aggregation of nanoparticles and to control their size [59]. The stabilizing effect can be achieved owing to charged surfaces and the resulting electrostatic repulsion, steric stabilization or a mix of them (see Figure 2.24) [57]. Another stabilization technique is the use of a (polymer) matrix, where nanoparticles are embedded in.

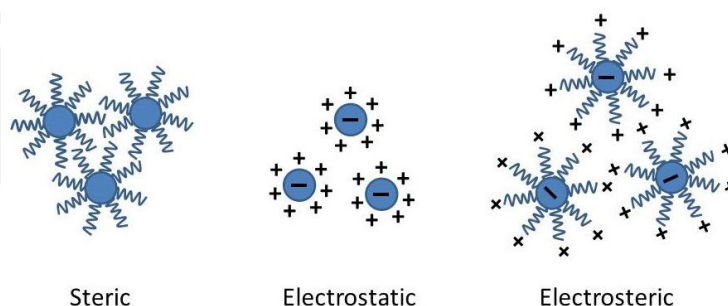


Figure 2.24: Mechanisms of nanoparticle stabilization [57]

In the present work a hydrogel matrix is used as a mechanical stabilizer and network where silver nanoparticles are dispersed statistically. The particles were formed in an aqueous environment using silver nitrate and sodium borohydride.

Biogenic silver nanoparticles can be produced by certain biological systems such as plants (geranium [73], ginkgo [74] or magnolia leaf extract [75]), fungi (*Fusarium oxysporum* [76]) or bacteria (*Pseudomonas stutzeri* AG259 [77], *Lactobacillus fermentum* [78]). The main principle persists in the interaction of fungi or bacteria protein with the silver salt solution (e.g. silver nitrate) [58]. The reduction of silver nanoparticles proceeds due to enzymatic reaction with electron donating species [58]. Thereby the reaction can take place inside (*Pseudomonas*

stutzeri AG259 [77]) or outside (*Fusarium oxysporum* [76]) the organism. Owing to biological synthesis harmful reducing agents like sodium borohydride can be relinquished [58]. The main disadvantage however is the hardly adjustable particle size distribution [58].

2.5.2 Antimicrobial effect

As mentioned before silver nanoparticles are vitally important for bactericidal applications. Nowadays silver nanocompounds of different forms can be found in numerous convenience goods such as clothing, household water filters, antibacterial sprays, cosmetics and so forth [79]. In order to evaluate the application potential of nanosilver and the risks associated therewith, it is crucial to understand the mechanism behind the antibacterial activity. Generally the antimicrobial effect of nano-scaled silver can be divided in three main processes: release of silver ions and their subsequent interaction with cell enzymes, generation of reactive oxygen species (ROS) as well as the direct cell damage by silver nanoparticles [79].

Silver nanoparticles can be oxidative dissolved to silver ions in the presence of oxygen or hydrogen peroxide combined with hydrogen protons as can be found in the bacteria cell membranes [79–81]. The resulted silver ions interact with respiratory and transport cell proteins disturbing their proper function [79].

ROS are naturally generated radicals during the metabolism process in respiring organisms. A small range of them can be managed by the antioxidant defensive forces of the cell [82]. Silver nanoparticles catalyze accessory reactions with oxygen. An excess of free radicals is toxic for a cell and leads to damage of cell components such as proteins, lipids and deoxyribonucleic acid (DNA) [82].

Furthermore nanoparticles themselves can interact with the bacteria cell membrane. They are reported to accumulate on the cell disturbing the respiration or even to penetrate into the cell leaving holes inside the cell membrane [60, 79].

In present work the antimicrobial effect on silver nanoparticles in hydrogel matrix was investigated using *Staphylococcus aureus*.

Feng et al. described the interactions between *Staphylococcus aureus* and silver ions using TEM and X-ray microanalysis [60]. According to this study after Ag^+ treatment silver ions could be detected inside the cell. The cytoplasm membrane shrank and detached from the cell wall. DNA molecules concentrated in the center of the cell protecting the important information. At the same time the DNA loses its replicating ability because the replication is only possible in a relaxed state. Then the protected region was surrounded by silver and finally ruptured. Furthermore owing to detection of sulfur in the energy-dispersive X-ray spectroscopy microanalysis (EDAX) silver (ions) were confirmed to interact with thiol groups in proteins disturbing their enzyme activity. [60]

2.6 Photosensitive glass

Glass is a non-crystalline solid with an internal structure more similar to a liquid than to a solid [83]. The glassy state can be achieved by rapid melt quenching (see Figure 2.25) [84]. Due to a rapid cooling the structural units of the glass do not have enough time to get ordered in a lattice structure (crystallization) and solidify in a disordered atomic configuration (amorphous state) [83]. For this reason glassy networks have merely a short-range order, but a long-range order is missing [83]. The transition between the liquid and the solid state is gradual and occurs at the transformation temperature T_g [84]. This temperature varies depending on the glass composition [83].

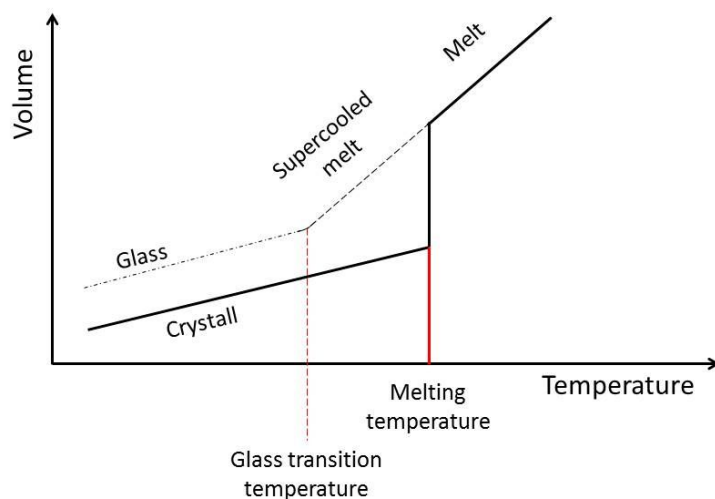


Figure 2.25: Formation of a crystalline and a glassy networks depending on cooling (according to [84])

Regarding the composition there are two main types of structural units in the glassy network. Network formers such as silica tetrahedra (SiO_4) constitute a continuous, but randomly distributed network. Network modifiers (metal oxides) interrupt this network partially due to the formation of non-bridging oxygens. The properties of the final product such as thermal expansion, density, electrical resistivity, etc. are determined by the internal structure and can be adjusted by a correct choice of used components. [83, 85]

Beside these main structural units photostructurable glasses contain photosensitive constituents. Exposed to laser or UV irradiation they induce (similar to photolithography) a structural transition inside the network and a change of solubility towards certain solvents.

2.6.1 Functional principle

Photosensitive glasses are lithium aluminosilicate glasses doped with small amounts of cerium oxide and silver oxide [83].

Although several types of photosensitive glasses with different compositions are known, the main compounds (even though in different percentages) and the functional principle are the same. Table 2.1 demonstrates composition of FOTURAN, a widely used photosensitive glass developed by SCHOTT, compared with FS21, a photosensitive glass developed at the TU Ilmenau and used in the present work [83,86].

Table 2.1: Chemical composition of two photostructurable glasses: FOTURAN (SCHOTT) and FS21 (TU Ilmenau) [83,86]

Component	FOTURAN	FS21
SiO ₂ [wt%]	79.1	74.29
Li ₂ O [wt%]	9.6	11.61
Na ₂ O [wt%]	1.7	2.74
K ₂ O [wt%]	3.69	4.16
Al ₂ O ₃ [wt%]	4.16	7.20
ZnO [wt%]	1.01	0
Ag ₂ O [wt%]	0.06	0.123
SnO [wt%]	<0.01	0.07
Sb ₂ O ₃ [wt%]	0.51	0.40
Ce ₂ O ₃ [wt%]	0.03	0.033

Exposed to UV light cerium (III) ions contained in the glass oxidize to cerium (IV) ions and release electrons [87]. Silver ions react with electrons released from cerium (III) ions to elemental silver. At this step the glass stays transparent, the exposed structure is latent [87]. Subsequently the glass is heated to temperatures above 500°C for several hours. The tempering varies depending on the glass type. Figure 2.26 presents recommended heating curves for FOTURAN and FS21 in comparison [86].

During the tempering elemental silver agglomerates to nanometer-sized clusters [87]. These clusters provide the nucleation of lithium metasilicate, a crystalline phase. After the heat treatment exposed areas become visible in an orange-brown colour (due to the silver clusters) [83].

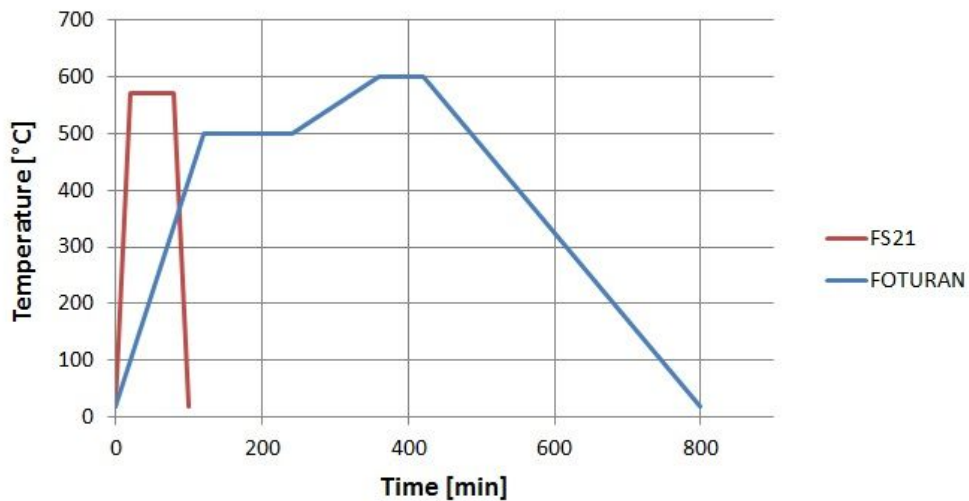


Figure 2.26: Recommended tempering curves for FOTURAN and FS21 (according to [86])

Compared to the non-exposed glassy regions, the partial crystallised areas are 18 times stronger attacked by hydrofluoric acid and can easily be removed this way leaving a structured glass substrate [83]. Optionally the whole substrate can be exposed and tempered a second time where lithium disilicate is formed. The whole process is shown in Figure 2.27.

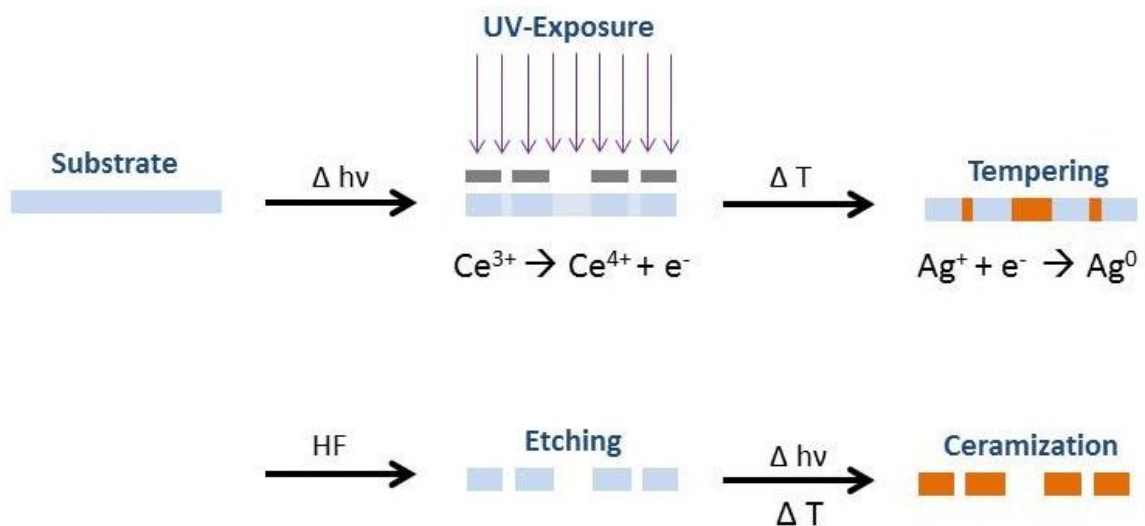


Figure 2.27: Schematic representation of photostructuring process

2.6.2 Properties and application of photosensitive glass

Photostructurable glasses are characterized by high optical transmission and high temperature resistance. By reason of the high etching ratio between glass and lithium metasilicate

phase small structures with high aspect ratio can be produced. Chemical and mechanical stability as well as pore-free structure make them suitable for biotechnical and biomedical applications, but also for microtechnological devices. Table 2.2 summarizes a few important characteristics. [86]

Table 2.2: Properties of two photostructurable glasses: FOTURAN (SCHOTT) and FS21 (TU Ilmenau) [86]

Property	FOTURAN	FS21
Therm. expansion coefficient $\alpha[10^{-6} \text{ K}^{-1}]$	8.6	10.3
Young's modulus [GPa]	78	82
Transformation temperature T_g [$^{\circ}\text{C}$]	465	450
Density [gcm^{-3}]	2.37	2.38
Thermal conductivity [$\text{Wm}^{-1}\text{K}^{-1}$]	1.35	1.2

Some already used devices made from photostructurable glasses are: middle ear implants, microvalves, microfluidic chips, different sensors and actuators, as well as micromechanical devices such as springs or grippers [83, 86, 88, 89].

The present work is aimed at the investigation of hydrogels and their use as coatings on photostructurable glass FS21 for biomedical applications. Hydrogel coatings are supposed to reduce the roughness of structured glass surfaces and (as a composite containing silver nanoparticles) to give an additional antimicrobial effect.

2.7 Basic principles of characterization methods used in present work

2.7.1 Nuclear magnetic resonance spectroscopy

Nuclear magnetic resonance spectroscopy, also known as NMR spectroscopy, is a common characterization technique in polymer research to confirm or to identify the chemical structure of materials.

The basis for this technique is the phenomenon of nuclear magnetic resonance, where certain NMR active nuclei (^1H in present work) absorb electromagnetic energy at a characteristic resonance frequency. The resonance frequency is dependent on the position inside the molecule and can be influenced by neighbouring functional groups. [90]

For the analysis some mg of the material are solved (or swollen in case of hydrogel samples) and placed in a NMR tube. A deuterated solvent (in this case CD_3OD for macromonomer and D_2O for hydrogel analysis) is used to avoid the interference between the sample and the

solvent signals. Inside the spectrometer the tube rotates in a magnetic field. A radiofrequency generator irradiates the solution causing resonance and energy absorption. Falling back to the low energy state (relaxation), the sample releases energy, which is recorded by the detector. [90]

In the High Resolution Magic Angle Spinning (HR-MAS) technique the sample is spinning at the angle of 54.7° to the magnetic field that provides narrower and better resolved spectra. Thus, samples with a low internal molecular motion such as hydrogels can be analysed. [91]

2.7.2 UV/Vis spectroscopy

Ultraviolet-visible (UV/Vis) spectroscopy relies on the absorption and scattering of light in the ultraviolet-visible spectral region. In the experimental setup the sample is placed between the light source and the detector. During the measurement the beam through the sample is compared to one without passing the sample or one through the "blank": a cuvette only filled with the solvent. For sample preparation of solids with low transparency it is necessary to pulverize the material and to prepare a low concentrated solution (eg. 1 mg/1 mL). Furthermore it is important to agitate the suspension to minimize the influence of sedimentation. [16, 92]

The recorded spectrum demonstrates the transmittance or absorbance of the material as a function of wavelength. The relationship between these values is shown below. [92, 93]

$$A = -\log_{10}(T) = -\log_{10}\left(\frac{I}{I_0}\right) \quad (2.3)$$

with

A = Absorbance

T = Transmittance

I = Intensity of the light beam without the sample

I_0 = Intensity of the light beam after passing the sample

Metal nanoparticles such as gold or silver nanoparticles show a characteristic absorption peak in UV/Vis measurements, which shifts to longer wavelengths with the increasing particle size. The reason for this phenomenon is the interaction of light with conductive electrons on the metal surface (surface plasmon resonance). Excited by the light of a specific energy they oscillate and show the increased extinction. Agglomeration of nanoparticles causes electronic coupling and a surface plasmon resonance at a lower energy. Due to this, UV/Vis spectroscopy can be used to demonstrate the presence of nanoparticles and to estimate their size. [94]

2.7.3 Fourier transformed infrared spectroscopy

Fourier transformed infrared spectroscopy analyses the energy absorption of a material at the infrared spectral region. Compared to other spectroscopy methods (e.g. UV/Vis spectroscopy) the sample is not irradiated by a monochromatic beam of light, which wavelength changes to get the full spectrum. In this case the starting beam contains the full desired spectrum of wavelengths. During the measurement it passes an interferometer, where a configuration of mirrors divides the initial beam in two partial beams and reunites them again inducing interference. Varying the mirror configuration the spectrum of the resulted beam (also called interferogram), which irradiates the sample, changes due to a consequent constructive or destructive interference effects. The detected transmitted light from every beam spectrum is analysed using Fourier transformation giving a wavenumber spectrum. Recorded bands are based on absorption of discrete energy values causing molecule vibrations and can be related to certain molecule groups. Thus, the chemical structure of a material can be clarified. [93,95]

2.7.4 Scanning electron microscopy

Scanning electron microscopy is an analysing technique where the sample is scanned by a focused electron beam. The interaction between the incident electrons and the sample occurs in different ways: they can be back-scattered (BSE), transmitted or can excite the sample generating secondary electrons (SE), characteristic X-rays or light (cathodoluminescence). The interaction signal is recorded by a detector and can be converted to an image containing information about the sample topography or material composition. The measurement proceeds under vacuum conditions to avoid collisions with air molecules. To prevent a surface charging the analysed sample should be electrically conductive or covered by a thin film of a conductive material. [96,97]

2.7.5 X-ray fluorescence spectroscopy

X-ray fluorescence spectroscopy (XRF) is used to determine the elemental composition of a material [98].

During the measurement the sample is irradiated with high-energy X-rays, which expel electrons from inner orbitals of the sample's atoms. The free position is immediately occupied by electrons from outer orbitals which change to a lower energy state emitting a photon. This process is called fluorescence. The energy of the photon is equal to the energy difference between the orbitals and is characteristic for each element. [98]

Emitted photons are recorded and analysed. As a result a spectrum with fluorescence intensities of included elements is given. Comparing the intensities a quantitative elemental

composition of a material can be given. However, it should be considered, that elements lighter than sodium ($Z = 11$) usually can not be detected [99].

2.7.6 Fluorescence microscopy

Fluorescence microscopy is an optical microscopy technique where the sample is irradiated by light of a specific wavelength, absorbing it and emitting a light of a longer wavelength. In this case the sample must be fluorescent or marked by fluorescent stains. [97]

During bacterial count tests the solution is marked by two different markers: a green and a red one. The green-fluorescent marker penetrates both bacterial cells: healthy cells with intact membranes and dead cells with damaged membranes. The red-fluorescent marker is only able to penetrate the damaged cell membranes covering the green fluorescence. By changing the excitation illumination green (healthy) and red (dead) fluorescent bacteria can be counted. [100]

Confocal laser scanning microscopy (CLSM) is a further development of fluorescence microscopy. Thereby the sample is illuminated pointwise in different depths, then the fluorescent signals at every point are collected to an image. Compared with a conventional fluorescence microscopy, CLSM has a higher resolution. [97]

2.7.7 Atomic force microscopy

Atomic force microscopy is a high-resolution microscopy technique based on the interaction of the sample and a scanning tip. The tip is arranged on a deformable cantilever, a focused laser beam transfers the cantilever deformation to the detector. The measured cantilever deflection is converted into an electrical signal, which is imparted to the feedback loop. The feedback control makes sure that a set force between the tip and the sample maintains, continuously correcting the position of the tip and the sample to each other. Thereby piezoelectric elements are used. The recorded information of every position is reconstructed to an image giving information about e. g. sample topography. [93, 101]

2.7.8 Profilometry

Profilometry is aimed at the measurement of the surface roughness. A diamond stylus moves vertically until it contacts the sample and then laterally for a certain distance. The stylus and the sample stay in contact during the measurement, while the force between them is regulated to a constant value, similar to an AFM. The recorded diagram demonstrates topography differences along the distance, from which roughness parameters can be calculated. [102]

Roughness is the irregularity of the surface and may occur due to different reasons, e.g. the production process or the ageing. Roughness parameters are defined to describe and to com-

pare surfaces. Some of the most commonly used parameters are the average peak-to-valley height R_z and the arithmetic roughness average R_a . To get the R_z , the measuring length is divided in five equal segments and the average of the highest asperity and the lowest valley (relative to the mean line) of every segment is calculated (see Figure 2.28). [103]

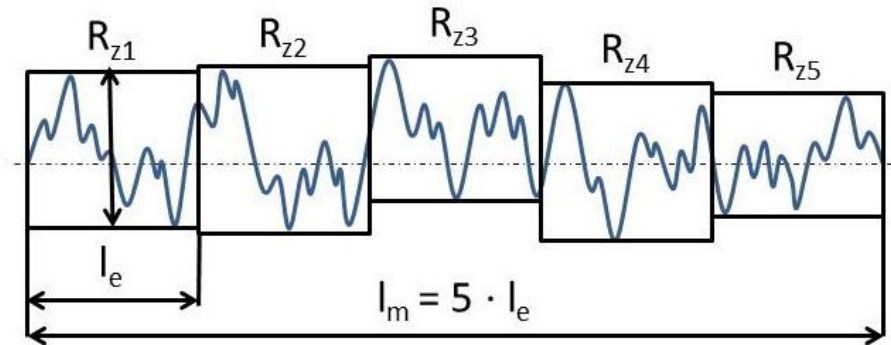


Figure 2.28: Schematic representation of the surface roughness and particularly of the average peak-to-valley height R_z (according to [104])

The arithmetic average R_a is the integral of all measured values (relative to the mean line) divided by the measuring length [103]. R_a and R_z are both commonly used in the industry, however, R_z is easier to determine and more reproducible in case of surfaces with several runaway values [103].

3 Experimental Part

3.1 Materials

3.1.1 Equipment

For the present work following devices were applied:

- **Atomic force microscope** Bruker Dimension Edge
- **Centrifuge** National Labnet Co. C-1200, 6000 rpm
- **Confocal laser scanning microscope** Zeiss LSM
- **Drying chamber** Heraeus T6060
- **Electronic balance** Sartorius BP 301S, accuracy 0.1 mg
- **Electronic balance** Sartorius BP 310S, accuracy 0.001 g
- **Electronic balance** Sartorius QUINTIX 124-1S, accuracy 0.0001 g
- **Fourier transform infrared spectrometer**
- **Nuclear magnetic resonance spectrometer** Bruker Avance III 500
- **Optical microscope** Olympus BX51 with
Reflected fluorescence system Olympus U-RFL-T
- **Scanning electron microscope** FIB Auriga Zeiss, resolution 1.9 nm at 1 kV
- **Scanning electron microscope** Hitachi S-4800, resolution 2 nm at 1 kV
- **Stylus profilometer** KLA-Tencor Alpha-Step 500
- **Thermostat** Fisherbrand FBH 604
- **UV/Vis/NIR spectrophotometer** PerkinElmer LAMBDA 950
- **X-ray fluorescence spectrometer** EDAX Orbis Micro XRF Analyzer

3.1.2 Reagents

Following chemicals were used:

- **2-Methoxycarbonylethyl-2-oxazoline (FOxa)**: $M = 157.11$ g/mol
self-synthesized, purified three times by vacuum assisted distillation using calcium hydride as a drying agent

- **2-Methyl-2-oxazoline (MeOxa)**: $M = 85.11$ g/mol
self-synthesized, purified three times in a reflux condenser using calcium hydride as a drying agent and distilled afterwards
- **3-Aminopropyltriethoxysilan ($C_9H_{23}NO_3Si$)** $M = 221.37$ g/mol
Evonik Industries
- **Acetone (CH_3COCH_3)**: $M = 58$ g/mol
VWR Chemicals, purity: 99.8 %, used as received
- **Acetonitril (CH_3CN)**: $M = 41.05$ g/mol
Aldrich, purity: 99 %, used as received
- **Ammonium persulfate (APS)**: $M = 228.2$ g/mol
Merck, purity: 98 %, used as received
- **Bacterial viability kit for microscopy** Molecular Probes LIVE/DEAD[®] BacLight[™]
- **Calcium hydride (CaH_2)**: $M = 42.09$ g/mol
Aldrich, purity: 98 %, used as received
- **Chloroform ($CHCl_3$)**: $M = 119.37$ g/mol
Merck, purity: 99.9 %, used as received
- **Chloromethylstyrene (CMS)**: mixture of *meta* (70 mol%) and *para* (30 mol%) isomers, $M = 152.62$ g/mol
Aldrich, purity: 97 %, purified twice by vacuum assisted distillation
- **Diethyl ether**: $M = 74.12$ g/mol
Aldrich, purity: 99 %, used as received
- **Distilled water**
- **Heptane**: $M = 100.21$ g/mol
Merck, purity: 99 %, used as received
- **Hydrochloric acid (HCl)**: $M = 36,46$ g/mol
VWR Chemicals, concentration: 37 ± 2 %
- **Hydroquinone**: $M = 110.11$ g/mol
Aldrich, purity: 99 %, used as received
- **Macromonomers (MM)**: hydrolysed random copolymers of 2-methoxycarbonylethyl-2-oxazoline ($M = 143.10$ g/mol (hydrolysed)) and 2-methyl-2-oxazoline ($M = 85.11$ g/mol):
MM1 ($M = 1961.6$ g/mol) with 11 mol% of 2-methoxycarbonylethyl-2-oxazoline and
MM2 ($M = 2100.8$ g/mol) with 23 mol% accordingly, self-synthesized
- **Methanol (CH_3OH)**: $M = 32.04$ g/mol
Merck, purity: 85 %, used as received
- **N,N'-methylenebisacrylamide (MBA)**: $M = 154.17$ g/mol
Merck, purity: 98 %, used as received
- **N,N,N',N'-tetramethylenediamine (TEMED)**: $M = 116.2$ g/mol
Aldrich, purity: 99 %, used as received

- **N-Isopropylacrylamide (NIPAM):** $M = 113.16$ g/mol
Aldrich, purity: 97 %, purified twice by recrystallizing in ethanol
- **Nitrogen (gas)**
purity: 99.999 %
- **Potassium hydroxide (KOH):** $M = 56.11$ g/mol
Merck, purity: 85 %, used as received
- **Silver nitrate (AgNO_3):** $M = 169.87$ g/mol
Merck, purity: 99 %, used as received
- **Sodium borohydride (NaBH_4):** $M = 37.83$ g/mol
Merck, purity: 96 %, used as received
- **Sodium hydroxide (NaOH):** $M = 39.997$ g/mol
Merck, purity: 99 %, used as received
- **Sodium iodide (NaI):** $M = 149.89$ g/mol
Aldrich, purity: 99.999 %, used as received
- **Tryptic Soy Broth**
Aldrich

3.2 Preparation methods

3.2.1 Macromonomer synthesis

The macromonomer was obtained via cationic ring-opening polymerization of 2-methyl-2-oxazoline (MeOxa) and 2-methoxycarbonylethyl-2-oxazoline (FOxa) in acetonitrile at 75 °C [4]. Chloromethylstyrene was used as an initiator and sodium iodide as a catalyst [4].

Before synthesis all chemicals were purified accurately to avoid any remainders of water. MeOxa was purified three times via dehydration with calcium hydride (CaH_2) in reflux condenser and subsequent distillation (see Figure A.2). FOxa and chloromethylstyrene (CMS) were purified three times by vacuum assisted distillation using CaH_2 as drying agent (see Figure A.1). The last distillation of CMS was just before the synthesis. To avoid a polymerization of CMS during the distillations, a small amount of hydroquinone as an inhibitor was added.

The typical procedure of the macromonomer synthesis was as follows: 1,48 g (9,87 mmol) sodium iodide (NaI) were filled under nitrogen atmosphere in a dry reactor. The reactor was closed and vacuum was applied for 30 minutes. 26 mL acetonitrile, 7,06 mL (83,5 mmol) MeOxa, 2,85 mL (20,87 mmol) FOxa and at the very end 0,7 mL (4,97 mmol) CMS were added. The mixture was stirred 7 hours at 75 °C to obtain a high polymerization yield. 3,258 g KOH were dissolved in 20 mL methanol. 2 mL of this solution (about 4,97 mmol KOH) were added after 7 hours long polymerization to terminate it. The obtained macromonomer was purified by dissolving in chloroform and precipitation in ether and heptane. Afterwards it

was dried under vacuum for 30 minutes. 5 g of macromonomer (MM) were added to 146 mL 0.1 N NaOH and heated 7 hours at 45 °C to hydrolyze side chain ester groups.

It should be considered that the macromonomer described here served only didactic purposes and was not used for hydrogel syntheses in the present work by reasons of time. However, the up front produced macromonomers MM1 and MM2, which were used here, were synthesized in the same way.

3.2.2 Synthesis of hydrogels

To obtain a higher grade of purity, NiPAAm was purified twice by recrystallizing in ethanol (see Figure A.3).

All in all six hydrogels were synthesized. The synthesis process was equal for all hydrogels produced in this work and is described below using the example of hydrogel (HG) S1. The amounts and ratios of monomers, however, differed from hydrogel to hydrogel and can be found in Table 3.1.

For the synthesis of HG S1 0,5 g of NiPAAm, 0,2 g of MM2, 0,034 g of MBA and 0,03 g of TEMED were dissolved in 5 mL of distilled water in a beaker glass. In an other beaker glass 0,02 g of APS were dissolved in 2 mL of distilled water. Both solutions were stirred 5 minutes under a dried nitrogen atmosphere and thereon cooled 7 minutes in a water and ice bath at 4 °C. Afterwards the solutions were mixed and rapidly poured in a cooled reaction vessel via syringe. The reaction vessel was composed of 2 glass slides separated by a 2 mm rubber insertion and clipped together (see Figure A.5). The reaction vessel was stored in a refrigerator at 8 °C for 24 h in order to complete the free-radical crosslinking polymerization. After opening the vessel, the HG was washed with distilled water for three days to eliminate any un-reacted chemicals. The water was changed twice a day.

Under equal reaction conditions, by varying the MM (MM1 and MM2 with a different number of carboxylic acid groups: 11 mol% in MM1, 23 mol% in MM2), MM/NiPAAm amount ratio (0 %, 2 % and 4 %) and MBA/NiPAAm amount ratio (2,5 %, 5 % or 10 %) hydrogels with different structures and properties were produced. The experimental details and results are summarized in Tables 3.1 and 4.1.

3.2.3 Synthesis of silver nanoparticles in hydrogels

For the purpose of comparison the procedure was carried out as in [16]. For preparation of Ag-NPs completely swollen hydrogels (ca. 70 % of total yield) were plunged in a 5 mM AgNO₃ solution for 1 day to generate loaded silver ions in a hydrogel network. The mass of AgNO₃ and the volume of the solution were calculated to represent the amount ratio of AgNO₃ to carboxylic acid groups about 2:1 (see Table 4.2).

Afterwards the carefully washed pieces of hydrogel were added in a 50 mM NaBH₄ solution. The amount ratio of NaBH₄ to AgNO₃ was about 4:1 (see Table 4.2).

Table 3.1: Chemicals used for synthesis of hydrogels S0-S5

	S0	S1	S2	S3	S4	S5	
NiPAAm ^a	0.5006	0.4999	0.5008	0.5008	0.5013	0.4989	g
	4.43	4.42	4.43	4.43	4.44	4.41	mmol
MM1 ^b	-	-	-	0.0358	0.3583	0.4041	g
	-	-	-	0.18	0.18	0.21	mmol
MM2 ^b	-	0.1952	0.3410	-	-	-	g
	-	0.09	0.16	-	-	-	mmol
MBA ^c	0.0347	0.0340	0.0343	0.0348	0.0706	0.0177	g
	0.23	0.22	0.22	0.23	0.46	0.11	mmol
APS ^d	0.0197	0.0200	0.0201	0.0203	0.0206	0.0206	g
	0.09	0.09	0.09	0.09	0.09	0.09	mmol
TEMED ^e	0.0336	0.0332	0.0370	0.0294	0.0301	0.0309	g
	0.29	0.29	0.32	0.25	0.26	0.27	mmol

Note:

a) NiPAAm: N-isopropylacrylamide

b) MM: Macromonomer: hydrolysed random copolymer of 2-methoxycarbonylethyl- and 2-methyl-2-oxazoline (20 monomer units), MM1 with 11 mol% (of 20 units) of (hydrolysed) 2-methoxycarbonylethyl-oxazoline (used for S3 and S4) and MM2 with 23 mol% accordingly (used for S1 and S2), mol%-values derive from NMR analysis

c) MBA: N,N'-methylenebisacrylamide

d) APS: Ammonium persulfate

e) TEMED: N,N,N',N'-tetramethylethylenediamine

Immediately after contact the colour of hydrogels changed from transparent to brown (see Figures A.6, A.7 and A.8). The intensity of brown colour increased with the amount ratio of acid groups in the macromonomer (AiMM) to NiPAAm (see Figure A.9). To guarantee complete reduction, the hydrogels were stored in NaBH₄ solution for 1 day and washed afterwards in distilled water for 3 days. The water was changed twice a day.

3.2.4 Coating of glass substrates

Photostructurable glass substrates (FS21) at different states of treatment (see Table 3.2) were firstly cleaned in 1 M NaOH and 1 vol% hydrochloric acid (HCl) for 1 minute each. Afterwards they were cleaned in deionized water and dried.

Dry substrates were placed in a Petri dish filled with 20 mL of a solution of acetone and 3-aminopropyltriethoxysilane (5 vol%) for 30 minutes to provide a better adhesion of hydrogels on glass surfaces.

Table 3.2: Photostructurable glass FS21 at different states of treatment

	Exposure ^a	Tempering ^b	Etching ^c
A	-	+	-
B	-	+	+
C	+	+	-
D	+	+	+

Parameters:

a) Exposure: illumination $\epsilon = 60 \text{ J/cm}^2$

b) Tempering: time $t = 1 \text{ h}$, temperature $T = 570 \text{ }^\circ\text{C}$

c) Etching: time $t = 5 \text{ min}$, concentration $c(\text{HF}) = 10 \text{ vol\%}$

After this the glasses were cleaned with acetone, dried and placed in a furnace for 1 hour at $100 \text{ }^\circ\text{C}$. Before coating the silanized glass substrates were cooled down to room temperature.

Different coating techniques were used to get hydrogel layers on glass surfaces:

For dip coating four square glass plates of ca. 1 cm^2 (one of every type) were attached to a plastic card using double-faced adhesive tape, which was dipped into a plastic beaker with the hydrogel solution. The beaker itself was placed in a vessel filled with ice to slow up the gelation of the hydrogel solution. To produce the hydrogel solution for dip coating 3.5006 g of NiPAAm, 0.2496 g of MBA and 0.2667 g of TEMED were solved in 35 mL water (H_2O) in one beaker glass and 0.1394 g of APS in 15 mL H_2O in an other beaker glass. Both solutions were stirred with nitrogen for 5 minutes and cooled in an ice bath before mixing together. Then the solutions were filled in a plastic beaker and the substrates were dipped into the solution. The dip coating programm lasted ca. 30 seconds, in which the samples were immersed with a velocity of 5 mm/s into the hydrogel solution, remained there for ca. 10 second and were finally withdrawn and dried at air.

For spin coating process 1.0044 g of NiPAAm, 0.0708 g of MBA and 0.0746 g of TEMED were solved in 10 mL H_2O in one beaker glass and 0.0413 g of APS in 4 mL H_2O in an other beaker glass. Both solutions were stirred with nitrogen and cooled afterwards as described before. For coating of every single square glass plate of ca. 1 cm^2 , which was attached to the rotary disc of the spin coater using double-faced adhesive tape, 3.5 mL of the solution from the first beaker glass (with NiPAAm, MBA, TEMED and H_2O) were mixed with 1 mL of the solution from the second beaker glass (with APS and H_2O) in a third beaker glass (new one for every sample). Then this mixture was put on the rotating glass plate in the spin coater via a disposable pipette. After the sample dried at air, it could be removed from the coater. The process was repeated for every of the four samples.

To get thicker layers a third method was applied: a frame of a 2 mm thick foamed rubber was adhered to every sample and filled with some drops of the mixed hydrogel solution from

the dip coating process. In order to get dried the form remained at room temperature and air for one day.

3.3 Characterization of bulk hydrogels

3.3.1 Nuclear magnetic resonance spectroscopy

For nuclear magnetic resonance spectroscopy (NMR) analysis of macromonomers a small amount (some mg) was solved in CD₃OD and filled in a NMR tube up to 4-5 cm. NMR tubes are uniformly thick borosilicate glass tubes, in the present work tubes with a 5 mm tube outer diameter were used. A ¹H NMR spectrum was recorded to analyse the structure. Due to insolubility of hydrogels, small amounts of dry HG samples were swollen with D₂O and analysed by means of ¹H HRMAS NMR.

3.3.2 Measurement of water absorption

To calculate the water absorption a part of completely swollen hydrogel was weighed and stored in a drying chamber at 35 °C for 1 day or more to get a completely dried hydrogel. Completely dried is defined as no weight decrease in a certain period of time, e.g. 30 minutes. Difference between swollen and dried hydrogel is ascribed to the absorbed water. Divided by the initial (dried) weight of hydrogel, water absorption in g per 1 g hydrogel can be calculated as described below:

$$Abs_{H_2O}(HG) = \frac{m_{sHG,p} - m_{dHG,p}}{m_{dHG,p}} \quad (3.1)$$

with

$Abs_{H_2O}(HG)$ = Water absorption of a hydrogel

$m_{sHG,p}$ = Mass of a swollen piece of hydrogel

$m_{dHG,p}$ = Mass of a dried piece of hydrogel

3.3.3 Determination of reaction yield

The mass of completely swollen hydrogel was determined. The total mass of dried hydrogel was calculated by means of dry to swollen HG ratio. To describe the reaction yield, the mass

of dried hydrogel and the sum of educts (NiPAAm, MM, MBA, TEMED and APS) were compared:

$$RY = \frac{\sum m(\text{product})}{\sum m(\text{educts})} = \frac{m_{dHG,t}}{\sum m(\text{educts})} \quad m_{dHG,t} = \frac{m_{dHG,p}}{m_{sHG,p}} \cdot m_{sHG,t} \quad (3.2)$$

with

RY = Reaction yield

$\sum m(\text{product})$ = Sum of product: total mass of dried hydrogel

$\sum m(\text{educts})$ = Sum of educts: sum of NiPAAm, MM, MBA, TEMED and APS

$m_{dHG,t}$ = Total mass of dried hydrogel

$m_{dHG,p}$ = Mass of a dried piece of hydrogel

$m_{sHG,p}$ = Mass of a swollen piece hydrogel

$m_{sHG,t}$ = Total mass of swollen hydrogel

3.3.4 Measurement of transition temperature

The weight of a piece of swollen hydrogel stored in water was measured every 40 minutes at different water temperatures between 20°C and 65°C. Thus, the contraction of hydrogel at different temperatures was evaluated in comparison to hydrogel weight at initial temperature, which was about 21°C. The transition temperature (T_{tr}) was determined from the recorded graph.

3.3.5 UV/Vis spectroscopy

In order to verify the generation of silver nanoparticles, UV/Vis spectrometry was used. Mortar and pestle were used to mill the dry hydrogels. Dry and powdered hydrogels were dispersed in distilled water (1 mg HG in 1 mL H₂O). The obtained suspension was filled in a measuring cuvette of 1 cm thickness. UV/Vis spectra of silver containing HGs and HGs without silver were recorded from 250 nm to 700 nm with 1 nm resolution by LAMBDA 950 UV/Vis/NIR spectrophotometer (PerkinElmer) at room temperature (about 21°C).

3.3.6 Fourier transform infrared spectroscopy

In order to analyze the hydrogel structure and the effect of silver nanoparticles on it, FTIR was used. Dry and powdered hydrogel was mixed with dry potassium bromide (KBr) powder and squelched intensively. This mixture was pressed in a steel cylinder under vacuum and high mechanical pressure to form a tablet. At this pressure, the KBr deforms plastically due to cold creep and forms transparent "compacts" which are placed in the beam path. FTIR

spectra of silver containing HGs and HGs without silver were recorded from 4000 cm^{-1} to 450 cm^{-1} .

3.3.7 Scanning electron microscope imaging

Silver nanoparticles inside the hydrogel matrix could be observed using scanning electron microscope. Firstly, hydrogels were powdered using mortar and pestle and added to some milliliters of distilled water. 1-2 drops of this suspension were put on a silicon wafer slice and dried at room temperature. Afterwards the slices were sputtered with wolfram to build a thin conductive film in order to guarantee undisturbed imaging without charge effects. Hydrogel covered glasses were sputtered without any previous modification with platinum. Pure hydrogel samples were analysed via scanning electron microscope FIB Auriga Zeiss (50000-fold magnification, acceleration voltage 5 V, working distance 5 mm).

3.3.8 X-ray fluorescence spectroscopy

The X-ray fluorescence analysis was realized as follows: small pieces of dried hydrogel of every type (S0-S5 with silver nanoparticles inside) were fixed on an acrylic glass plate and put inside the analyzer, where vacuum was applied. The reference sample S0 without silver nanoparticles inside, which was only available in its powder form, was placed between two thin polymer films clamped between a specific sample holder. X-ray fluorescence spectra of every single sample were recorded using a 1 mm diameter aperture (voltage $U = 45\text{ kV}$, current $I = 500\text{ }\mu\text{A}$) in the first run and a 30 μm diameter polycapillary (voltage $U = 45\text{ kV}$, current $I = 100\text{ }\mu\text{A}$) in the second run at a different test point. Then the hydrogels were compared among each other using the intensity of the silver peak, which is (under equal conditions) proportional to the silver content inside the hydrogel.

3.3.9 Examination of antibacterial activity towards *Staphylococcus aureus*

The antibacterial activity of Ag-NPs in hydrogel network was determined quantitatively by bacterial count tests. Therefore hydrogels S0-S5 containing silver nanoparticles were analysed. S0 without silver nanoparticles was used as a reference.

The incubation was executed in a 24-well-plate, where three wells were filled with one type of hydrogel (see Figure A.12). In every well 20 mg of powdered hydrogel (milled using mortar and pestle) were added to 400 μL *Staphylococcus aureus* culture (10^4 cells/mL) in Tryptic Soy Broth (TSB), stirred and incubated for 15 hours.

For count tests hydrogel-bacteria mixtures were transferred to micro centrifuge tubes, rinsed with 400 μL of phosphate buffered saline (PSB) each and stirred using a mini vortexer. 0.6 μL of yellow colourant and 0.3 μL of red colourant from LIVE/DEAD[®] BacLight[™] bacterial

viability kit were added to every micro centrifuge tube. Thoma cell counting chamber (with 0.02 mm depth and 0.025 mm² area of the smallest square) was filled on either side and placed under a fluorescence microscope. Alive bacteria which fluoresce green were counted firstly, dead bacteria which fluoresce red afterwards.

The described preparation and tests were repeated twice to generate a reliable average value.

3.4 Characterization of glass substrates

3.4.1 Atomic force microscopy

Atomic force microscopy was used to observe surface differences of photostructurable glass FS21 due to different treatments such as exposure, tempering and etching and to evaluate the quality of hydrogel layers on these surfaces. Atomic force microscope Bruker Dimension edge was operated in PeakForce Tapping[®] mode using ScanAsyst-Air AFM Probes. The scan size was 10 μm x 10 μm, the scan rate 1 Hz.

3.4.2 Profilometry

Profilometric measurements were prepared with KLA Tencor Alpha-Step IQ to evaluate the changes of surface roughness owing to glass treatment processes and the effect of the hydrogel coating. To determine one roughness value pair (R_a and R_z) five measurements were done and the average values were calculated. The measured distance was 800 μm, which was scanned with a velocity of 20 μm/s (10 μm/s for 21C glasses) and a resolution of 0.1 μm.

3.4.3 Scanning electron microscopy

Scanning electron microscope images were taken using Hitachi S-4800 operating at 10 kV. FS21A glass sample (with a hydrogel coating containing silver nanoparticles) was analysed as an example to evaluate the coating quality as well as the particle distribution. To guarantee a charge-free imaging, the glass sample was sputtered with a thin conductive film of platinum.

4 Results and discussion

4.1 Materials syntheses

4.1.1 Macromonomer synthesis

The synthesis of macromonomer was realized in acetonitrile via cationic ring opening polymerization of 2-methyl-2-oxazoline (MeOxa) and 2-methoxycarbonylethyl-2-oxazoline (FOxa) using chloromethylstyrene (CMS) as an initiator and sodium iodide (NaI) as a catalyst [4]. The entire reaction equation is shown in Figure 4.1 [4].

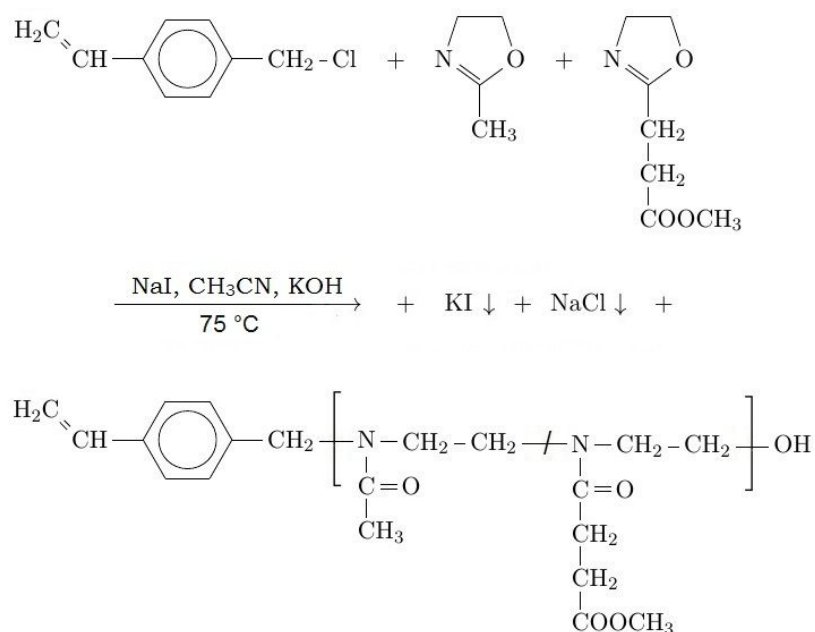


Figure 4.1: Cationic ring opening polymerization of sodium iodide (NaI), 2-methyl-2-oxazoline (MeOxa) and 2-methoxycarbonylethyl-2-oxazoline (FOxa) in acetonitrile initiated by chloromethylstyrene (CMS) and terminated by potassium hydroxide (KOH)

By reason of initiator role of CMS, the obtained macromonomer contains a vinyl group as a starting group on one chain end [105]. At the other chain end it contains a hydroxy group (OH) due to termination with potassium hydroxide (KOH) [105]. The synthesis was carried out 7 hours at 75 °C to avoid the polymerization of CMS double bonds (at this point),

but to implement the polymerization of 2-oxazolines. Such a low temperature and a short reaction time as well as the low concentration of CMS allow controlled conditions for a polymerization reaction and enable a very high reaction yield up to almost 100%. The polymerization reaction was initiated by iodomethylstyrene (IMS), which is a product of CMS and NaI beside sodium chloride (NaCl) (see Figure 4.2) [106].

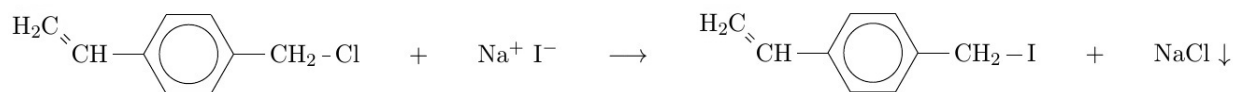


Figure 4.2: Macromonomer synthesis: Initiation 1: Formation of iodomethylstyrene (IMS)

In the second step of the initiation reaction IMS is attacked by nitrogen atom of MeOxa or FOxa monomer at the carbon atom next to iod, that leads to formation of propagation species with iod as a counterion (see Figure 4.3).

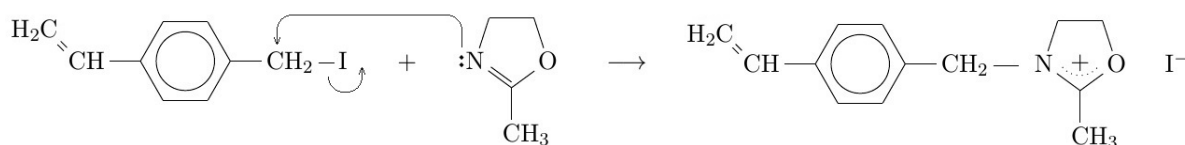


Figure 4.3: Macromonomer synthesis: Initiation 2: Formation of propagating species

In the following propagation phase, the propagation species react with further MeOxa and FOxa monomers and form macromonomer molecules with a defined polymerization degree (see Figures 4.4 and 4.5) [4].

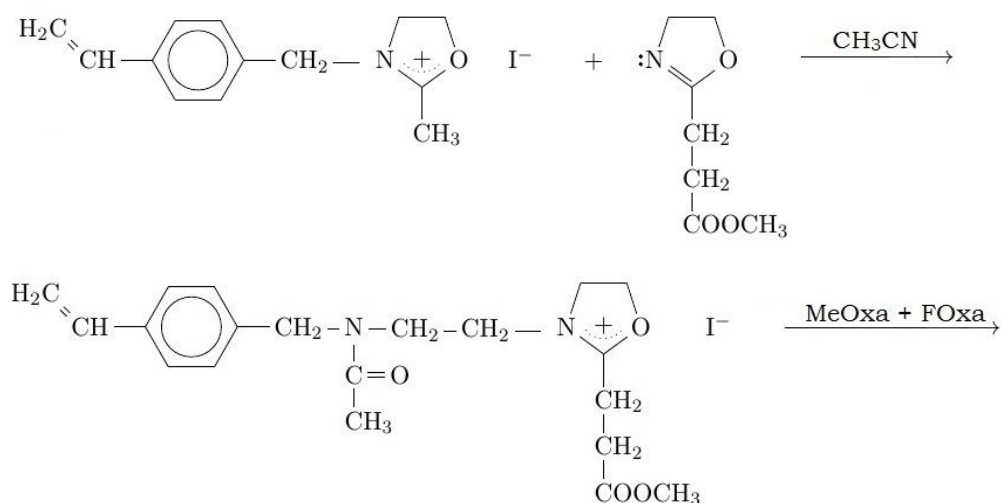


Figure 4.4: Macromonomer synthesis: Propagation reaction: Polymerization of 2-oxazoline monomers (Part 1)

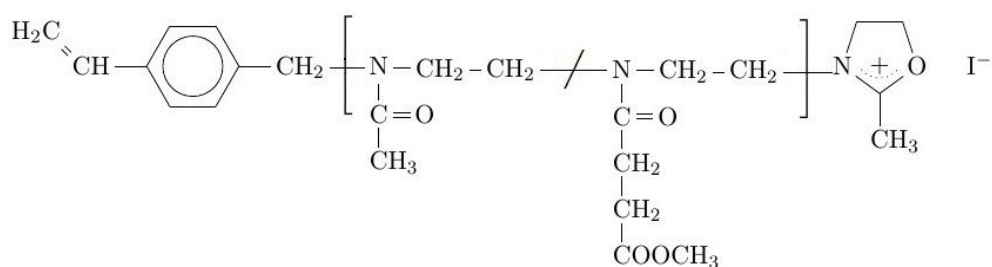


Figure 4.5: Macromonomer synthesis: Propagation reaction: Polymerization of 2-oxazoline monomers (Part 2)

The polymerization is terminated by using KOH/methanol solution (see Figure 4.6). Negative OH groups from KOH in the solution react with positive oxazoline ends and build the new end group of the macromonomer.

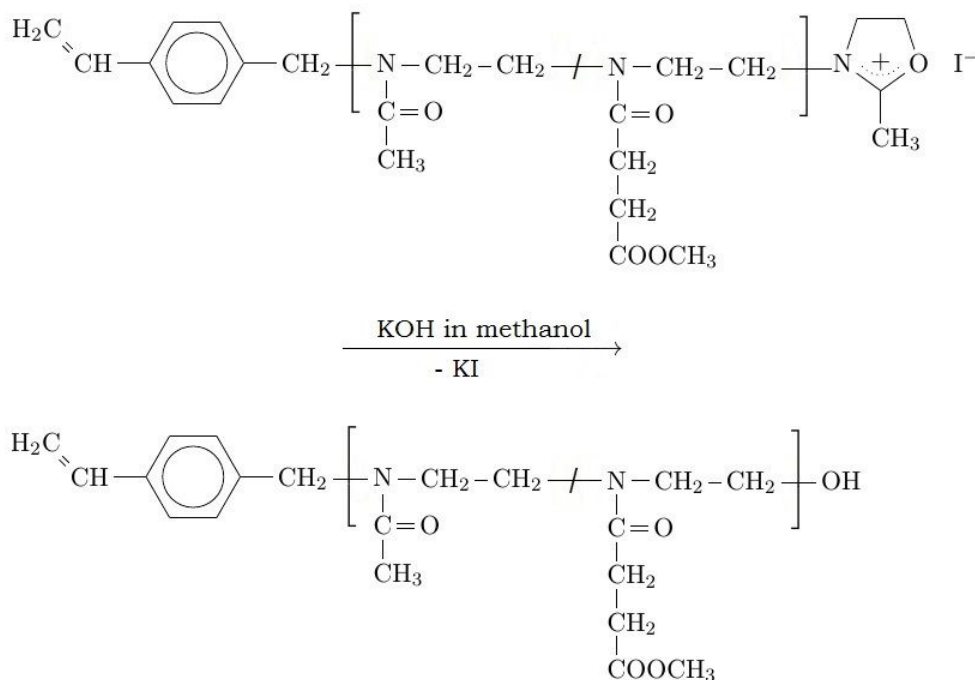


Figure 4.6: Macromonomer synthesis: Termination by KOH/methanol solution under elimination of KI

The obtained macromonomer was purified and characterized using NMR spectroscopy. Recorded spectrum (see Figure 4.8) demonstrate the presence of MeOxa, FOxa and CMS parts in the macromonomer. The signal at approximately 3,65 ppm correspond to the ester group of FOxa. The signals at 4.6-4.7 ppm (CH_2 next to the aromatic ring), 5,3 ppm and 5,8 ppm ($\text{CH}_2=$), 6.7-6.8 ppm ($-\text{CH}=\text{}$) and 7.1-7.5 ppm ($\text{H}_{\text{aromatic}}$) point the existence of CMS in the macromonomer. The signal at 2,1 ppm ($\text{CH}_3\text{C}=\text{O}$) shows the presence of MeOxa.

Using this analysis the degree of polymerization and molar ratio of MeOxa and FOxa can be determined. Comparing the integrals of 2.6-2.8 ppm peak (CH_2CH_2 in FOxa), 2,1 ppm peak ($\text{CH}_3\text{C}=\text{O}$ in MeOxa) and 6.7-6.8 ppm peak ($-\text{CH}=\text{}$ in CMS) the polymerization degree of 22 ± 2 could be calculated, which is close to the desired theoretical degree of polymerization of 21. The content of MeOxa was determined at 78.5 ± 2 mol% and of FOxa at 21.5 ± 2 mol%. Spectra of MM1 and MM2, which were synthesized in advance and used for syntheses of hydrogels below, are presented in Figure 4.9 and 4.10. The content of MeOxa is 89 ± 2 mol% in MM1 and 77 ± 2 mol% in MM2 and of FOxa 11 ± 2 mol% in MM1 and 23 ± 2 mol% in MM2 respectively.

In order to obtain COOH groups in the macromonomer, it was hydrolysed in 0.1 N NaOH (see Figure 4.7).

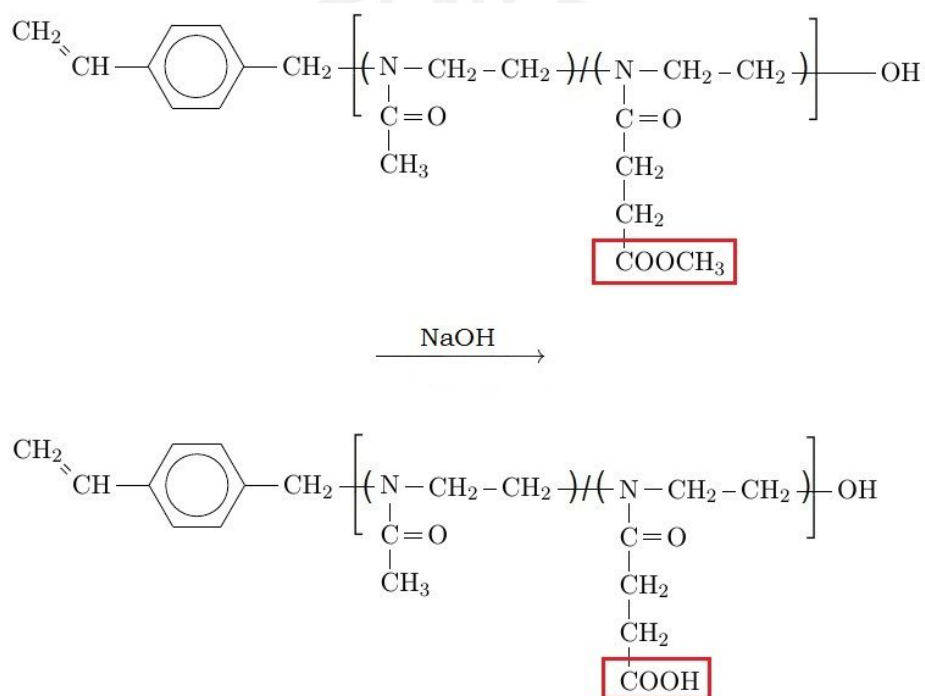


Figure 4.7: Hydrolysis of the macromonomer

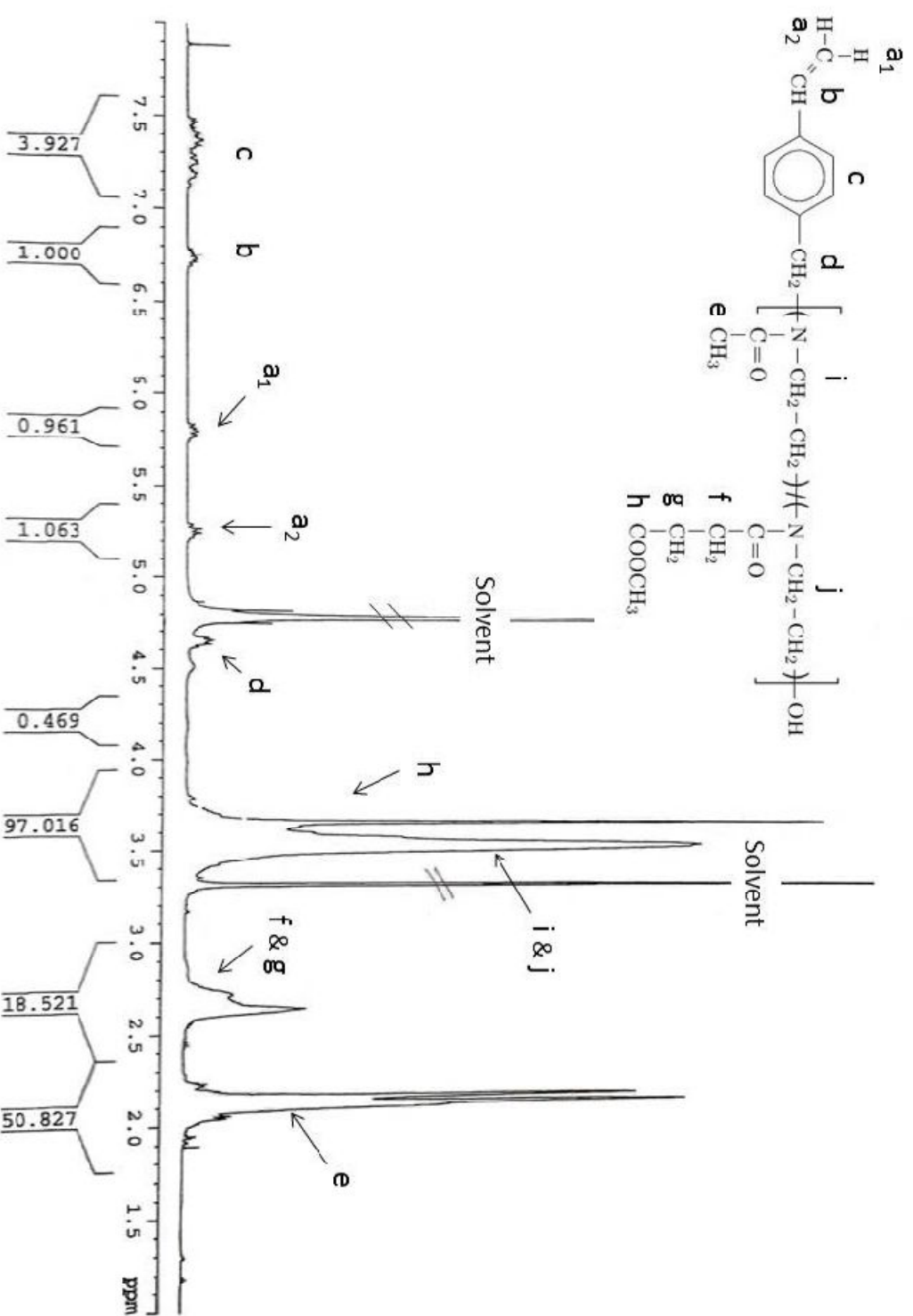


Figure 4.8: $^1\text{H-NMR}$ spectrum of MM synthesized in present work, but not used for further hydrogel formation (dissolved in CD_3OD , measured at $30\text{ }^\circ\text{C}$)

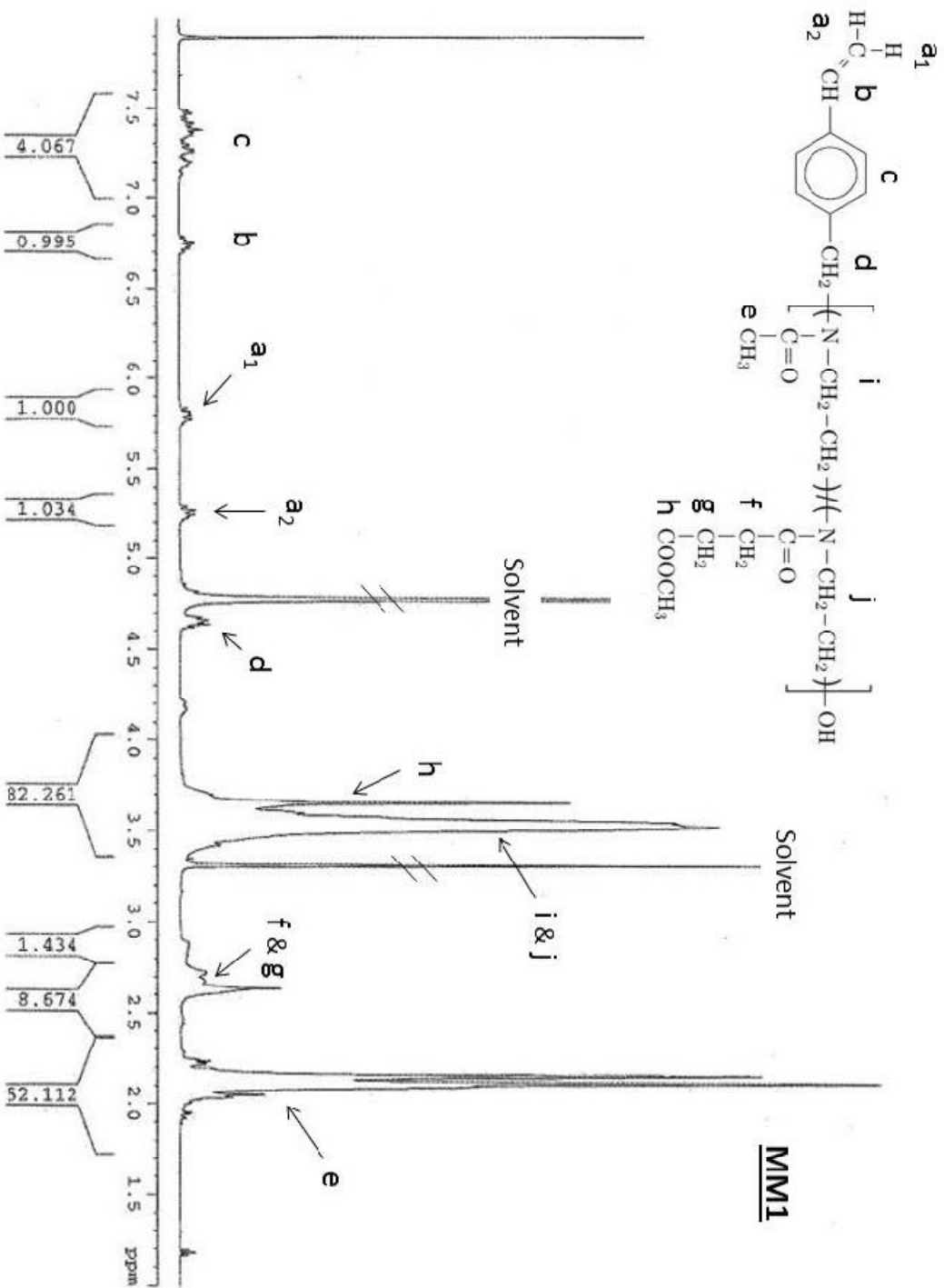


Figure 4.9: ¹H-NMR spectrum of MM1 (dissolved in CD₃OD, measured at 30 °C)

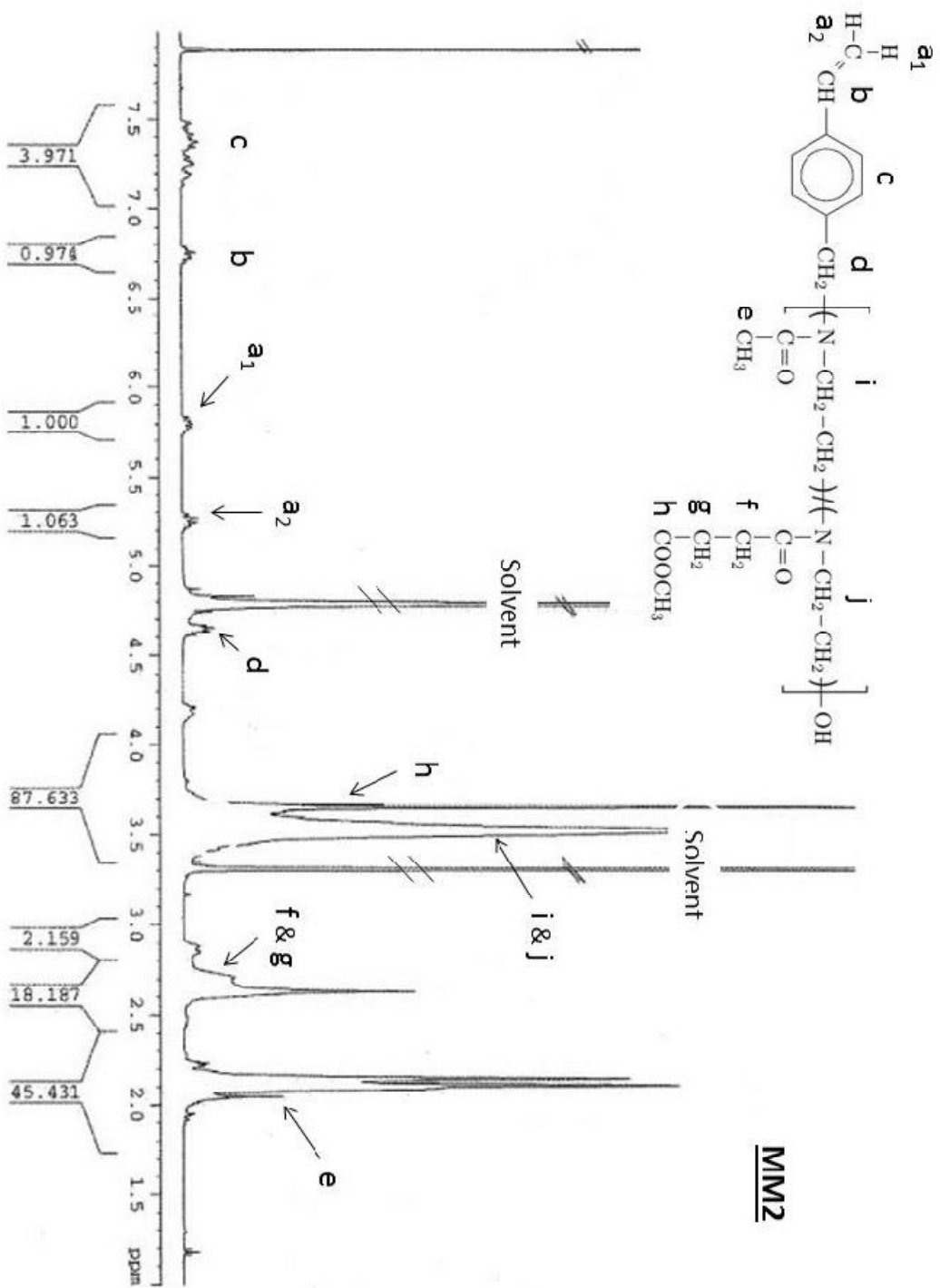
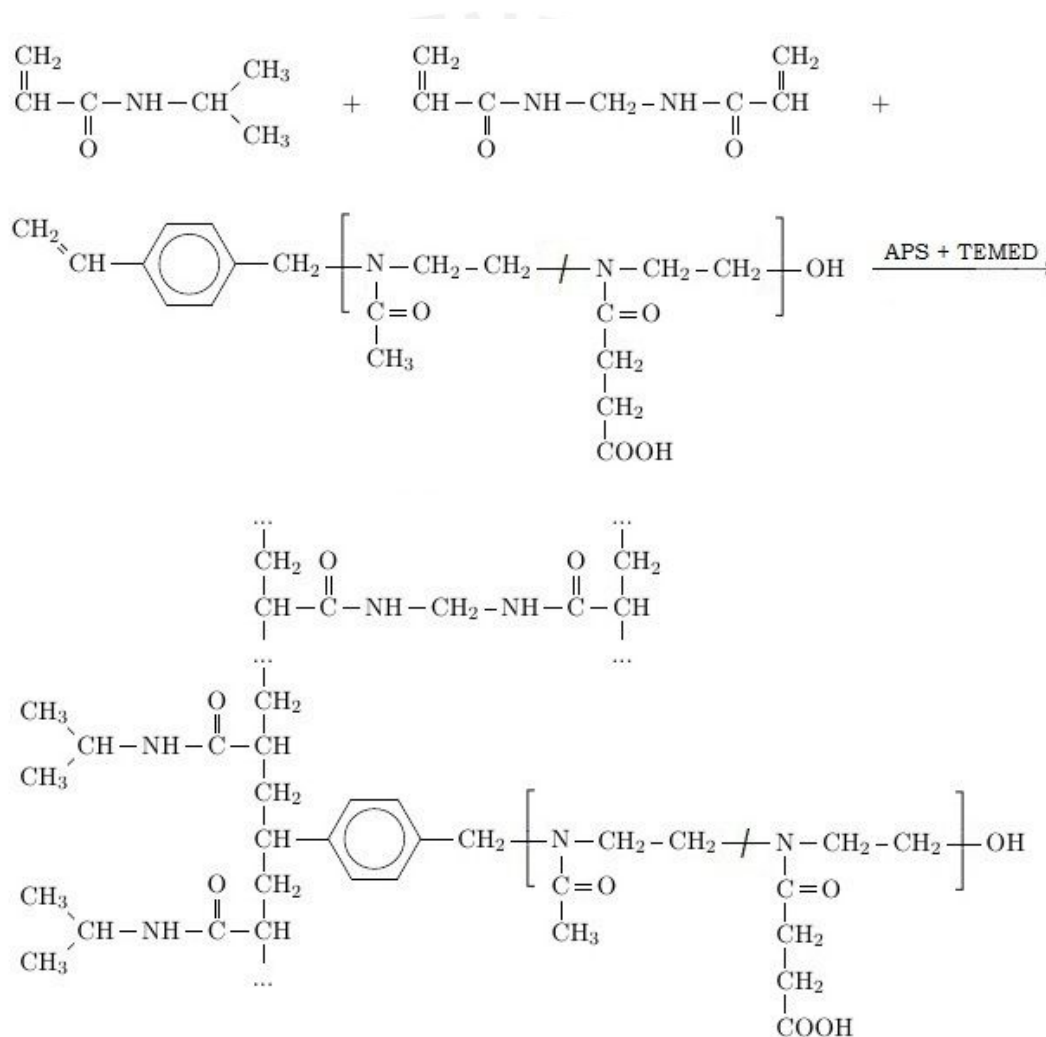


Figure 4.10: ¹H-NMR spectrum of MM2 (dissolved in CD₃OD, measured at 30 °C)

4.1.2 Hydrogel synthesis

The free radical copolymerization of N-isopropylacrylamide (NiPAAm), macromonomer (MM) and N,N'-methylene bisacrylamide (MBA) was initiated by ammonium persulfate (APS) in the presence of N,N,N',N'-tetramethylene diamine (TEMED) as a catalysator. The type of MM (11 mol% or 23 mol% of acid groups in the macromonomer (AiMM)) and its content were varied to determine the effect of MM on several properties of the hydrogels (HG). The reaction was carried out in water at 8°C. The reaction vessel (see Figure A.5) was stored in a refrigerator for 24 hours in order to complete the free-radical crosslinking polymerization, although the gelation already occurred after 10-15 minutes. The detailed reaction is shown in Figure 4.11 [4].



Note: The number of monomer units is 20 for both MMs, but MM1 contains 89 mol% of 2-methyl-2-oxazoline and 11 mol% of 2-methoxycarbonylethyl-2-oxazoline (hydrolyzed) as well as MM2 77 mol% and 23 mol% respectively.

Figure 4.11: Hydrogel synthesis from NiPAAm, MBA and MM

In the initiation phase APS forms in the presence of the catalyst TEMED free radicals. Feng et al. give a proposal for this redox initiation system. Thus, especially four species could act as initiating radicals (see Figure 4.12) [107].

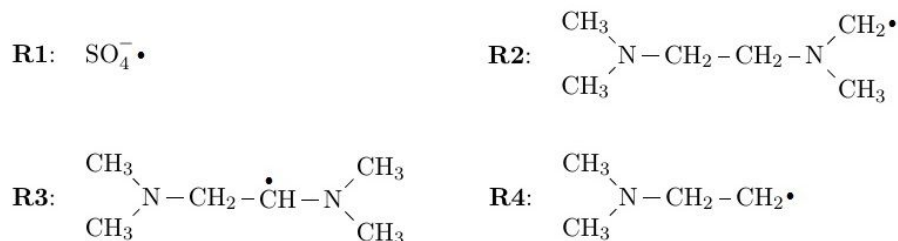


Figure 4.12: Possible radicals from the reaction of APS and TEMED

R1 and R2 are initial radicals. Depending on reaction conditions, R3 and R4 can be formed. At higher concentrations of TEMED a transfer reaction leads to formation of R3. After more than 30 minutes without monomer presence, initial radical R2 decomposes and forms R4 [107].

Free radicals created by APS and TEMED attack molecules with double bonds such as NiPAAm and generate thereby further radicals (see Figure 4.13).

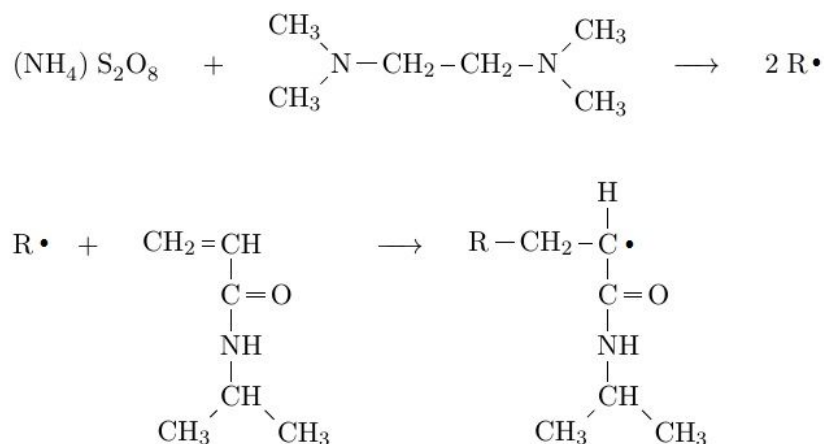


Figure 4.13: Initial reaction for hydrogel synthesis

In the propagation phase MM is also attacked on its double bond and is integrated as a side chain in the NiPAAm main chain (see Figure 4.14).

MBA acts due to its two double bonds as a crosslinking agent and connects two NiPAAm main chains to each other (see Figure 4.15). Therewith a three-dimensional structure can be formed (Gelation).

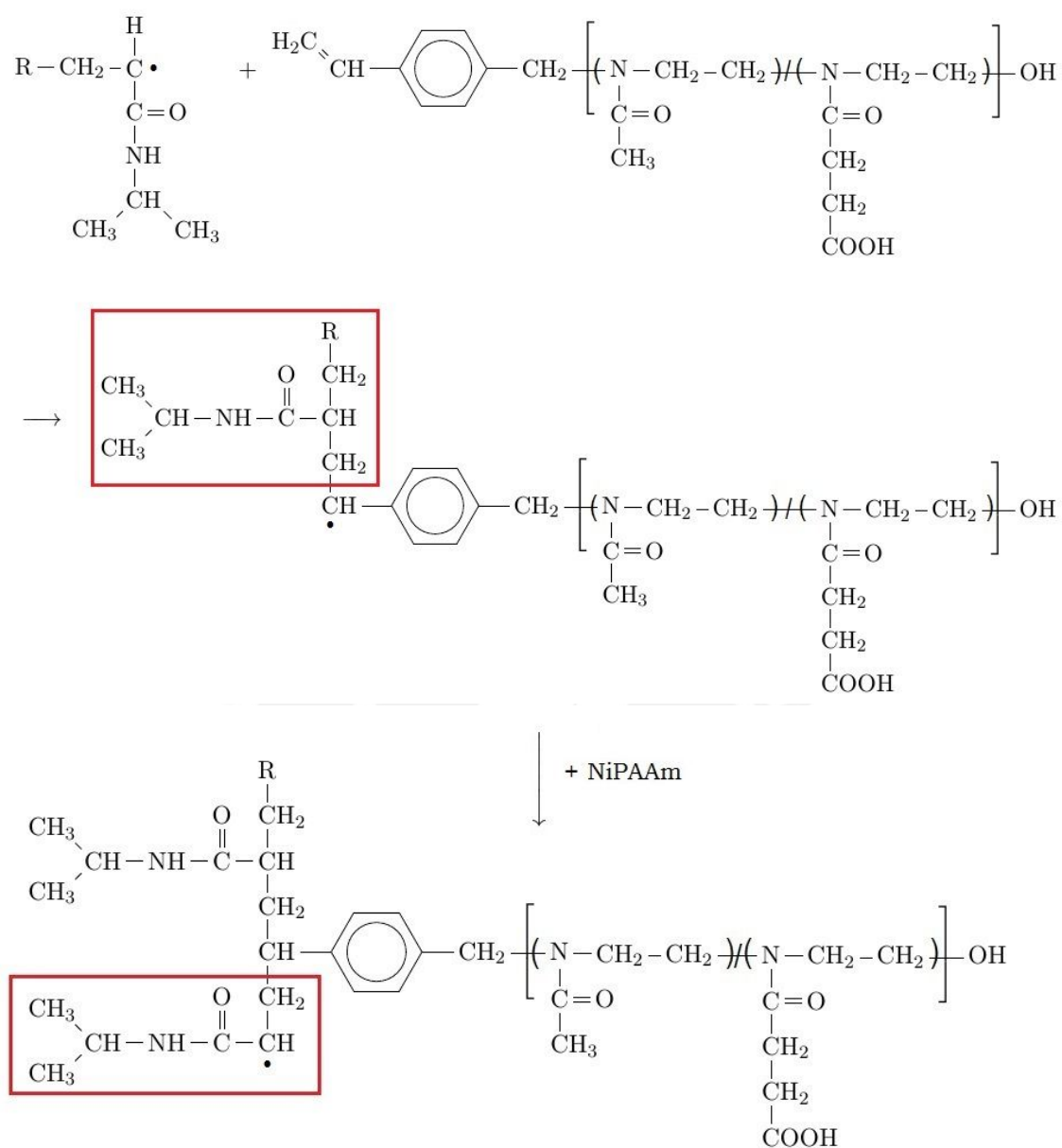


Figure 4.14: Propagation reaction in hydrogel synthesis

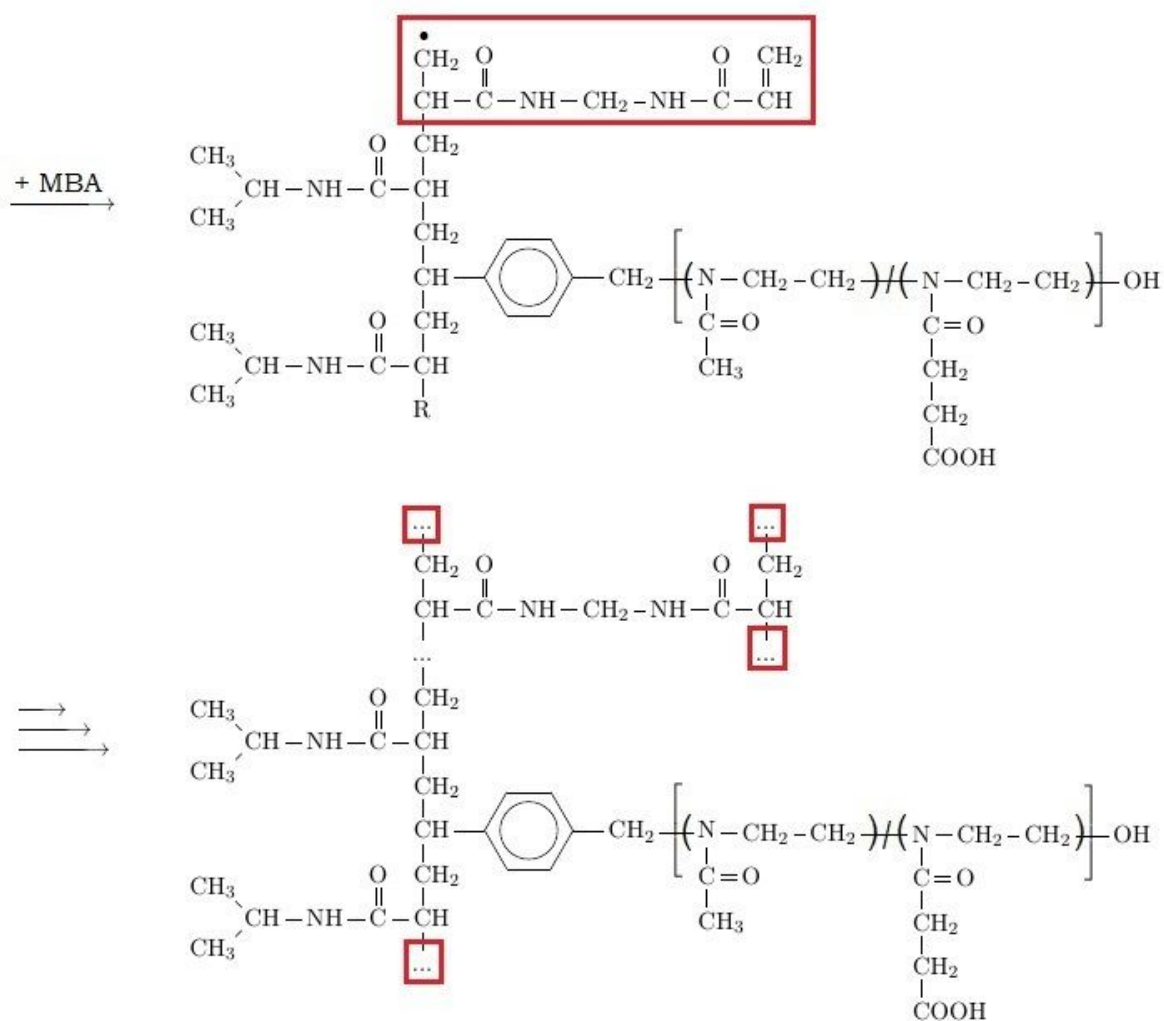


Figure 4.15: Gelation reaction: Formation of a hydrogel

Table 4.1 gives the exact reaction data and the achieved results. Hence reaction yield decreases with increasing content of MM. It means that the macromonomer does not react completely in the used amount ratio or period of time. The reason therefore is a slower mobility and thus the slower polymerization of MM compared to NiPAAm because of its higher molar mass.

All the fabricated hydrogels were washed repeatedly in distilled water and analysed using NMR spectroscopy. Recorded spectra (see Figure 4.17) confirmed the presence of NiPAAm, and MM parts in the hydrogel (see Section 4.2.1).

Table 4.1: Composition and characteristics of hydrogels S0-S5 (without silver nanoparticles)

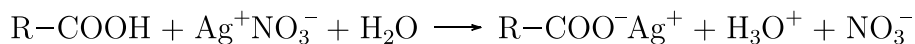
	S0	S1	S2	S3	S4	S5
NiPAAm ^{a)} [mmol]	4.43	4.42	4.43	4.43	4.44	4.41
MM ^{b)} [mmol]	0	0.09	0.16	0.18	0.18	0.21
AiMM ^{c)} [mmol]	0	0.42	0.77	0.40	0.40	0.45
MBA ^{d)} [mmol]	0.23	0.22	0.22	0.23	0.46	0.11
TEMED ^{e)} [mmol]	0.29	0.29	0.32	0.25	0.26	0.27
APS ^{f)} [mmol]	0.09	0.09	0.09	0.09	0.09	0.09
MM/NiPAAm ^{g)} [mol%]	0	2	3.6	4.1	4.1	4.8
AiMM/NiPAAm ^{h)} [mol%]	0	9.5	17.4	9.0	9.0	10.2
MBA/NiPAAm ⁱ⁾ [mol%]	5.2	5.0	5.0	5.2	10.4	2.5
APS/NiPAAm ^{j)} [mol%]	2.0	2.0	2.0	2.0	2.0	2.0
APS/TEMED ^{k)} [mol%]	31	31	28	36	35	33
RY ^{l)} [%]	87	75	72	97	98	87
T _{tr} ^{m)} [°C]	35	46	50	45	45	45
Abs H ₂ O ⁿ⁾ [g H ₂ O/g HG]	9.48	23.66	27.63	17.20	10.78	18.42

Note:

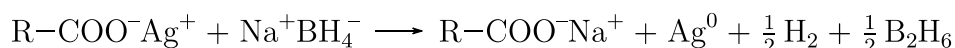
- a) NiPAAm: N-Isopropylacrylamide: 0.5 g were used for every hydrogel
- b) MM: Macromonomer: hydrolysed random copolymer of 2-methoxycarbonylethyl- and 2-methyl-2-oxazoline (20 monomer units), MM1 with 11 mol% (of 20 units) of 2-methoxycarbonylethyl-oxazoline (used for S3,S4 and S5) and MM2 with 23 mol% accordingly (used for S1 and S2), mol%-values derive from NMR analysis
- c) AiMM: Acid groups in macromonomer: calculated values, MM1 (S3, S4 and S5) contains 11 mol% (of 20 units) of acid groups, MM2 (S1 and S2) 23 mol% respectively
- d) MBA: N,N'-Methylenebisacrylamide
- e) TEMED: N,N,N',N'-Tetramethylethylenediamine
- f) APS: Ammonium persulfate
- g) Molar ratio MM/NiPAAm in percent
- h) Molar ratio AiMM/NiPAAm in percent
- i) Molar ratio MBA/NiPAAm in percent
- j) Molar ratio APS/NiPAAm in percent
- k) Molar ratio APS/TEMED in percent
- l) Reaction yield RY = Total mass of obtained dried hydrogel/ sum of masses of educts
- m) Transition temperature T_{tr} was determined by measuring weight difference of swollen hydrogel in water compared to weight at starting temperature (21 °C) at different water temperatures (21 °C - 65 °C)
- n) Water absorption: Abs H₂O = (mass of swollen hydrogel - mass of dry hydrogel)/ mass of dry hydrogel, measured at 25 °C and pH = 5.5

4.1.3 Synthesis of silver nanoparticles in hydrogels

After polymerization reaction hydrogels were washed with distilled water for three days to eliminate any un-reacted chemicals. The water was changed twice a day. Thereon the completely swollen hydrogels were put in silver nitrate solution to generate charged silver ions in a hydrogel network:



After 1 day the pieces of hydrogels were carefully cleaned and added to sodium borohydride solution to reduce silver ions to elemental silver [39]:



The reaction data as well as results are listed in Table 4.2.

The colour of the hydrogel changed immediately after contact with NaBH_4 from transparent to yellowish brown. This is due to the surface plasmon resonance (SPR) of silver nanoparticles. The energy required for SPR corresponds to wavelengths from 400 nm to 500 nm (dependent on the particle size) and is absorbed by the material. The reflected light has the complementary colour, which is yellow or brown. The intensity of brown colour increased with the amount ratio of carboxylic acid groups (AiMM) to NiPAAm. The reason is a higher concentration of electron-rich species like N, O and COOH which promote the reception of silver ions [15]. Due to this hydrogel S0, which does not contain COOH groups, has the lightest colour, as can be seen in Figure 4.16.

The described observations are in concordance with other hydrogel-Ag-NPs systems in the literature [15, 16, 33].

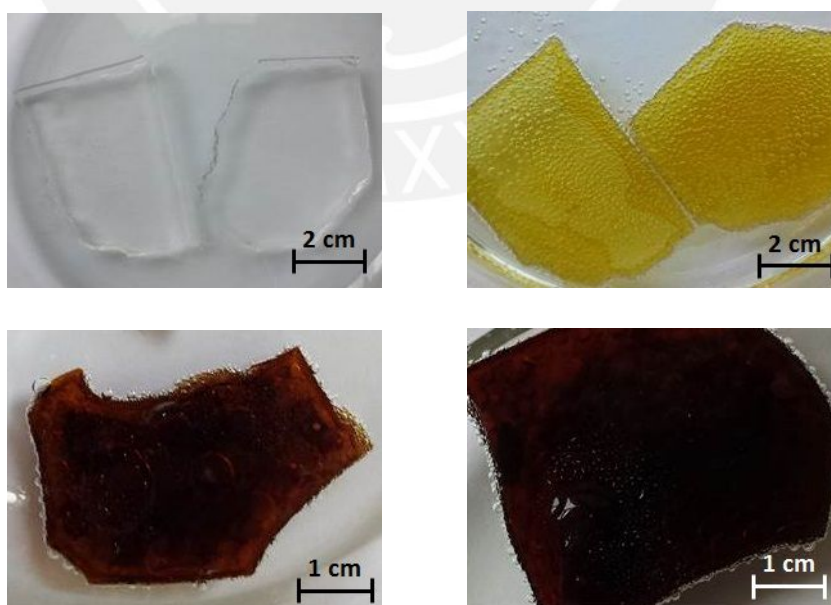


Figure 4.16: Swollen hydrogel S0 without silver nanoparticles as well as hydrogels S0, S1 and S2 containing silver nanoparticles (from left to right)

Table 4.2: Composition and characteristics of hydrogels S0-S5 containing silver nanoparticles

	S0	S1	S2	S3	S4	S5
Mass (dry) ^{a)} [g]	0.193	0.406	0.455	0.676	0.735	0.563
NiPAAm ^{b)} [mmol]	1.45	2.29	2.16	3.17	3.32	2.56
MM ^{c)} [mmol]	0	0.05	0.08	0.13	0.14	0.12
AiMM ^{d)} [mmol]	0	0.22	0.36	0.28	0.30	0.26
MBA ^{e)} [mmol]	0.07	0.11	0.11	0.16	0.34	0.06
AgNO ₃ ^{f)} [mmol]	0.24	0.47	0.78	0.59	0.59	0.52
NaBH ₄ ^{g)} [mmol]	1.05	2.11	3.16	2.37	2.37	2.08
MM/NiPAAm ^{h)} [mol%]	0	2.2	3.7	4.1	4.2	4.7
AiMM/NiPAAm ⁱ⁾ [mol%]	0	9.6	16.7	8.8	9.0	10.2
AgNO ₃ /AiMM ^{j)} [mol%]	-	214	211	211	197	200
NaBH ₄ /AgNO ₃ ^{k)} [mol%]	438	449	416	402	402	400
NaBH ₄ /AiMM ^{l)} [mol%]	-	959	877	846	790	800
λ_{max} ^{m)} [nm]	401	414	411	413	414	409
Abs H ₂ O ⁿ⁾ [g H ₂ O/g HG]	8.85	23.4	26.5	15.39	10.03	18.42

Note:

- a) Mass of dry hydrogel before complexion and reduction, ca. 70 % of total yield
- b) NiPAAm: N-isopropylacrylamide: calculated value is a weight proportion NiPAAm/mass of all educts multiplied by the mass of dry hydrogel.
- c) MM: Macromonomer: hydrolysed random copolymer of 2-methoxycarbonylethyl- and 2-methyl-2-oxazoline (20 monomer units), MM1 with 11 mol% (of 20 units) of 2-methoxycarbonylethyl-oxazoline (used for S3, S4 and S5) and MM2 with 23 mol% accordingly (used for S1 and S2), mol%-values derive from NMR analysis
- d) AiMM: Acid groups in macromonomer: calculated values, MM1 (S3, S4 and S5) contains 11 mol% (of 20 units) of acid groups, MM2 (S1 and S2) 23 mol% respectively
- e) MBA: N,N'-methylene bisacrylamide
- f) AgNO₃: Silver nitrate, concentration: 20 mg/30 mL [40]
- g) NaBH₄: Sodium borohydride, concentration: 1 g/500 mL
- h) Molar ratio MM/NiPAAm in percent
- i) Molar ratio AiMM/NiPAAm in percent
- j) Molar ratio AgNO₃/AiMM in percent
- k) Molar ratio NaBH₄/AgNO₃ in percent
- l) Molar ratio NaBH₄/AiMM in percent
- m) Wavelength λ_{max} marks the characteristic plasmon peak in UV/Vis spectrum
- n) Water absorption Abs H₂O = (mass of swollen hydrogel - mass of dry hydrogel)/ mass of dry hydrogel, measured at 25 °C and pH = 5.5

4.2 Characterization of hydrogels

4.2.1 Nuclear magnetic resonance spectroscopy of hydrogels

The structure of hydrogels was analysed via ^1H HRMAS NMR. Figure 4.17 shows signals referred to NiPAAm and MM: 4.6-4.7 ppm (CH_2 next to the aromatic ring), 1,1 ppm (CHCH_3), 2.0-2.2 ppm (COCH_3), 2.4-2.6 ppm (CH_2COOH and COCH_2), 3.4-3.8 ppm (NCH_2CH_2) and 3.9-4.0 ppm (CH). MBA could not be measured due to a low concentration.

Figure 4.18 shows the region between 3.3 ppm and 4.2 ppm in detail. The graph was normed at the CH-peak of polyNiPAAm to determine the real MM to NiPAAm ratio in produced hydrogels. For the calculation the integrals of NCH_2CH_2 -peak had to be divided by 80, because 80 protons contribute to this signal (20 monomer units \times 4 protons, no difference between MeOxa and FOxa). Table 4.3 summarizes obtained values. The real MM to NiPAAm ratio is lower than the theoretical value in all samples. This is due to the higher molar mass of MM and consequently a slower polymerization, that correlates with values from reaction yield (see Table 4.1).

Furthermore, the effect of silver nanoparticles was examined in hydrogels S0 and S1 (see Figure 4.19). As can be seen, no clear influence can be observed. The peak at 2.96 ppm, which can be seen in S1, but disappears in S1 with silver (Ag), can be interpreted as contamination with succinic acid, which can be formed during the hydrolysis. Such a huge amount remaining even after repeated washing can not be explained, however.

Table 4.3: Theoretical and experimental values for MM to NiPAAm ratios

	S0	S1	S2	S3	S4	S5
NiPAAm [mmol] ^{a)}	4.43	4.42	4.43	4.43	4.44	4.41
MM [mmol] ^{b)}	-	0.09	0.16	0.18	0.18	0.21
MM/NiPAAm theor. [%] ^{c)}	-	2.0	3.6	4.1	4.1	4.8
MM/NiPAAm exp. [%] ^{d)}	-	1.6	2.4	3.1	3.2	3.3

Note:

a) NiPAAm: N-isopropylacrylamide: calculated value is a weight proportion NiPAAm/mass of all educts multiplied by the mass of dry hydrogel.

b) MM: Macromonomer: hydrolysed random copolymer of 2-carboxyethyl- and 2-methyl-2-oxazoline (20 monomer units), MM1 with 11 mol% (of 20 units) of 2-carboxyethyl-oxazoline (used for S3, S4 and S5) and MM2 with 23 mol% accordingly (used for S1 and S2), mol%-values derive from NMR analysis

c) Theoretical molar ratio MM/NiPAAm, calculated from amounts of chemicals used in synthesis

d) Molar ratio MM/NiPAAm, calculated from ^1H HRMAS NMR signal integral, estimated relative error: $\pm 10\%$

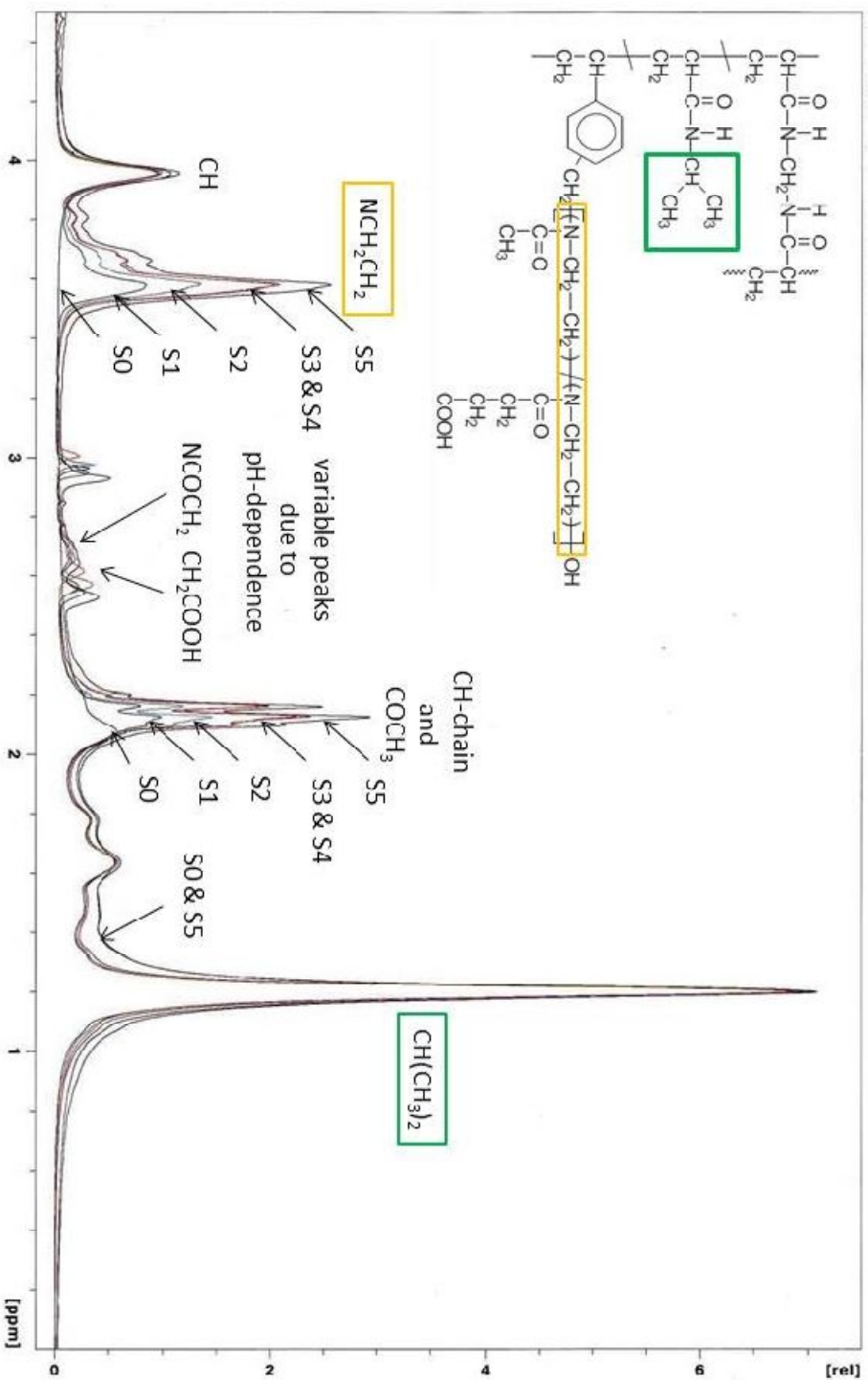


Figure 4.17: ^1H HRMAS NMR spectrum of HG S0-S5 (swollen with D_2O)

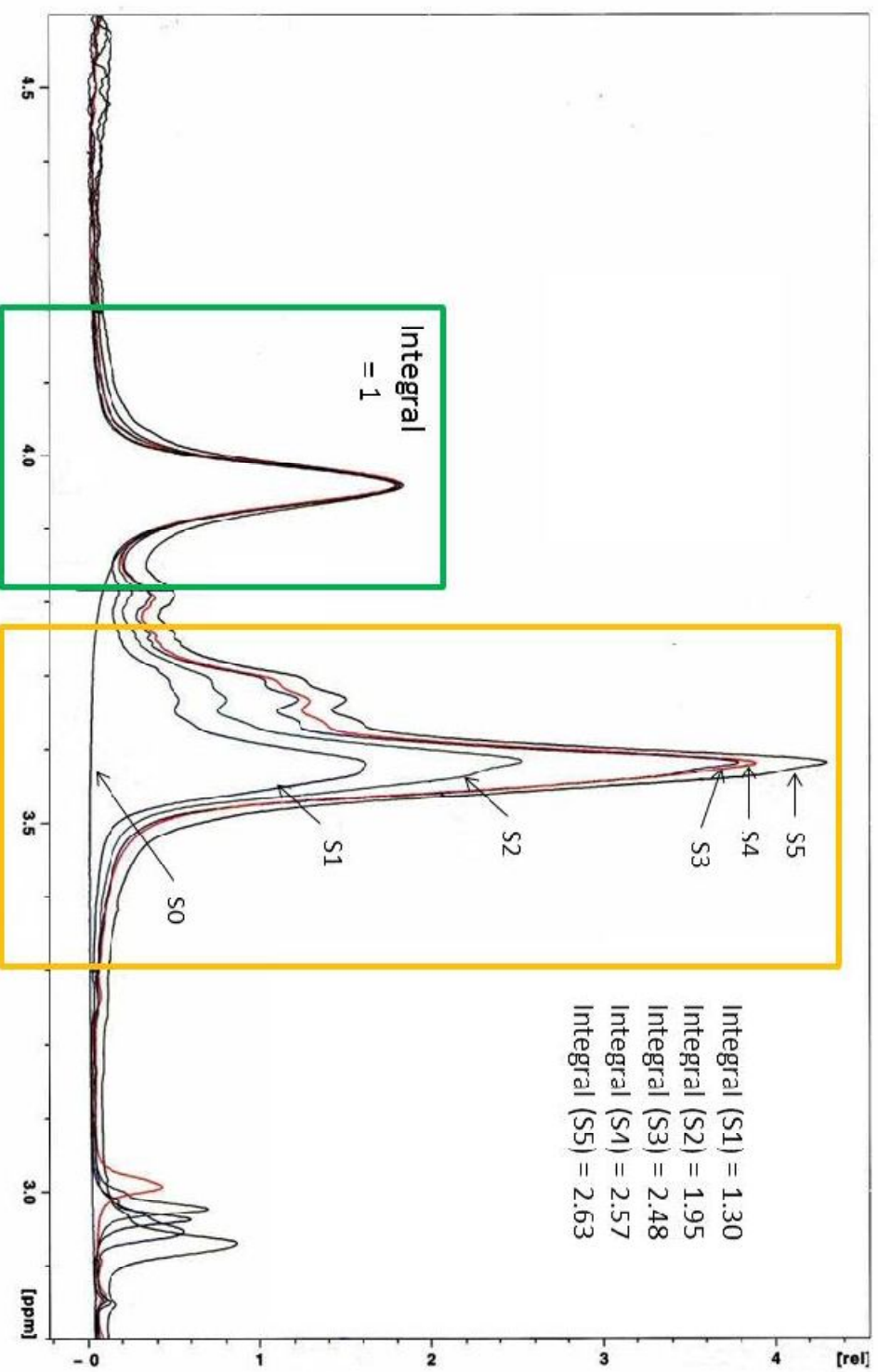


Figure 4.18: Detailed ^1H HRMAS NMR spectrum of hydrogels S0-S5 (swollen with D_2O) with integral values for calculation of the real MM to NiPAAm ratio

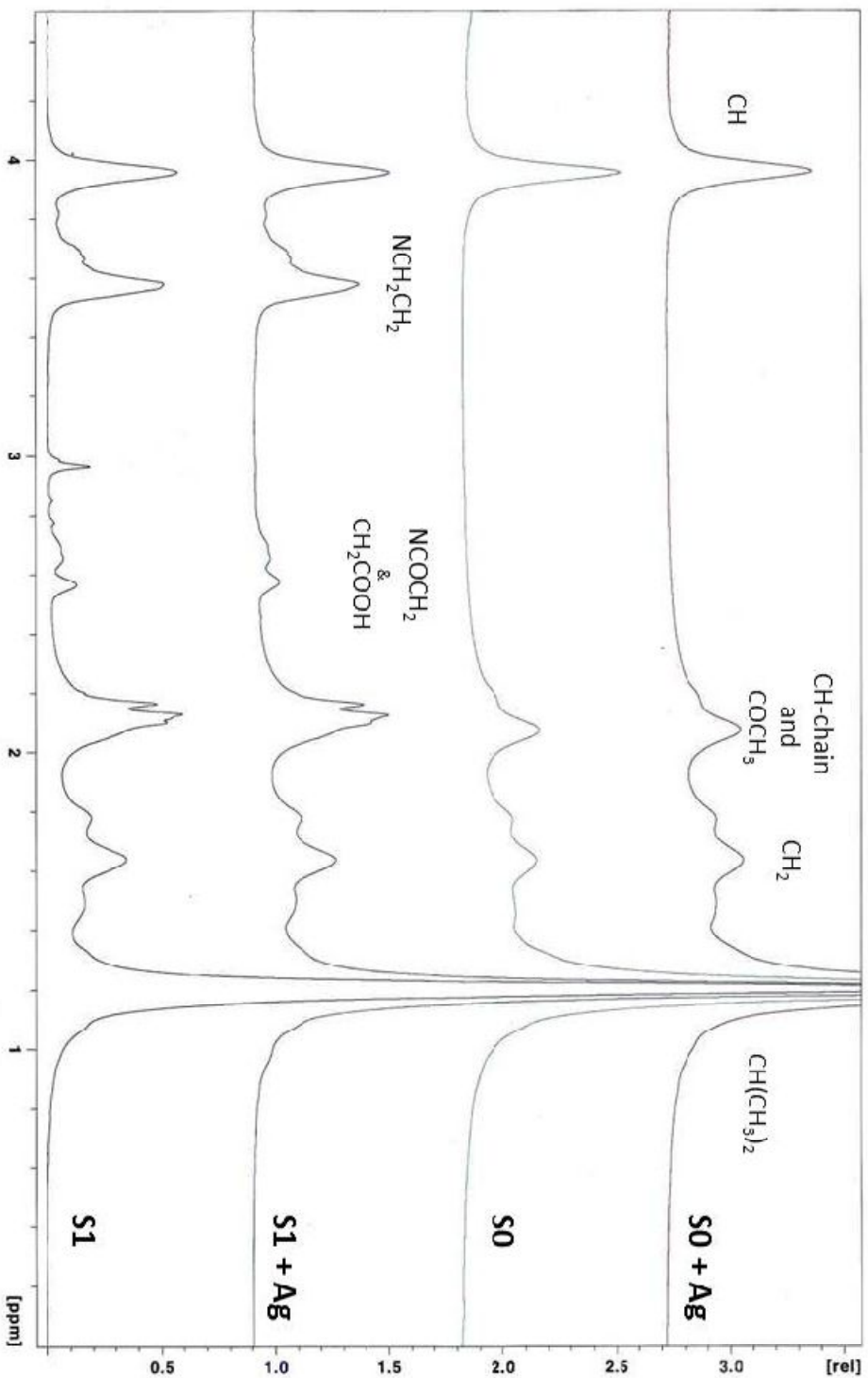


Figure 4.19: ^1H HRMAS NMR spectrum of hydrogels S0 and S1 with and without silver nanoparticles (swollen with D_2O)

4.2.2 Measurement of water absorption

The absorption of water was tested at $\text{pH} = 5.5$. It was determined that water absorption increases with increasing MM content or MM/NiPAAm amount ratio (see Table 4.1 and Table 4.2). This is likely due to higher polarity of MM (caused by carboxylate and carboxylic groups) in comparison to NiPAAm [4].

Moreover, the type of MM is important. HG S1 (with MM2) shows higher water absorption in comparison to HG S3 (with MM1), although the number of acid groups is almost the same. The reason is presumable that S3 contains more MM and consequently more phenol groups that are hydrophobic and decrease water absorption of the hydrogel.

The amount ratio MBA/NiPAAm affects water absorbance considerably. Higher MBA to NiPAAm ratio causes a more crosslinked hydrogel structure with smaller free spaces between molecules that limits the water absorbance [4].

The content of silver nanoparticles does not change the absorption value remarkable. This result is different to the findings of Mohan et al. [16], where incorporation of silver reduced the absorption of water to one-third, but similar to Deen and Chua's results [33], where both values were nearly the same. The reason seems to be in the hydrogel structure: Mohan et al. used NiPAAm, MBA and sodium acrylate as monomers which are all small molecules. As a result they are able to build a hydrogel network with small pores. Disadvantageously the ability to absorb water decreases rapidly when the pores are filled with silver nanoparticles. In present work (as well as in Deen and Chua's work [33]) longer molecules such as MM (or N-acryloyl-N'-ethyl piperazine [33]) were used, which may effectuate bigger pores. Filled with small silver nanoparticles the hydrogels still have enough space for water, so that the absorption value does not change considerable.

Summarized water absorption seems to be driven by following factors:

- **The amount ratio of the crosslinker** The higher the crosslinker concentration the less the absorption due to smaller pores inside the hydrogel.
- **The amount of hydrophilic groups** Polar groups promote water absorption, so the more polar groups in the hydrogel network the higher water absorption.
- **Fillers** Silver particles which fill free spaces inside the hydrogel affect the water absorption taking space which could be filled with water. In hydrogels with short monomers (and small pores) the absorption decreases greatly after formation of silver nanoparticles, in hydrogels with longer monomers (and larger pores) the decrease is very small.

4.2.3 Measurement of transition temperature T_{tr}

The sensitivity to temperature of HG was verified with measuring of the transition temperature (see Table 4.1).

S1 and S2 show a slow transition in comparison to S0, which does not contain MM and shows a sharper transition from a swollen hydrated state to a shrunken dehydrated state at 35 °C (Figure 4.20). S2 which contains the highest amount of MM shows the slowest transition. Furthermore, the transition of HGs containing MM is not only smoother, but also at higher temperature (at 46 °C for S1 and 50 °C for S2). The contraction of hydrogels with MM is clearly stronger. This is on the one hand due to a higher water absorption ability. On the other hand acid and amide groups are reported to undergo hydrogen bonds, which increase the contraction above T_{tr} [108].

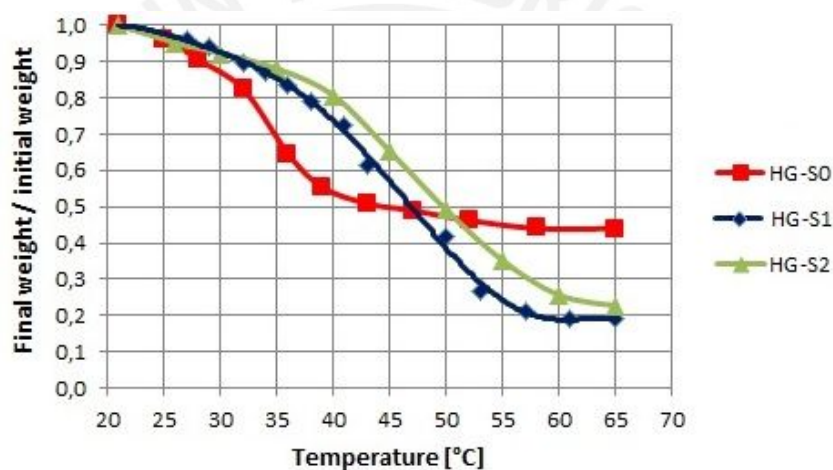


Figure 4.20: T_{tr} measurement of S0 (red), S1 (blue) and S2 (green): Weight loss as a function of temperature

The transition temperature of S3, S4 and S5, which contain the same amount of MM1 is at 45 °C (Figure 4.21). This is near to transition temperature of S1 which contain almost the same amount of acid groups (but MM2). Thus, transition temperature increases with the content of hydrophilic acid groups or their amount ratio to NiPAAM that was already discussed in other publication with similar systems [4].

The transition of S4 is smoother and ends at higher weight relation due to higher MBA content and lower water absorbance.

The strong shrinkage due to a higher water absorption (compared to S0) and hydrogen bonds between acid and amide groups [108] is observable here as well.

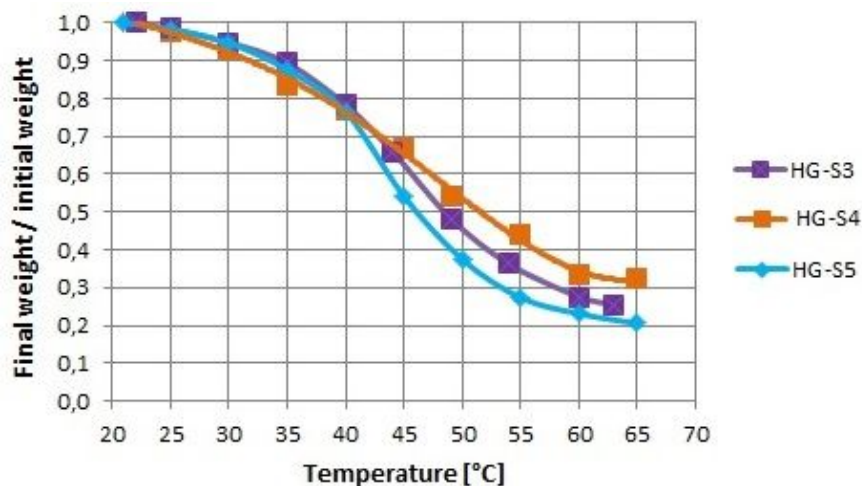


Figure 4.21: T_{tr} measurement of S3 (purple), S4 (orange) and S5 (light blue): Weight loss as a function of temperature

4.2.4 UV/Vis spectroscopy

In order to verify the generation of silver nanoparticles, UV/Vis spectra were recorded. Hydrogels with Ag-NPs content are distinguished by a very clear peak at around 410 nm (see Table 4.2) due to the plasmon resonance of silver nanoparticles. The spectral response of silver nanoparticles is a function of diameter and is characterized by a peak plasmon resonance shift to longer wavelengths with increasing diameter [94]. At diameters greater than 80 nm, a second peak at a shorter wavelength becomes visible [94]. For e.g. 100 nm silver nanoparticles there are two peaks: main peak at approx. 520 nm and the second peak at approx. 410 nm [94]. With smaller particle size the main peak grows and shifts to shorter wavelength and the second peak disappears [94]. Due to this effect it can be claimed that synthesized particles are smaller than 80 nm in diameter.

Furthermore, it can be asserted that Ag-NPs in S0 (without macromonomer) are smaller than in S1-S4 that are similar in size (see Table 4.2).

The content of MM or AiMM affects the peak height which is higher with increasing MM to NiPAAm ratio. Although the sedimentation of HG-Ag compound particles (same for all HGs) should be considered due to possible noticeable influence on the peak height.

HGs S3, S4 and S5 contain nearly the same amount of acid groups and should consequently include the same amount of Ag-NPs. But S4 contains more MBA. Due to this, the amount of silver related to the entire hydrogel is lower and the peak height accordingly too.

The weaker peaks between 200-300 nm, which occur in hydrogels containing silver nanoparticles, are probably caused by Ag^+ ions [109, 110].

UV/Vis serves as estimate; the more accurate particle size measurement is carried out with scanning electron microscope (SEM).

All the measured peaks (401-414 nm) correlate with values from similar studies [15, 16, 33].

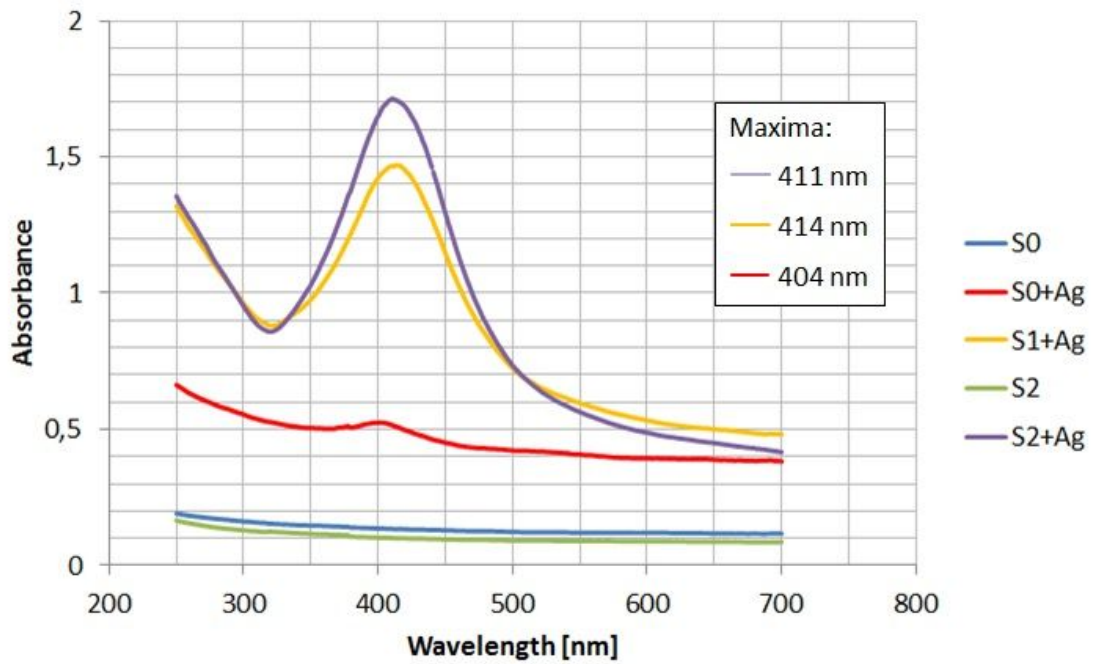


Figure 4.22: UV/Vis spectra of S0, S1 and S2 with and without Ag-NPs

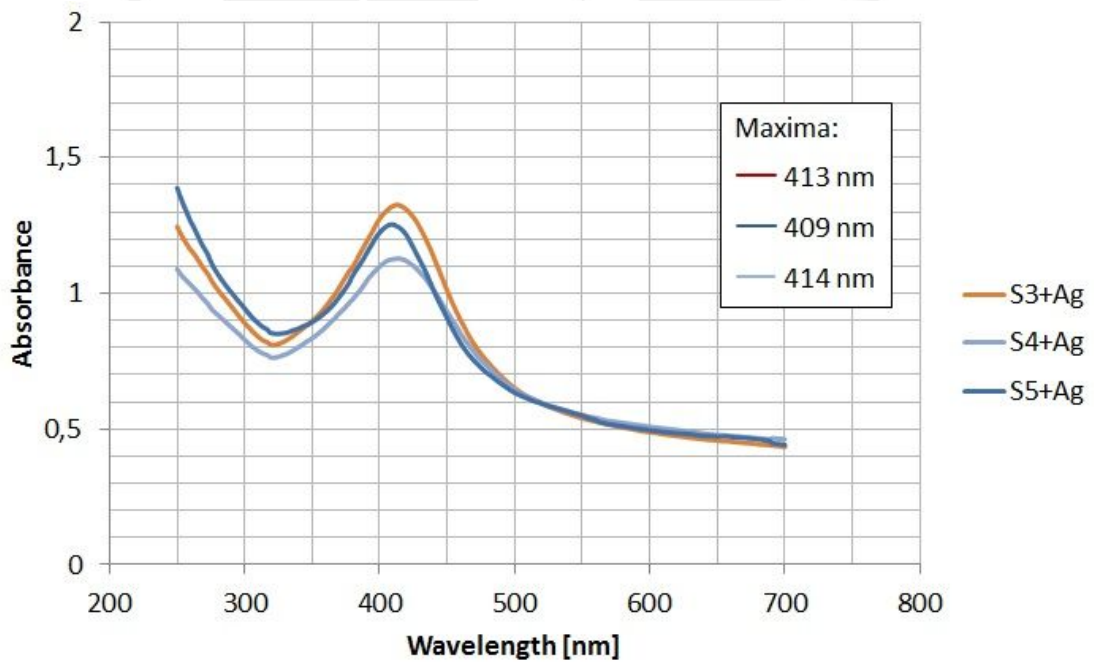


Figure 4.23: UV/Vis spectra of S3 and S4 containing Ag-NPs

4.2.5 Fourier transform infrared spectroscopy

In order to analyze the hydrogel structure and the effect of silver nanoparticles on it, Fourier transform infrared spectroscopy (FTIR) was recorded.

Both measures spectra (S2 and S2+Ag-NP) coincide for the most part. The main peak assignments are as follows [111]:

- 3500-3300 cm^{-1} : N-H stretch in NiPAAm and MBA
- 3000-2850 cm^{-1} : $-\text{CH}_3$ stretch in NiPAAm and 2-methyl-2-oxazoline monomer in MM
- 1650 cm^{-1} : C=O stretch in NiPAAm, MBA and MM
- 1550 cm^{-1} : N-H bend/ C-N stretch in NiPAAm and MBA
- 1450-1350 cm^{-1} : C-H stretch in aromatic rings in MM side chains
- 1300-1100 cm^{-1} : C-O stretch due to carboxylic acid groups in 2-carboxyethyl-2-oxazoline monomer in MM
- 1020 cm^{-1} : aliphatic C-N stretch in NiPAAm and MBA
- 700-500 cm^{-1} : C-C-C bend in NiPAAm, MBA and MM

The theoretical structure as a network of NiPAAm, MBA and MM could be confirmed. The effect of silver nanoparticles is particularly perceivable at 3000-3200 cm^{-1} , 2800-2000 cm^{-1} , 1650 cm^{-1} and 1100-450 cm^{-1} , which correlates with the typical finger-print FTIR spectra of Ag-NPs [112]. Reported horizontal shifting of C=O peak at about 1650 cm^{-1} ([15], [113]) could not be observed.

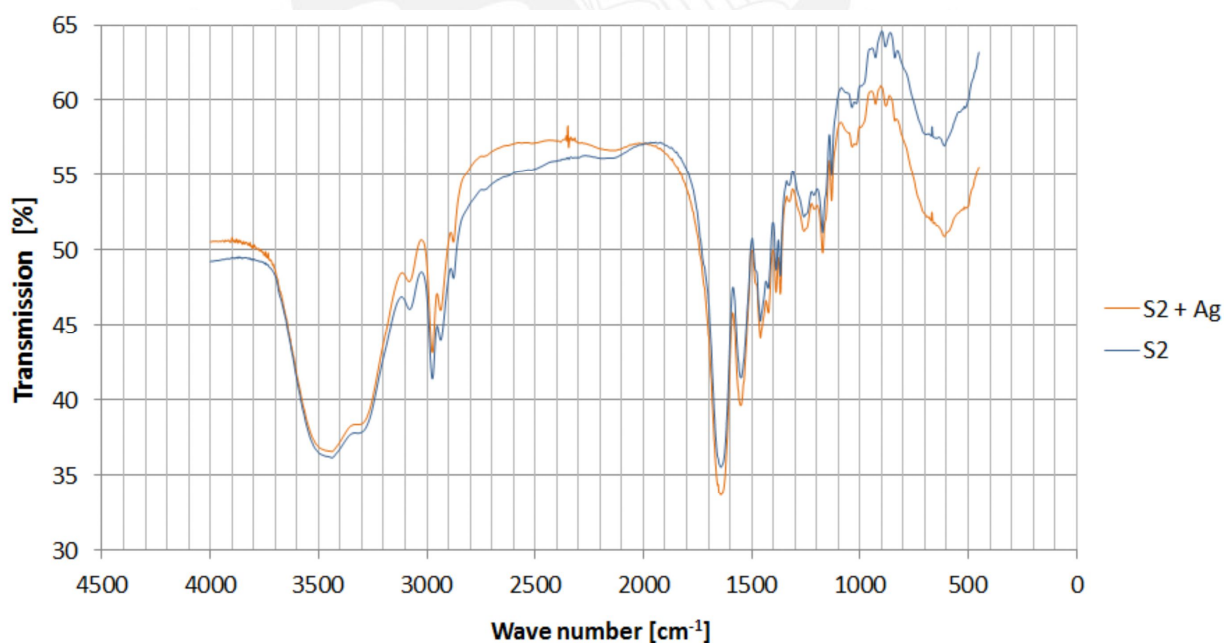


Figure 4.24: FTIR spectra of hydrogel S2 with and without silver nanoparticles

4.2.6 Scanning electron microscope analysis

SEM images were taken to analyse the hydrogel-Ag-NPs hybrid structure as well as the size and morphology of silver nanoparticles.

As can be seen in Figures 4.25, 4.26, 4.27, 4.28, 4.29 and 4.30, the particle size is nonuniform and is between 15 nm up to 200 nm, wherein the most are between 20 nm and 45 nm.

Such a wide range of particle size distribution correlates partially with other studies about hydrogel-Ag-NPs [15, 16, 33]. Indeed most authors report about precise particle formation, the size varies by a multiple [16]. The comparison with other publications is difficult due to different used monomers. The reported influence of MBA is an important factor, but the amount of MBA used in the present work could be too little to see great differences in SEM images. Another explanation could be the use of longer monomers in present work compared with Mohan et al. [16] with smaller particles and a narrow particle size distribution. Due to longer monomer chains the pores inside the hydrogel are bigger and particles can keep growing. On the other hand it is logical that nanoparticles do not fill the whole pore due to defined concentration of silver nitrate in the solution and osmotic pressure. According to this assumption the size of the nanoparticle inside the pore depends on the amount of silver ions and (at a certain concentration) on the pore volume. A variation in pore volumes analogously affects the particle size. Longer monomers may tend to a wider pore size distribution and hence a wider particle size distribution. However, this assumption do not consider the formation of several particles inside one pore as well as diffusion between pores. Electron-rich species (such as COO^-) act as attraction poles for silver ions. A higher concentration of these may lead to generation of more attraction poles for silver ions and thus smaller nanoparticles.

Summarized there are many supposable factors which may affect the formation of Ag-NPs inside the hydrogel matrix: the concentration of MBA and electron-rich species as well as the size of used monomers seems to be the most important. However, the present work does not clearly confirm all observations made in other studies. A possible reason for this could be the agglomeration of nanoparticles during a long period of time between the fabrication of hydrogels and their analysis via SEM (ca. 4-5 months).

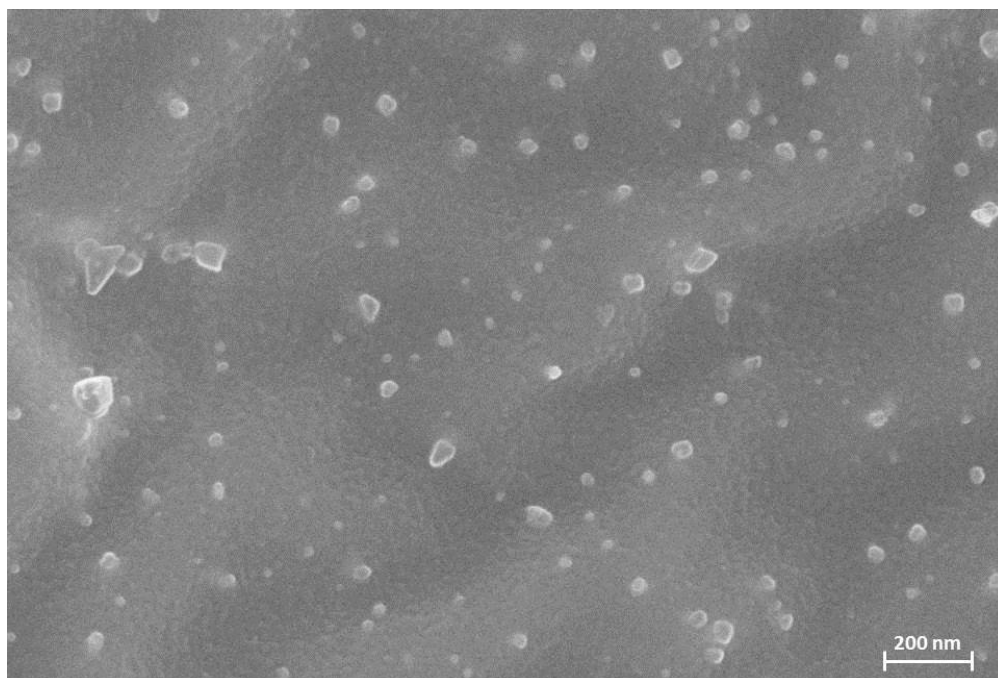


Figure 4.25: SEM image of hydrogel S0 containing silver nanoparticles

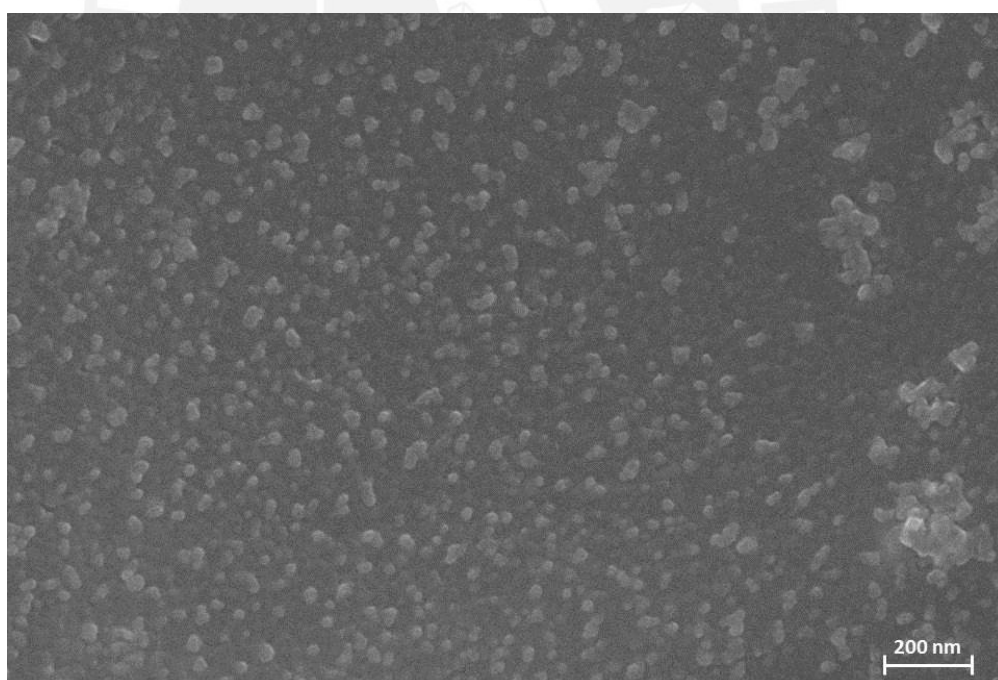


Figure 4.26: SEM image of hydrogel S1 containing silver nanoparticles

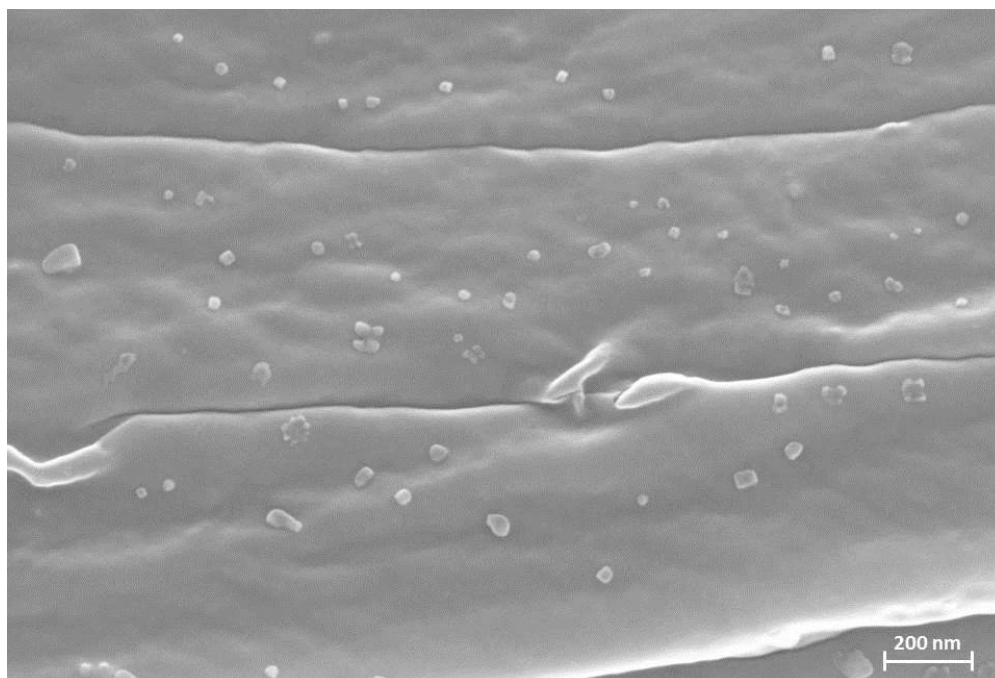


Figure 4.27: SEM image of hydrogel S2 containing silver nanoparticles

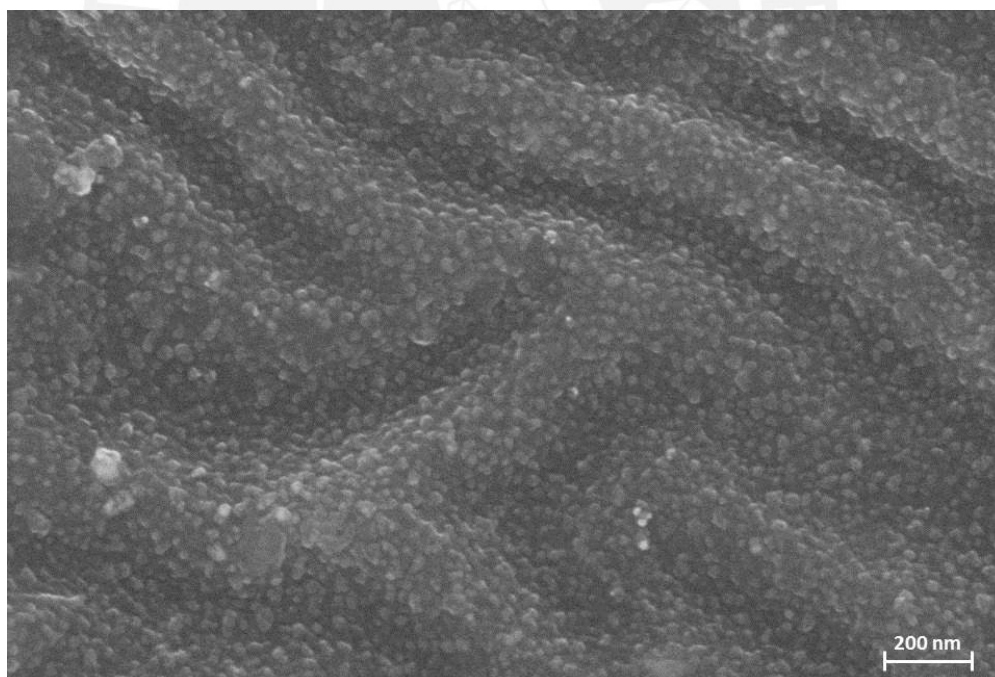


Figure 4.28: SEM image of hydrogel S3 containing silver nanoparticles

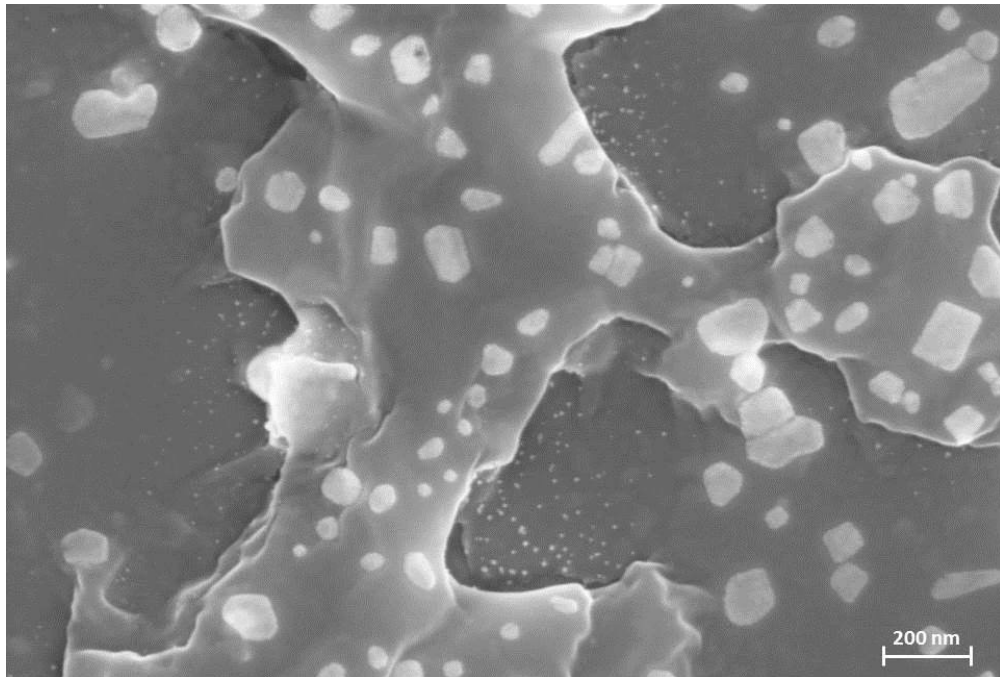


Figure 4.29: SEM image of hydrogel S4 containing silver nanoparticles

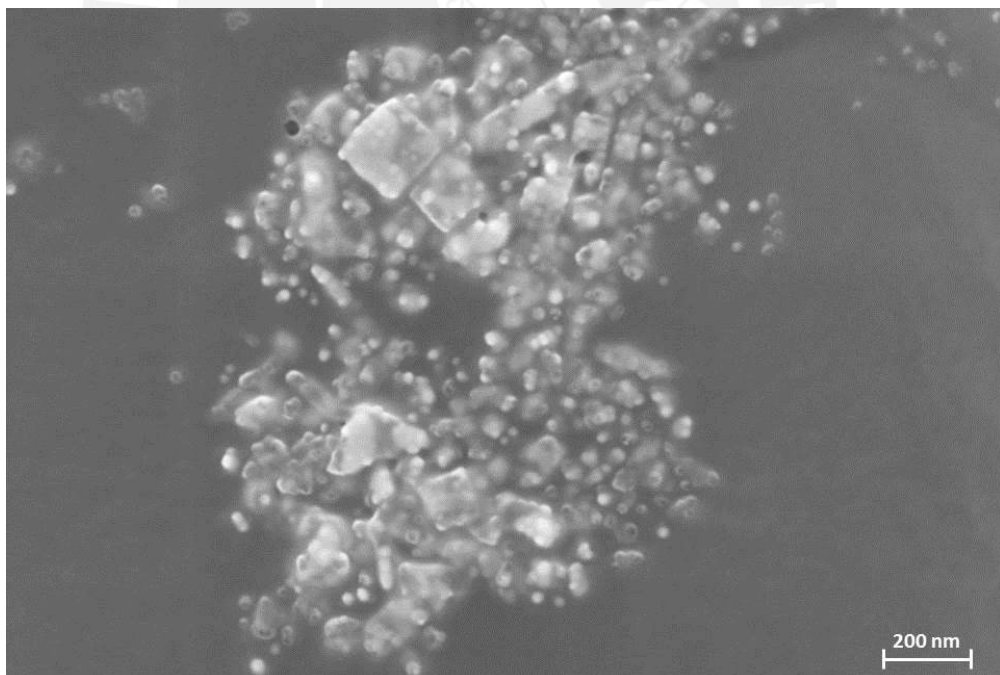


Figure 4.30: SEM image of hydrogel S5 containing silver nanoparticles

4.2.7 X-ray fluorescence spectroscopy

X-ray fluorescence spectroscopy allows a local measurement of silver content in hydrogels due to the proportionality of the silver L-peak intensity to the silver content inside the gel. Figure 4.31 shows the intensities of silver L-peak in different hydrogels S0-S5.

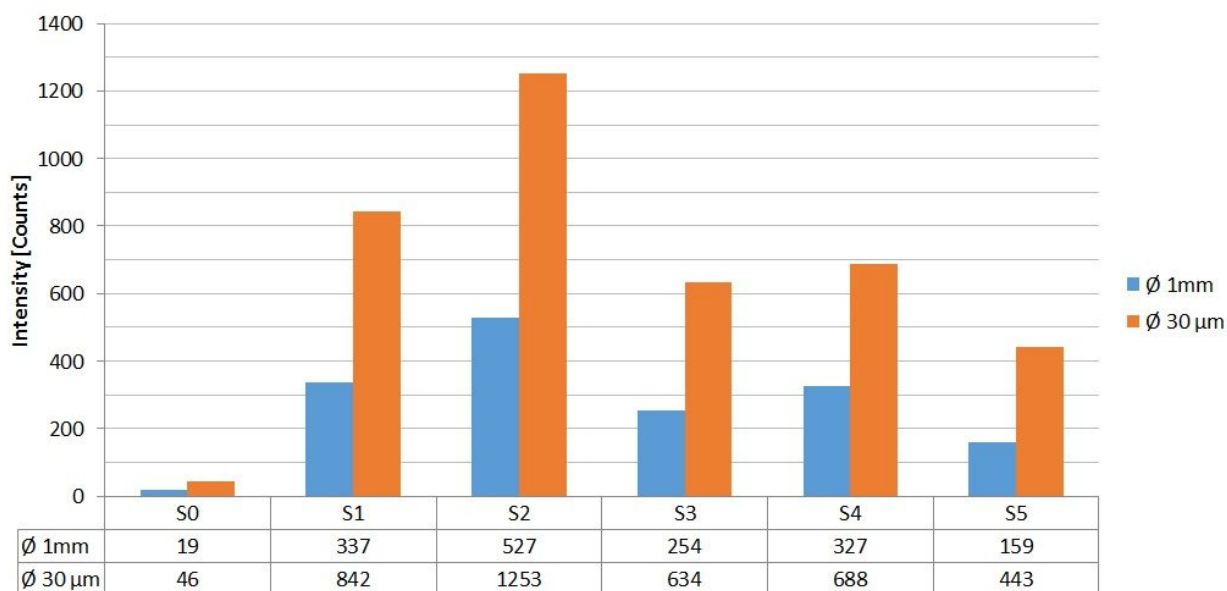


Figure 4.31: Intensities of silver L-peak from X-ray fluorescence spectra of hydrogels S0-S5 containing silver nanoparticles (measured with 1 mm diameter aperture and 30 µm polycapillary)

As can be seen, there is no trend difference between the measurements with 1 mm aperture diameter and such with 30 µm polycapillary. This is an important indication of a good distribution of silver nanoparticles inside the hydrogels and consequentially a good reproducibility of measurements.

S0 has the lowest peak intensity and thus the lowest content of silver nanoparticles in comparison with other hydrogels S1-S5. This is due to the absence of macromonomer units as additional electron-rich species. This effect can be observed optically by a lighter yellowish brown colour of S0 in comparison with brown coloured hydrogels with macromonomer and thus more silver nanoparticles inside.

The silver content increases from S0 to S2 due to the increasing content of (the same) macromonomer. Hydrogels S1 and S3, where different types of macromonomers were used, show a different content of silver, although the content of acid groups and the crosslinker is the same. The reason is a higher content of additional less electron-rich species inside the macromonomer and the hydrogel and consequentially a lower concentration of acid groups and thus silver nanoparticles relating to an area or volume unit in hydrogel S3.

Hydrogels S3-S5 with the same type of macromonomer and nearly the same content of it, still have a different content of silver. This is the result of the different content of the crosslinker

MBA in hydrogels. Thus MBA, which contains electron-rich amide groups, influence the content of silver (nanoparticles) inside hydrogels as well. S4 with the highest content of MBA from hydrogels S3-S5 (with the same content of macromonomer) has the highest content of silver and S5 with the lowest content of MBA, the lowest content of silver nanoparticles inside the gel.

Summarized these are the main factors, which influence the silver content in hydrogels: the content of the macromonomer as additional electron-rich species and the content of these species in it as well as the content of the crosslinker with electron-rich amide groups. These influences were clearly observed during X-ray fluorescence spectroscopy measurements, a high-precision materials analysis technique.

4.2.8 Antibacterial tests

The antibacterial activity of the produced hydrogel-Ag-NPs composites against *Staphylococcus aureus* was determined via count tests. Figure 4.32 shows the obtained results.

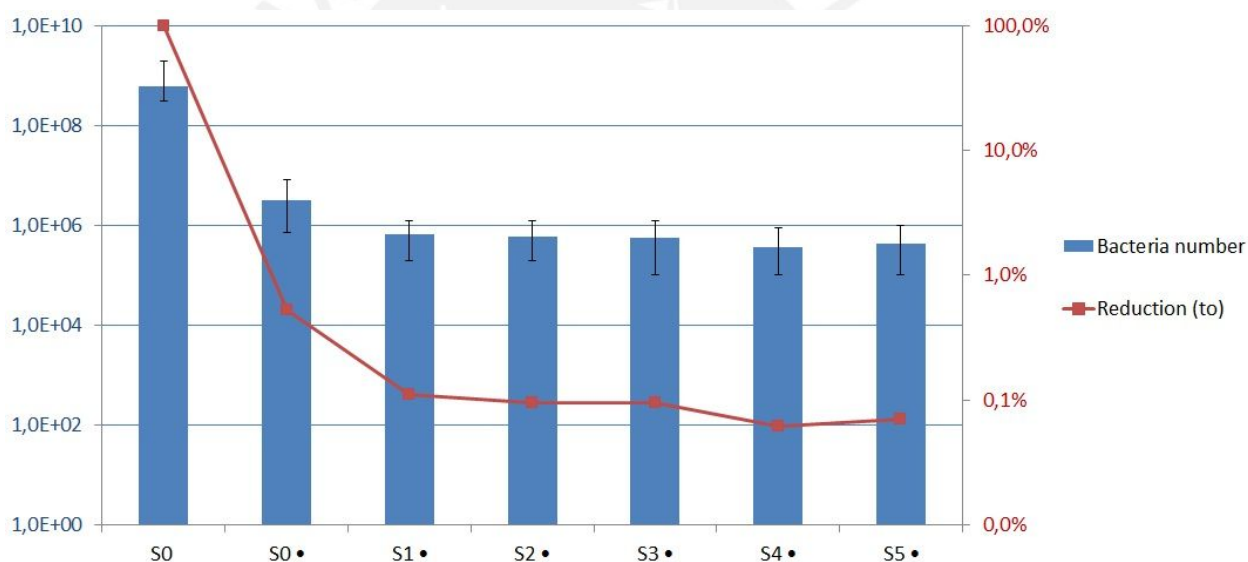


Figure 4.32: Bacteria number counted using Thoma chamber and grossed up to 1 mL (blue) as well as the reduction of this compared to the reference sample S0 (red). The point behind the hydrogel denotation symbolizes the presence of silver nanoparticles inside it.

As can be seen, the bacteria number decreases clearly from S0 without Ag-NPs (reference) to S0 with Ag-NPs and further to S1-S5 due to a higher amount of silver nanoparticles inside the hydrogel. The considerable difference between S1 with Ag-NPs and S0 with Ag-NPs is based on the use of the macromonomer and thus a higher amount of electron-rich species, which promote a higher amount of silver inside the hydrogel. However, there is no further noticeable difference between hydrogels S1-5. The structural differences between these hydrogels may possibly be too small to see a clear effect in bacterial tests.

Furthermore, the reduction of bacteria number compared to the reference could be shown. Assuming the reference sample S0 as 100 %, the number of bacteria could be reduced to approximately 0.1 % of the original value.

The antibacterial study made in present work correlates with investigations made by Feng et al. [60], according to which silver ions destroy the replication ability of bacterial DNA. Hence, it can be assumed that the considerable reduction of bacteria number observed in the present study is based on the ability of silver (ions) to prevent cell division of the bacterial culture.

The obvious reduction of the bacteria number from S0 without Ag-NPs (reference) to S0 with Ag-NPs and further to S1 with Ag-NPs is also demonstrated by confocal laser scanning microscope images shown in Figures 4.33, 4.34 and 4.35.

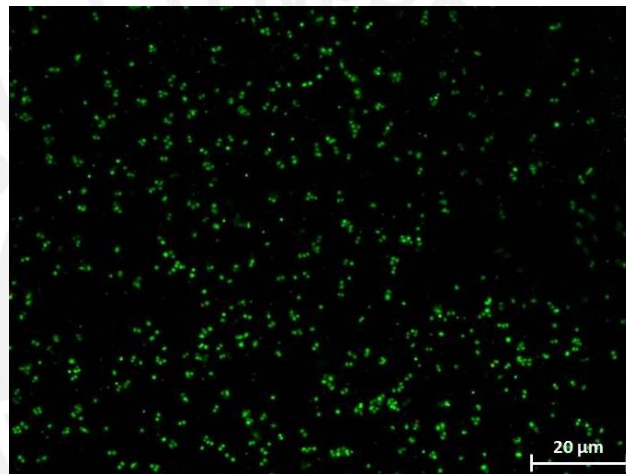


Figure 4.33: CLSM image of bacteria charged with hydrogel S0 without silver nanoparticles

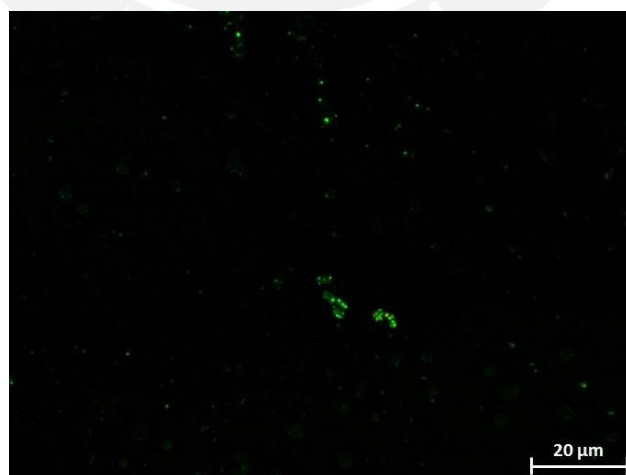


Figure 4.34: CLSM image of bacteria charged with hydrogel S0 with silver nanoparticles

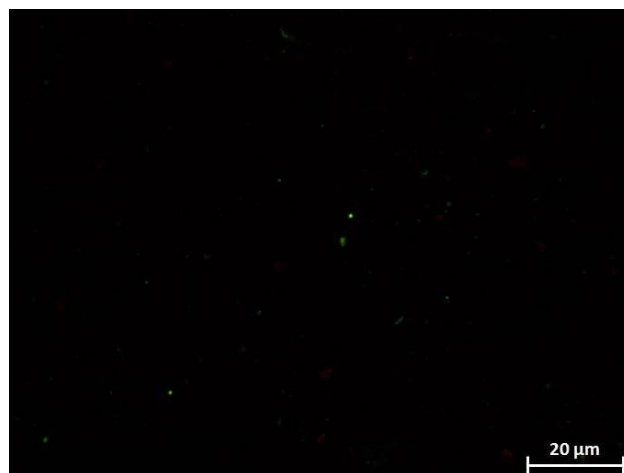


Figure 4.35: CLSM image of bacteria charged with hydrogel S1 with silver nanoparticles

4.3 Characterization of glass surfaces

4.3.1 Visual control

In many cases (e.g. rough surfaces) the quality of the surface and/ or the coating can already be observed by visual control.

Figure 4.36 (top) shows FS21 glass plates of approx. 1 cm² area at different states of treatment:

- after tempering (A),
- after tempering and etching (B),
- after exposure and tempering (C) as well as
- after exposure, tempering and etching (D).

Glass plates shown in Figure 4.36 (top) are already coated with a hydrogel layer via dip coating, however, the formed transparent hydrogel layer did not change the visual nature of the glass, so that uncoated glasses as well as glass surfaces coated with a thin hydrogel film via dip or spin coating have the same macroscopic/ visual appearance: Exposure causes formation of silver clusters (and subsequent formation of lithium metasilicate ceramic phase) inside the glass, changing the colour from transparent (A and B) to brown (C and D), etching is the reason for rough and mat surface (B and D).

Glass plates shown in Figure 4.36 (bottom) with equal hydrogel films and a reference (type A) without a coating were additionally treated with AgNO₃ and NaBH₄. Due to the formation of silver nanoparticles inside the gel layer the colour changed from transparent to brown (A and B) or got darker (C and D). Although the reference plate did not get as brown as samples A and B, nevertheless, the colour changed to light yellowish. A possible reason therefor may be a small amount of physisorbed silver nanoparticles on glass surfaces.

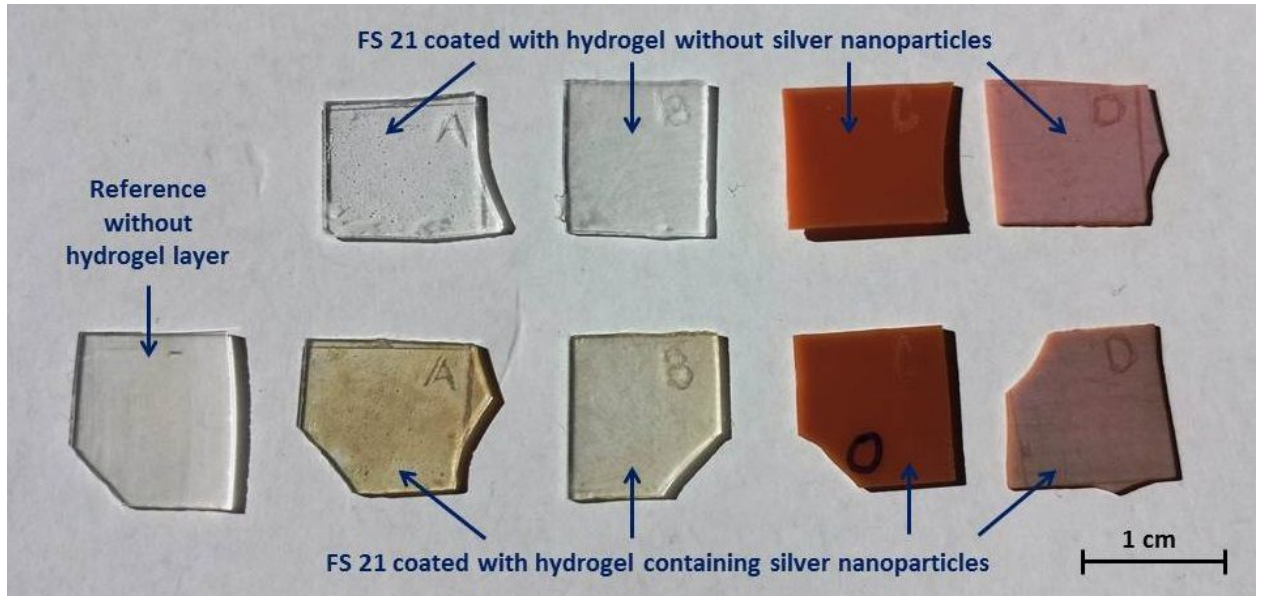


Figure 4.36: Glass surfaces coated with hydrogel via dip coating with and without silver nanoparticles inside, the reference sample without hydrogel layer was treated with AgNO_3 and NaBH_4 as well to demonstrate the importance of hydrogel layer for reception of silver nanoparticles

In order to observe the drying behaviour of hydrogel coating, thick layers were deposited. As can be seen in Figure 4.37 formerly thick (approx. 1.5-2 mm) layers with straight borders shrunk and were deformed due to mechanical stress inside the coating and at the boundary surface. Owing to the considerable shrinkage the hydrogel coating/ structure corrugated, however, flatter areas could be observed as well.

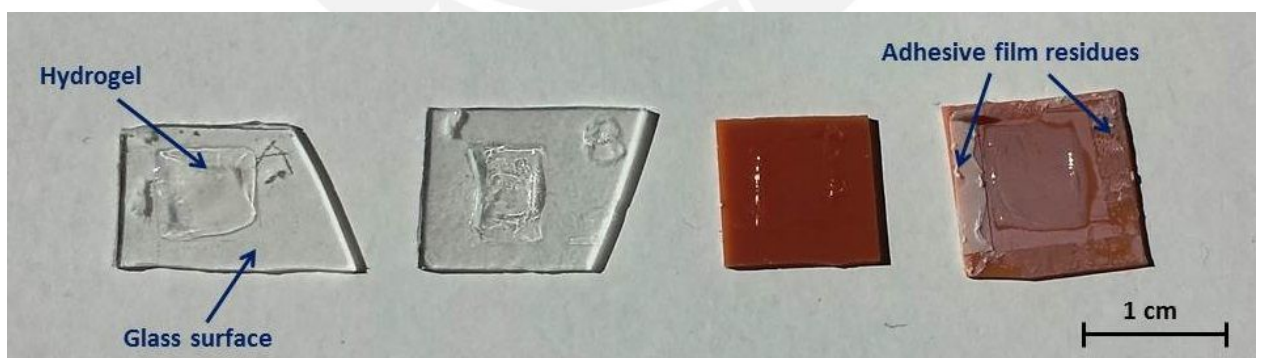


Figure 4.37: Thick hydrogel structures on glass surfaces

4.3.2 Atomic force microscopy

Atomic force microscopy was used to evaluate the surface quality before and after coating with hydrogel. While topography mode was used to visualize the surface structure and roughness, adhesion mode was applied to demonstrate the quality of the hydrogel coating.

As can be seen in Figure 4.38 the topography depends strongly on the processing step. In Figure 4.38 a), which shows the glass surface without any further treatment, the surface is flat, only polishing marks are observable.

After tempering, the surface roughness increases due to surface crystallization, which can be seen in Figure 4.38 b) in terms of tapered star-shaped crystallites. Surface crystallization occurs owing to heat supply during tempering process. The energy supply results in a transition to a more stable crystalline state, which starts at surface imperfections [114].

The surface crystallites are dissolved during etching. Etching pits, which are shown in Figure 4.38 c), remain. As a result, the surface roughness increases.

After UV light exposure and subsequent tempering, the formation of surface crystallization could be observed. In contrast to Figure 4.38 b), the crystals appear snowflake-shaped, as can be seen in Figure 4.38 d). Due to former observation [83, 86], they are interpreted as a crystalline lithium metasilicate phase.

Etching and removing of the lithium metasilicate phase results in a rough surface, which is shown in Figure 4.38 e).

After dip coating the topography of glass surfaces did not change remarkably. The few changes can be observed in Figures 4.39 a) and c), where the hydrogel coating seems to accumulate at crystallite borders, emphasizing the primary surface structure.

However, the quality of the hydrogel coating can not be evaluated using topography information only. Therefore adhesion images are advantageous. Figure 4.39 shows AFM images based on adhesion interaction of cantilever probe and glass surfaces before and after hydrogel coating. While Figures 4.39 a), c) and e) before coating are very similar to topographic images in Figure 4.38, Figures 4.39 b), d) and f) contain new information caused by hydrogel coating. Thus it appears that the coating is not homogenous and differs depending on primary surface structure.

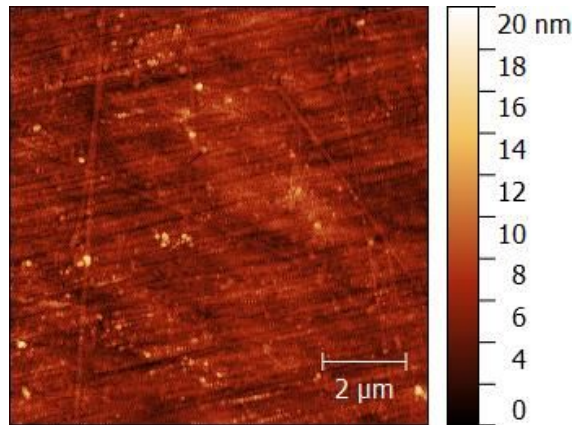
In Figure 4.40 b), which shows the glass surface after tempering, the hydrogel coating is formed along surface crystallites. It can be assumed that drying on air forced the entire coating to contraction and led to shrinkage and microcracks. Due to the fact that the coating did not change the topography considerably, it can be supposed that the thickness of the hydrogel layer is too low to cover surface roughness of the glass. More precise predictions can be done comparing roughness parameters (see Section 4.3.3).

While the layer in Figure 4.40 b) is largely homogenous, the layer formation in Figures 4.40 d) and f) is not completed. Due to different surface tensions (even after silanization) and

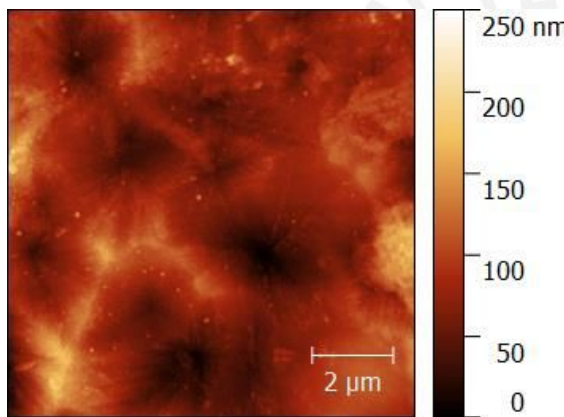
high contraction forces the hydrogel forms drops or islands on rough glass surfaces. A high roughness of the surface before coating is most likely the reason for dewetting of hydrogel in Figure 4.40 d), which can be compared with hydrophobic or super hydrophobic surfaces, where dewetting is achieved by means of surface structuring [115].

Figure 4.40 f) shows that the formation of hydrogel layer starts at lithium metasilicate crystals as surface imperfections. Compared with surrounding glass area, lithium metasilicate crystals are rougher and seem to be preferred by hydrogel molecules for layer formation. Relating to thin-film growth modes it corresponds to Volmer-Weber mode, where the layer formation proceeds out of single islands [116].

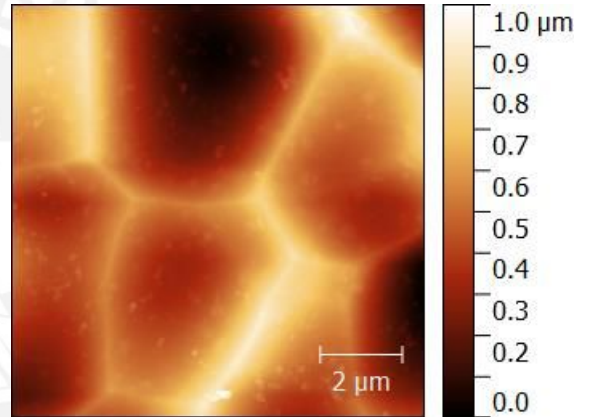




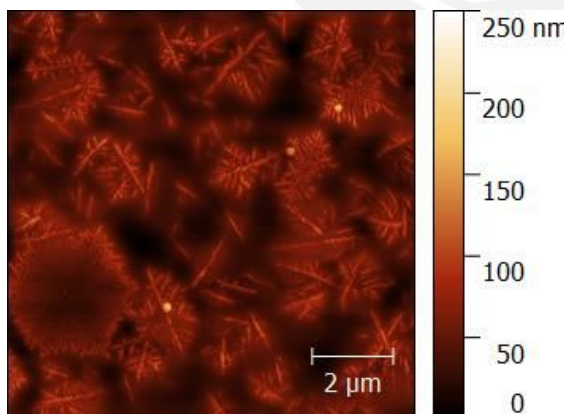
a) Polished FS21 glass surface without any further treatment



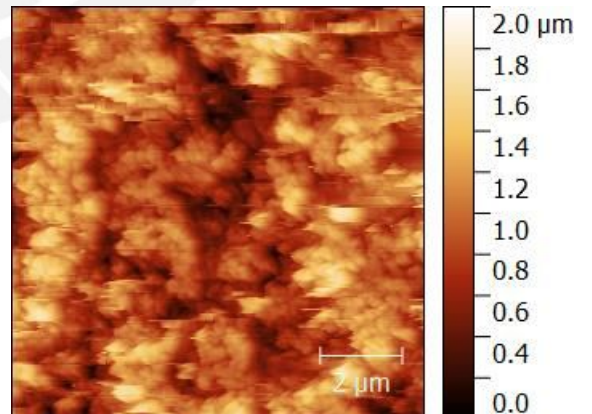
b) FS21 glass surface A (after tempering)



c) FS21 glass surface B (after tempering and etching)

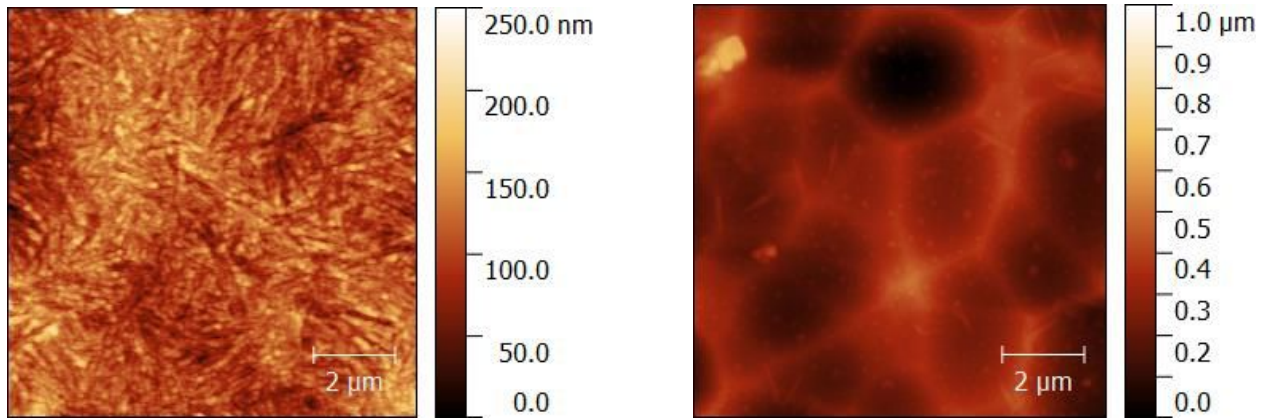


d) FS21 glass surface C (after exposure and tempering)



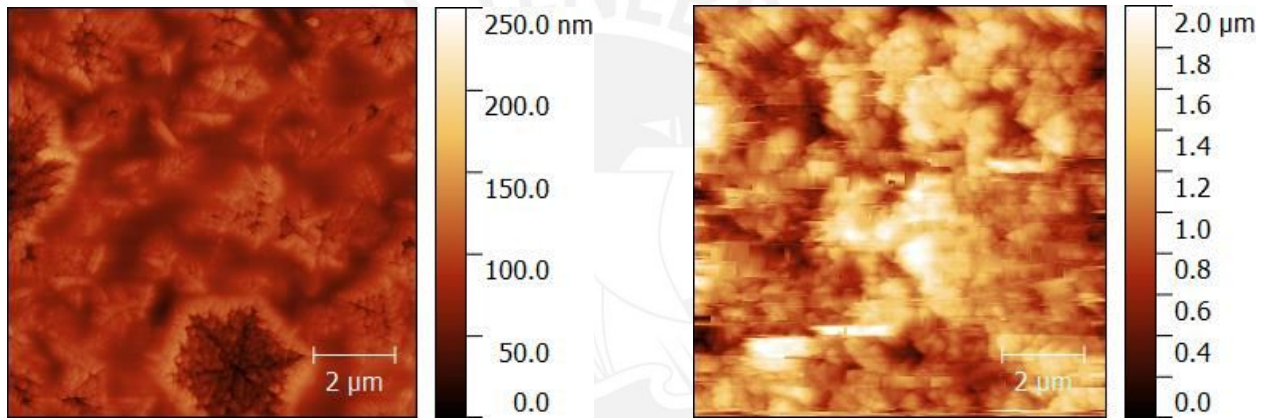
e) FS21 glass surface D (after exposure, tempering and etching)

Figure 4.38: AFM topography images of uncoated FS21 glass surfaces at different states of treatment



a) FS21 glass surface A (after tempering) coated with hydrogel

b) FS21 glass surface B (after tempering and etching) coated with hydrogel



c) FS21 glass surface C (after exposure and tempering) coated with hydrogel

d) FS21 glass surface D (after exposure, tempering and etching) coated with hydrogel

Figure 4.39: AFM topography images of FS21 glass surfaces at different states of treatment after dip coating with hydrogel

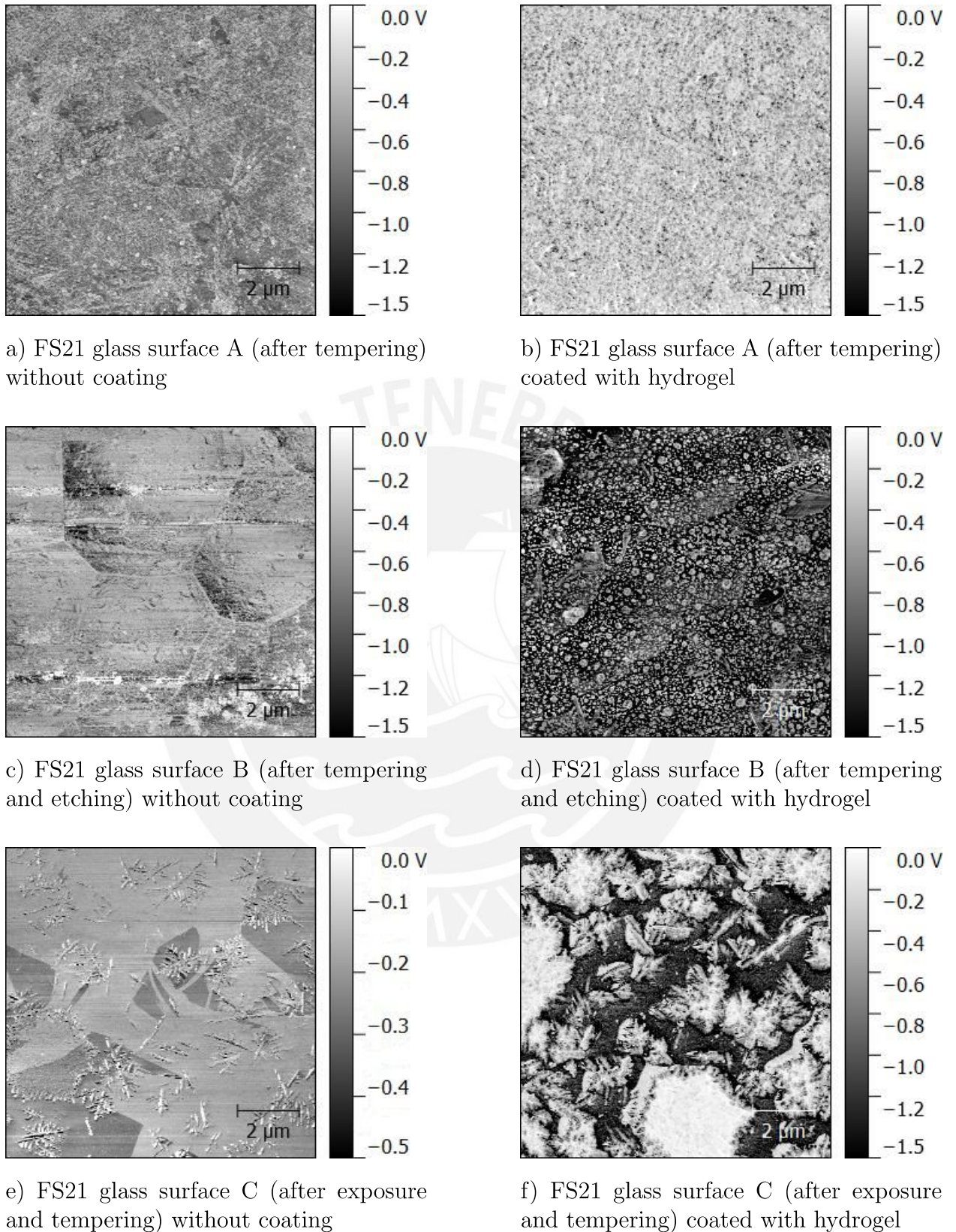


Figure 4.40: AFM adhesion images of FS21 glass surfaces (at different states of treatment) before and after coating with hydrogel

4.3.3 Profilometry

In order to evaluate the quality of glass surfaces, their change due to different treatment processes as well as the influence of the gel coating, profilometric measurements were done. The results are graphed in Figures 4.41 and 4.42.

Firstly, the influence of structuring processes on uncoated glasses was examined. As can be seen on R_a and R_z values in Figures 4.41 and 4.42, the roughness increases initially after tempering and increases once more after etching (see Figures 4.41 and 4.42, uncoated samples 0, A and B). This is due to surface crystallization (A) and remained etching pits (B), which both were observed during AFM-measurements (see Fig. 4.38). The same trend can be observed at samples C and D, albeit with lower values. The reason is that owing to exposure newly formed lithium metasilicate crystals (C) are smaller and finer than surface crystals in case of glass A, so that the roughness of exposed plates is lower.

As already mentioned in previous sections, a thin hydrogel layer did not change the glass surface remarkable. Considering adhesion images of AFM in Figure 4.40, it is clear that the reason is the incomplete layer formation (B and D). An exception is the glass sample A, where the best coating could be achieved. In this case the coating retraces the imperfections of the glass surface. A high mechanical stress due to hydrogel shrinkage may cause layer deformation increasing the roughness.

In case of thick hydrogel layers the roughness strongly differs from that of uncoated glasses and is approximately in the same range (except of sample D). In all probability the appearance of the hydrogel surface of such thick structures is no more influenced by the initial roughness of the glass, but by mechanical deformation due to shrinkage. Hence, roughness values of the accidentally distorted gel layers vary largely (see error bars in Figures 4.41 and 4.42). Sample D with lower roughness, but similarly high variation as samples A, B and C, might be subject to more advantageous drying conditions.

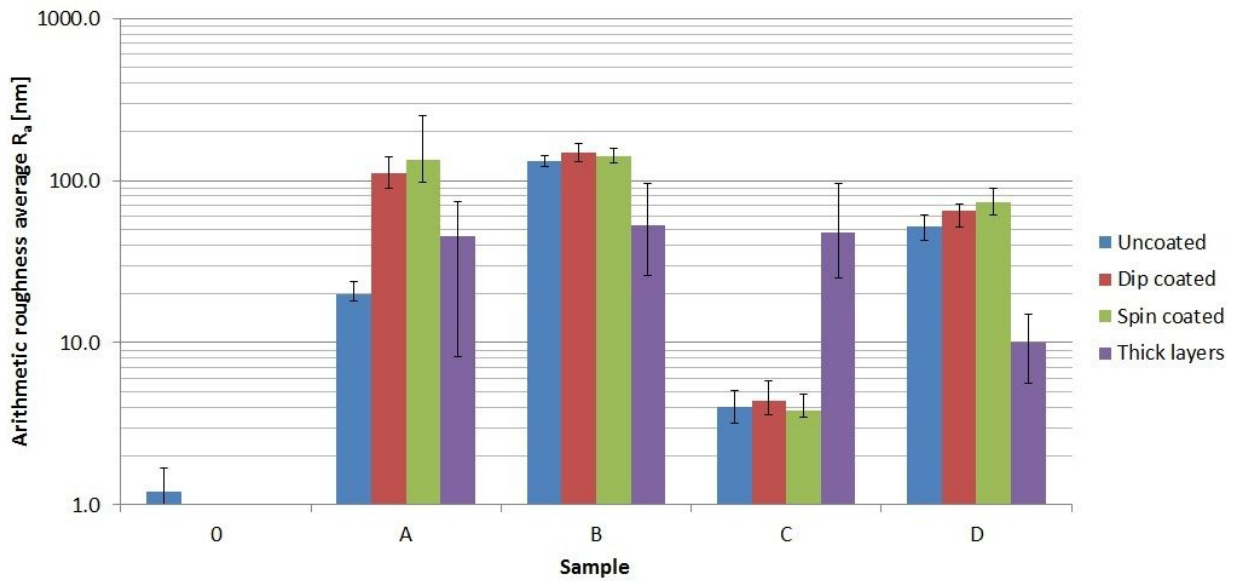


Figure 4.41: Arithmetic roughness average R_a of FS21 glass surfaces (at different states of treatment) before and after coating with hydrogel; coloured bars show the average value of five measurements, error bars the highest and the lowest value

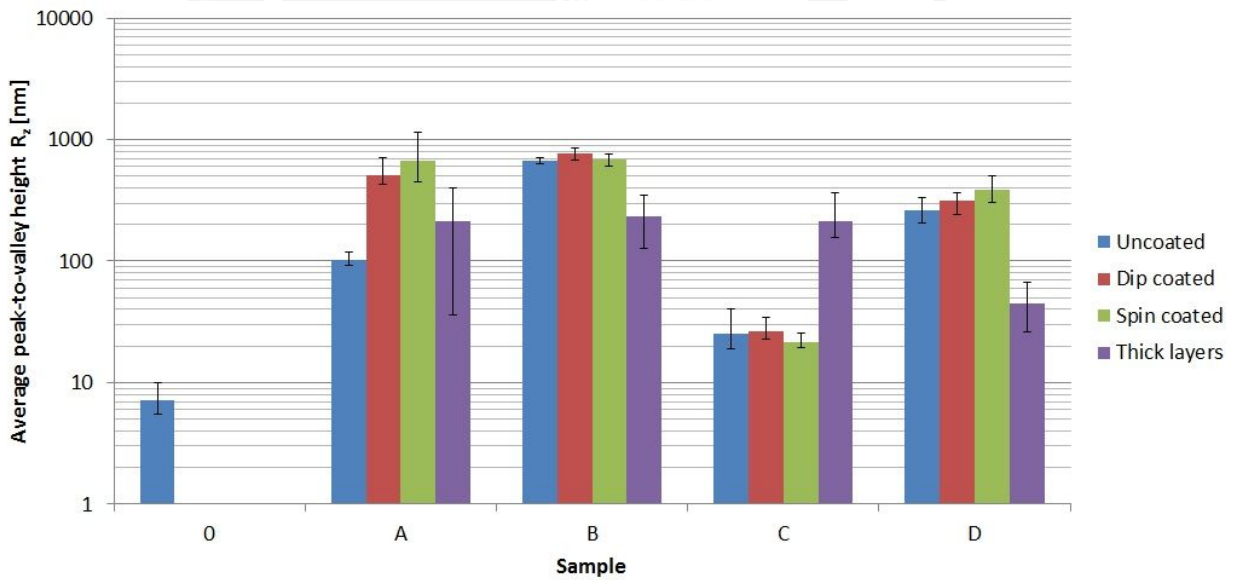


Figure 4.42: Average peak-to-valley height R_z of FS21 glass surfaces (at different states of treatment) before and after coating with hydrogel, coloured bars show the average value of five measurements, error bars the highest and the lowest value

4.3.4 Scanning electron microscope imaging of glass surfaces

FS21A glass (after tempering, but without exposure and etching), which showed the best coating quality according to AFM adhesion imaging results, was examined via SEM after nanoparticle formation inside the hydrogel layer. Surface crystallization, similar to AFM topography images, could be observed as well, as can be seen in Figure 4.43. Thus, it is clear too, that the hydrogel coating is too thin to cover the surface roughness caused by this process. Except this, the layer seems to be homogenous as well as the silver nanoparticle distribution.

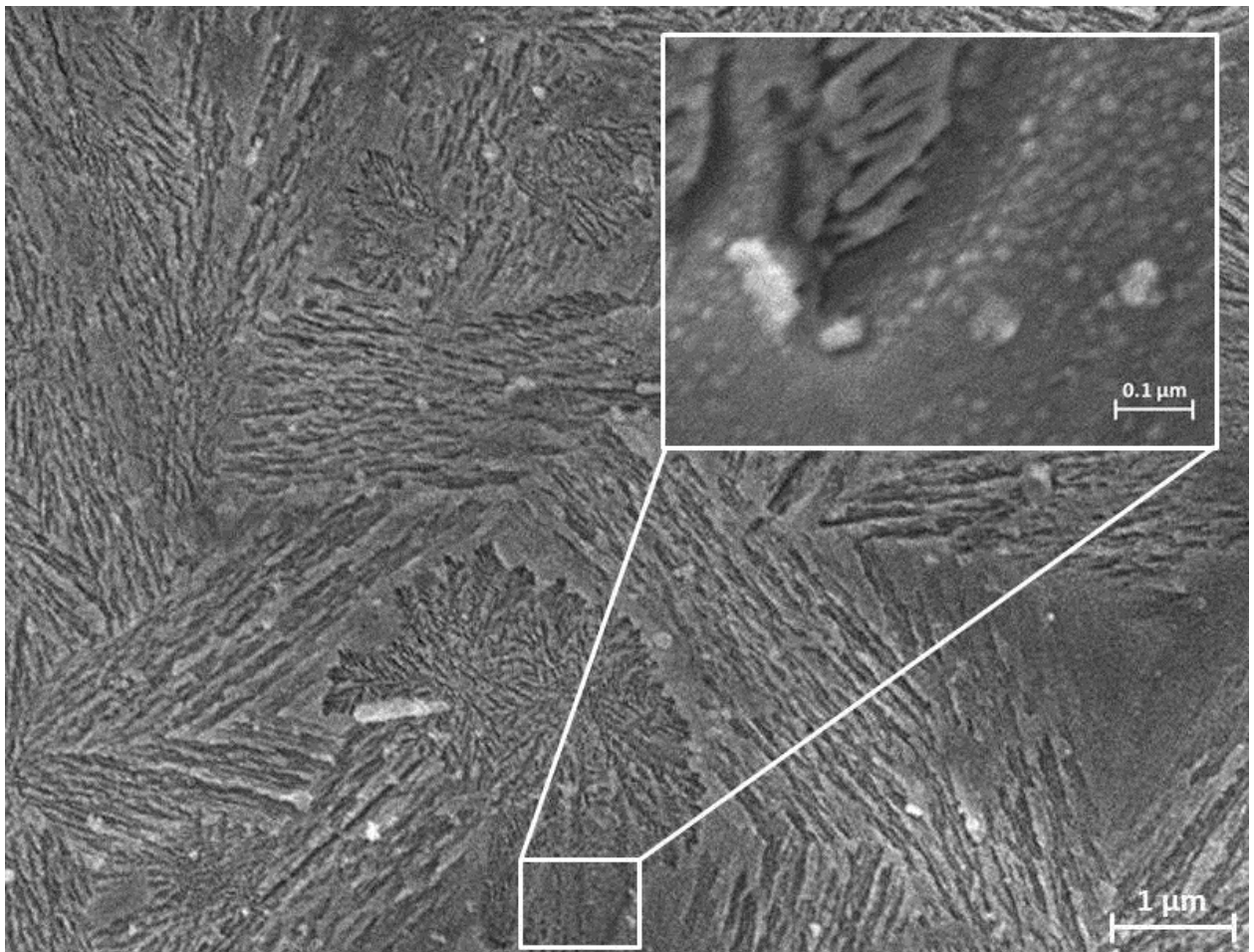


Figure 4.43: SEM image of an FS21A glass surface covered with hydrogel containing silver nanoparticles

4.4 Discussion

In this chapter the achieved results should firstly be reviewed and then compared to the latest publications in this field of research.

The hydrogel synthesis was successful and conformed to theoretical scheme, that could be confirmed via FTIR and NMR measurements. While FTIR spectra verify the presence of main functional groups, NMR allows a precise positioning of a functional group and even a quantification of certain groups (e.g. macromonomer content) inside the network. The determined macromonomer content in hydrogels was lower than calculated theoretically, but that was expected due to a lower mobility of macromonomer molecules with a high molar mass. The achieved reaction yields were high (up to 98 %), which indicates a good chemical reactivity at selected conditions and a small amount of remained unreacted chemicals. Achieved results correlate with previous work about hydrogels with similar compositions [4]. The use of macromonomer inside a NiPAAm-based hydrogel network has a strong influence on its main characteristic: the absorbance of water. Carboxylate and carboxylic groups in macromonomer units induce a higher polarity and thus a higher water absorption compared with hydrogel without macromonomer molecules, which was observed in previous work as well [4]. An increasing content of MBA as a crosslinker decreases the water absorption by reason of a stronger networking of polymer chains and subsequently less space for water reception inside the gel. This effect was already reported, too [4], and could be confirmed in this work.

The generation of silver nanoparticles inside a hydrogel network containing a macromonomer based on functionalized 2-oxazolines was new. The formation of silver nanoparticles could be confirmed using UV/Vis spectroscopy, SEM imaging as well as X-ray fluorescence spectroscopy. Compared to other work [16,33], the particle size distribution was nonuniform and varied between 15 and 200 nm, wherein the largest portion was between 20 nm and 45 nm. A possible reason may be the use of macromonomer, which is a long molecule compared with monomers used in other studies [16,33,40]. Such long chains could restrain the formation of small pores inside the hydrogel network, which act as reaction vessel for nanoparticles. This would explain, why in spite of different concentrations of MBA in hydrogels S3-5 there is no difference in particle size or antibacterial activity of these gels. A further possibility could be the agglomeration of nanoparticles inside the gel due to a long period of time between the fabrication of hydrogels and their analysis via SEM (ca. 4-5 months).

Furthermore, the observed silver nanoparticles inside are not only distributed nonuniformly in their size, but also in their position. This may be due to mobility differences between macromonomer and NiPAAm molecules, where longer and heavier macromonomer molecules react at last, so that these areas with a higher concentration of electron-rich groups contain more silver nanoparticles. Another reason may be the higher concentration of MBA

(2.5-10 %) compared to 1.5 % used by Mohan et al. [16] and Deen and Chua [33], which could restrict the diffusion and lead to a nonuniform distribution of silver nanoparticles as reported by Deen and Chua [33].

X-ray fluorescence spectroscopy was an important method to evaluate the amount of silver inside the hydrogel network. However, the exact (absolute) amount could not be determined, relative values provide significant information about the chemical composition of the hydrogel and its influence on silver content inside the polymer network. Thus, it could be observed, that the silver content increases not only with an increasing amount of macromonomer with electron-rich acid groups, but also with a higher content of MBA, which contain electron-rich amide groups.

It is important to consider the advantages and limitations of analysing methods used for silver nanoparticle characterisation as well. While UV/Vis spectroscopy allows to confirm the presence of silver nanoparticles inside the gel, a precise determination of particle size or their amount is hardly possible, especially due to strong sedimentation. SEM imaging enables to see the particles, but the few measurements are local and can not be generalized for the whole network. X-ray fluorescence spectroscopy, however, provides information not only from superficial silver, but also from silver particles inside the hydrogel. Furthermore, there was no sample preparation, such as milling or sputtering, needed. Each with its disadvantages, there is no perfect characterisation method, so that different techniques have to be applied.

Produced hydrogels are aimed for use in the biomedical field due to antibacterial properties of silver nanoparticles. On account of this it was important to evaluate the antimicrobial activity of the obtained samples. Although this evaluation was done qualitatively in all similar publications [15, 16, 117], in this case quantitative analysis using count tests were realized. Compared to a reference sample without silver nanoparticles, the bacteria number was reduced to approximately 0.1 %. Thus, the antibacterial effect of hydrogels containing silver nanoparticles was confirmed. Due to a wide particle size distribution, however, the most convenient composition could not be determined (all hydrogels with macromonomer show nearly the same results). Not at least the experimental setup should be considered. In antibacterial tests in the present work the hydrogel is milled and used as powder. On the one hand it is necessary to get more sample material, but on the other hand the form of the sample influence the measurements greatly, especially those, where surface plays an important role. It means, that the antibacterial activity of the final product, where hydrogel may be used as a bulk material or as a coating and not as a powder, could differ strongly. In this case it is proposed to repeat the measurements using the final bulk product.

In the present work, previously described hydrogels were furthermore evaluated in terms of application possibility in combination with photostructurable glass FS21. Firstly, uncoated glass surfaces were analysed and it was observed, that treatment processes influence greatly the glass surface: Tempering of un-exposed glasses causes surface crystallization and thus a

higher roughness. Lithium metasilicate crystals were observed on exposed and tempered glass surfaces, where the surface roughness was lower than this of unexposed FS21, but higher than roughness values of untreated (polished) glass. The formation of snowflake-shaped lithium metasilicate crystals, as observed in the present work, was reported numerously [83,86,118]. During etching the crystalline phase was removed, but the remaining etching pits increase the surface roughness dramatically. As reported by Stookey [118], hydrofluoric acid dissolves lithium metasilicate crystals first, whereon lithia-deficient glass dissolves due to a high surface area. Hence, these spongy areas [83] remain after etching exposed and tempered photostructurable glasses increasing the surface roughness.

The use of hydrogels as coatings or layer structures is of great interest for microtechnological applications such as sensors or actuators [14,34], however, their formation is coupled with difficulties. On the one hand high forces due to shrinkage should be considered, which deform or even destroy the hydrogel layer. On the other hand the influence of the substrate surface (e.g. material and initial roughness) is of importance. In case of the present work, FS21 glasses were silanized to improve the adhesion between the hydrogel layer and the glass substrate. In most cases the coating was not complete and tended to island formation or even dewetting. A possible reason may be an insufficient adhesion even after silanization. The experimental setup may be an other reason. Possibly the volume of hydrogel solution that remained on glass surface after dip or spin coating was not sufficient to form a layer, so that polymer monomers were not able to build a large network due to a fast evaporation of water.

Although the combination of hydrogels with other materials may be of note for many applications, not least for biomedical devices, disadvantageously there are not many studies about thin film hydrogel layers based on similar systems. The described systems are usually used in combination with other polymers, where a NiPAAm based hydrogel is embedded in a porous matrix [119] or in a polymer network as a microgel [120,121]. But there are other hydrogel systems as well, e.g. polyvinyl alcohol/ polyacrylic acid networks [122] or polymethacrylic acid/ polyethylene glycol dimethacrylate [43], which were reported to be coated homogenously. Insufficient coating quality is not necessarily based on the used hydrogel composition, it also could be caused by a weak adhesion promoter or a deficient substrate surface quality. Spin coating with lower rotation velocity or other coating methods could help to understand the observed phenomena.

5 Conclusions and Perspectives

The main achievements of this work were:

- A successful synthesis (reaction yield up to 98 %) of new hydrogel/ silver nanoparticle composites based on N-isopropylacrylamide and a macromonomer of 2-oxazolines (functionalized with acidic groups) was demonstrated, where N,N'-methylene bisacrylamide was used as a cross-linker, ammonium persulfate and N,N,N,N'-tetramethylene diamine as an initiator system.
- The chemical structure of hydrogels was as expected and could be confirmed via NMR and FTIR analysis.
- The formation of silver nanoparticles inside the gel (by complexation with AgNO_3 and a subsequent reduction by NaBH_4) was verified via UV/Vis spectroscopy, SEM imaging and X-ray fluorescence spectroscopy.
- The antibacterial activity of the obtained composite (against *Staphylococcus aureus*) was determined quantitatively using count tests. A reduction to 0.1 % of bacteria (compared to a reference value without silver) could be achieved.
- It could be observed that a higher concentration of macromonomer increases the water absorption as well as the amount of silver nanoparticles and thus the antibacterial activity. A higher concentration of the cross-linker, in contrast, decreases the absorbed water, but influences the formation of silver nanoparticles similarly positive.
- Moreover, the obtained hydrogels were evaluated as coatings on photostructurable glass FS21. The quality of the coatings varied depending on the initial surface conditions (e.g. roughness).

In spite of a wide coverage of this topic in the present work, there are numerous uninvestigated aspects, which could be interesting for future research:

- Investigations relating to porous structure of hydrogels (e.g. distribution of pore size inside the gel) could help on further understanding of the particle formation process.
- Measurements of the long-term stability of hydrogel/ silver nanoparticles composite are inevitable for their application in medical field as well as a detailed investigation of a possible nanoparticle release and its toxic effect on healthy human body cells (such as reported in [58, 79, 81, 123]).
- An achievement of a homogenous and narrow distribution of silver nanoparticles could be desirable.

- For application in biomedical devices, the use of un toxic and biocompatible chemicals (such as reported in [58]) should be considered.
- The antibacterial activity of the final product could differ from the results measured on hydrogel powder, so that separate examinations could be reasonable.
- Mechanical properties (e.g. abrasion resistance) were not investigated in this thesis, but they are of great importance for the final products and should not be neglected.
- The influence of the substrate roughness on the internal stress in the hydrogel layer would be interesting for thin film applications.
- A desirable homogenous and complete coating could be possibly achieved by following suggestions:
 - an other surface functionalization treatment (e.g. using Surface-Initiated Atom Transfer Radical Polymerization (ATRP) method [124, 125]),
 - fabrication of thicker hydrogel layers, which would compensate the surface imperfections of substrate material and
 - minimization of mechanical stress due to hydrogel drying and shrinkage by a gradual drying (step by step minimization of atmospheric humidity).
- An interesting topic would be the investigation of the lower limit of film thickness or bulk dimensions for good performance.
- Coating of textile fibers with hydrogel layers containing silver nanoparticles could be interesting for several applications, e.g. sportswear or bandaging materials.

Bibliography

- [1] A. Makino and S. Kobayashi. Chemistry of 2-Oxazolines: A Crossing of Cationic Ring-Opening Polymerization and Enzymatic Ring-Opening Polyaddition. *Journal of Polymer Science, Part A: Polymer Chemistry*, 48:1251–1270, 2010.
- [2] K. Aoi and M. Okada. Polymerization of oxazolines. *Progress in Polymer Science*, 21:151–208, 1996.
- [3] R. H. Wiley and L. L. Bennett. The Chemistry of the Oxazolines. *Chemical Reviews*, 44(3):447–476, 1949.
- [4] J. C. Rueda et al. Synthesis and characterization of new pH- and thermo-responsive hydrogels based on N-isopropylacrylamide and 2-oxazolines. *Designed Monomers and Polymers*, 17:208–216, 2013.
- [5] H. Witte and W. Seeliger. Cyclische Imidsäureester aus Nitrilen und Aminoalkoholen. *Justus Liebig's Annalen der Chemie*, 1974(6):996–1009, 1974.
- [6] D. M. Roush and M. M. Patel. A Mild Procedure for the Preparation of 2-Oxazolines. *Synthetic Communications*, 15(8):675–679, 1985.
- [7] M. Malasquez. Síntesis de nuevos hidrogeles a partir de N-isopropilacrilamida, macromonómeros de 2-oxazolinas y Laponita. Master's thesis, Pontificia Universidad Católica del Perú, 2015.
- [8] A. Levy and M. Litt. Polymerization of Cyclic Iminoethers. IV. Oxazoline Polymerization in Solvents Containing Different Functional Groups. *Journal of Polymer Science, Part A: Polymer Chemistry*, 6(1):63–72, 1968.
- [9] M. Miyamoto et al. Preparation of Poly[(N-acetylimino)ethylene] Having (Perfluoroacrylimino)ethyl End Group and Its Surface Activity. *Polymer Journal*, 27(5):461–468, 1995.
- [10] B. Jeong et al. Thermosensitive sol-gel reversible hydrogels. *Advanced Drug Delivery Reviews*, 54:37–51, 2002.
- [11] Y. Qiu and K. Park. Environment-sensitive hydrogels for drug delivery. *Advanced Drug Delivery Reviews*, 53:321–339, 2001.
- [12] H.G. Schild. Poly(N-Isopropylacrylamide): Experiment, Theory and Application. *Progress in Polymer Science*, 17:163–249, 1992.
- [13] Y. Guan and Y. Zhang. PNIPAM microgels for biomedical applications: from dispersed particles to 3D assemblies. *Soft Matter*, 7:6375–6384, 2011.
- [14] A. Richter et al. Review on Hydrogel-based pH Sensors and Microsensors. *Sensors*, 8:561–581, 2008.
- [15] S. K. Bajpai et al. In Situ Formation of Silver Nanoparticles in Poly(N-Isopropyl Acrylamide) Hydrogel for Antibacterial Applications. *Designed Monomers and Polymers*, 14:383–394, 2011.

- [16] Y. Murali Mohan et al. Hydrogel networks as nanoreactors: A novel approach to silver nanoparticles for antibacterial applications. *Polymer*, 48:158–164, 2007.
- [17] H. Plaut and J. J. Ritter. A New Reaction of Nitriles. VI. Unsaturated Amides. *Journal of the American Chemical Society*, 73(9):4076–4077, 1951.
- [18] Jr. H. W. Cooper and Jr. N. H. Shearer. Continuous method of making n-substituted amides, Eastman Kodak Co, United States patent US 2719176 A, 1955 Sept 27.
- [19] M. Shibayama et al. The Properties of Copolymer Gels Containing N-Isopropylacrylamide. *Macromolecules*, 29:2019–2024, 1996.
- [20] S. Van Vlierberghe et al. Biopolymer-Based Hydrogels As Scaffolds for Tissue Engineering Applications: A Review. *Biomacromolecules*, 12:1387–1408, 2011.
- [21] M. Heskins and J. E. Guillet. Solution Properties of Poly(N-isopropylacrylamide). *Journal of Macromolecular Science: Part A - Chemistry*, 2(8):1441–1455, 1968.
- [22] A. H. E. Müller and O. Borisov. *Self Organized Nanostructures of Amphiphilic Block Copolymers II*. Springer Science & Business Media, Berlin Heidelberg, 2011.
- [23] A. S. Hoffman. Applications of thermally reversible polymer and hydrogels in therapeutics and diagnostics. *Journal of Controlled Release*, 6:297–305, 1987.
- [24] C. A. Cole et al. Reversible Polymeric Gels and Related Systems. *ACS Symposium Series*, 350:245–254, 1987.
- [25] A. D. McNaught and A. Wilkinson. *IUPAC. Compendium of Chemical Terminology*. Blackwell Scientific Publications, Oxford, 2nd edition, 1997.
- [26] Y. Chujo. *Chemistry and Industry of Macromonomers - Macromonomer Synthesis*. Huethig & Wepf, Basel, 1993.
- [27] Y. Yamashita. *Chemistry and Industry of Macromonomers - Molecular Design of Block and Graft Copolymers*. Huethig & Wepf, Basel, 1993.
- [28] K. Matyjaszewski et al. Hydrogels by Atom Transfer Radical Polymerization. I. Poly (N-Vinylpyrrolidinone-g-Styrene) via the Macromonomer Method. *Journal of Polymer Sc*, 36:823–830, 1998.
- [29] Arvind M. Mathur et al. Methods for Synthesis of Hydrogel Networks: A Review. *Journal of Macromolecular Science, Part C*, 36(2):405–430, 1996.
- [30] Y. Tsukahara et al. *Chemistry and Industry of Macromonomers - Hydrogels and Contact Lenses*. Huethig & Wepf, Basel, 1993.
- [31] R. L. Whistler. Synthetische und natürliche Hydrogele. *TAPPI Journal*, 60:64–67, 1977.
- [32] Y. Kohno et al. Thermoresponsive polyelectrolytes derived from ionic liquids. *Polymer Chemistry*, 6:2163–2178, 2015.
- [33] G. R. Deen and V. Chua. Synthesis and Properties of New "Stimuli" Responsive Nanocomposite Hydrogels Containing Silver Nanoparticles. *Gels*, 1:117–134, 2015.
- [34] I. Tokarev and S. Minko. Stimuli-responsive hydrogel thin films. *Soft Matter*, 5:511–524, 2009.
- [35] P. Schexnailder and G. Schmidt. Nanocomposite polymer hydrogels. *Colloid and Polymer Science*, 287:1–11, 2009.
- [36] P. C. Thomas et al. Nanoparticle-crosslinked hydrogels as a class of efficient materials for separation and ion exchange. *Soft Matter*, 7:8192–8197, 2011.

- [37] T. Y. Liu et al. Study on controlled drug permeation of magnetic-sensitive ferrogels: effect of Fe_3O_4 and PVA. *Journal of Controlled Release*, 126(3):228–236, 2008.
- [38] I. Tokarev et al. Gold-Nanoparticle-Enhanced Plasmonic Effects in a Responsive Polymer Gel. *Advanced Materials*, 20(14):2730–2734, 2008.
- [39] Sally D. Solomon et al. Synthesis and Study of Silver Nanoparticles. *Journal of Chemical Educatio*, 84:322–325, 2007.
- [40] V. Thomas. A versatile strategy to fabricate hydrogel-silver nanoparticles and investigation of their antimicrobial activity. *Journal of Colloid and Interface Science*, 45:107–119, 2007.
- [41] M. E. Harnon et al. A Surface Plasmon Resonance Study of Volume Phase Transitions in N-Isopropylacrylamide Gel Films. *Macromolecules*, 35(15):5999–6004, 2002.
- [42] T. Tanaka et al. Mechanical instability of gels at the phase transition. *Nature*, 325:796–798, 1987.
- [43] R. Bashir et al. Micromechanical cantilever as an ultrasensitive pH microsensor. *Applied Physics Letters*, 81(16):3091–3093, 2002.
- [44] M. Lake. *Oberflächentechnik in der Kunststoffverarbeitung*. Carl Hanser Verlag, München, 2009.
- [45] P.-G. de Gennes et al. *Capillarity and Wetting Phenomena*. Springer-Verlag New York, 2004.
- [46] Y. Yuan and T. R. Lee. *Surface Science Techniques*, volume 51 of *Springer Series in Surface Sciences*, chapter Contact Angle and Wetting Properties, pages 3–34. Springer Berlin Heidelberg, 2013.
- [47] R. Benedix. *Chemie für Bauingenieure*. B. G. Teubner Stuttgart Leipzig, 1999.
- [48] N. Nuraje et al. Superhydrophobic electrospun nanofibers. *Journal of Materials Chemistry A*, 1:1929–1946, 2013.
- [49] P. Schönherr. *Multiple Oberflächenfunktionalisierung von Mischgläser- und Siliziumdioxidnanopartikeln als Komponenten für Kompositmaterialien*. PhD thesis, TU Chemnitz, 2013.
- [50] E.P. Plueddemann. *Silane Coupling Agents*. Springer Science & Business Media New York, 1991.
- [51] B. Müller and W. Rath. *Formulierung von Kleb- und Dichtstoffen*. Vincentz Network, Hannover, 2004.
- [52] G. P. Bierwagen. *Paint and Coating Testing Manual*, chapter Surface Energetics, pages 369–382. ASTM Manual Series. American Society for Testing and Materials, Philadelphia, PA, 1995.
- [53] L. E. Scriven. Physics and Applications of Dip Coating and Spin Coating. *Materials Research Society Symposium Proceedings*, 121:717–729, 1988.
- [54] L. Landau and B. Levich. Dragging of a Liquid by a Moving Plate. *Acta Physicochimica U.R.S.S.*, XVII(1-2):42–54, 1942.
- [55] H. Kumar Raut et al. Anti-reflective coatings: A critical, in-depth review. *Energy & Environmental Science*, 4:3779–3804, 2011.
- [56] C. J. Brinker et al. *Metallurgical and Ceramic Protective Coatings*, chapter Sol-gel derived ceramic films - fundamentals and applications, pages 112–148. Chapman &

- Hall, London, 1996.
- [57] A. D. Pomogailo and V. N. Kestelman. *Metallpolymer Nanocomposites*. Springer-Verlag Berlin Heidelberg, 2005.
- [58] S. Prabhu and E. K. Poullose. Silver nanoparticles: mechanism of antimicrobial action, synthesis, medical applications, and toxicity effects. *International Nano Letters*, 2:32–42, 2012.
- [59] T. M. Tolaymat et al. An evidence-based environmental perspective of manufactured silver nanoparticle in syntheses and applications: A systematic review and critical appraisal of peer-reviewed scientific papers. *Science of the Total Environment*, 408:999–1006, 2010.
- [60] Q. L. Feng et al. A mechanistic study of the antibacterial effect of silver ions on *Escherichia coli* and *Staphylococcus aureus*. *Journal of Biomedical Materials Research*, 52(4):662–668, 2000.
- [61] J. R. Morones et al. The bactericidal effect of silver nanoparticles. *Nanotechnology*, 16:2346–2353, 2005.
- [62] K. Awazu et al. A Plasmonic Photocatalyst Consisting of Silver Nanoparticles Embedded in Titanium Dioxide. *Journal of the American Chemical Society*, 130(5):1676–1680, 2008.
- [63] W.-J. Yoon et al. Plasmon-enhanced optical absorption and photocurrent in organic bulk heterojunction photovoltaic devices using self-assembled layer of silver nanoparticles. *Solar Energy Materials and Solar Cells*, 94(2):128–132, 2010.
- [64] L. Ye et al. Effect of Ag Particle Size on Electrical Conductivity of Isotropically Conductive Adhesives. *IEEE Transactions on Electronics Packaging Manufacturing*, 22(4):299–302, 1999.
- [65] H. Jiang et al. Conductivity Enhancement of Nano Silver-Filed Conductive Adhesives by particle Surface Functionalization. *Journal of Electronic Materials*, 34(11):1432–1439, 2005.
- [66] Z.-J. Jiang et al. Catalytic Properties of Silver Nanoparticles Supported on Silica Spheres. *Journal of Physical Chemistry B*, 109(5):1730–1735, 2005.
- [67] A. C. Patel et al. Electrospinning of Porous Silica Nanofibers Containing Silver Nanoparticles for Catalytic Applications. *Chemistry of Materials*, 19(6):1231–1238, 2007.
- [68] D. K. Tiwari et al. Time and dose-dependent antimicrobial potential of Ag nanoparticles synthesized by top-down approach. *Current Science*, 95(5):647–655, 2008.
- [69] T. R. Jensen et al. Nanosphere Lithography: Tunable Localized Surface Plasmon Resonance Spectra of Silver Nanoparticles. *Journal of Physical Chemistry B*, 104(45):10549–10556, 2000.
- [70] J. C. Hulteen et al. Nanosphere Lithography: Size-Tunable Silver Nanoparticle and Surface Cluster Arrays. *Journal of Physical Chemistry B*, 103(19):3854–3863, 1999.
- [71] F. Mafuné et al. Formation and Size Control of Silver Nanoparticles by Laser Ablation in Aqueous Solution. *Journal of Physical Chemistry B*, 104(39):9111–9117, 2000.
- [72] J. García-Barrasa et al. Silver nanoparticles: synthesis through chemical method in solution and biomedical applications. *Central European Journal of Chemistry*, 9(1):7–19, 2011.

- [73] S. S. Shankar et al. Geranium Leaf Assisted Biosynthesis of Silver Nanoparticles. *Biotechnology Progress*, 19(6):1627–1631, 2003.
- [74] J. Y. Song and B. S. Kim. Rapid biological synthesis of silver nanoparticles using plant leaf extracts. *Bioprocess and Biosystems Engineering*, 32:79–84, 2009.
- [75] J. Y. Song et al. Biological synthesis of gold nanoparticles using *Magnolia kobus* and *Diopyros kaki* leaf extracts. *Process Biochemistry*, 44(10):1133–1138, 2009.
- [76] A. Ahmad et al. Extracellular biosynthesis of silver nanoparticles using the fungus *Fusarium oxysporum*. *Colloids and Surfaces B: Biointerfaces*, 28(4):313–318, 2003.
- [77] T. Klaus et al. Silver-based crystalline nanoparticles, microbially fabricated. *Proceedings of the National Academy of Sciences of the United States of America*, 96(24):13611–13614, 1999.
- [78] L. Sintubin et al. Lactic acid bacteria as reducing and capping agent for the fast and efficient production of silver nanoparticles. *Applied Microbiology and Biotechnology*, 84(4):741–749, 2009.
- [79] C. Marambio-Jones and E. M. V. Hoek. A review of the antibacterial effects of silver nanomaterials and potential implications for human health and the environment. *Journal of Nanoparticle Research*, 12:1531–1551, 2010.
- [80] L. Jeong et al. Cellular response of silk fibroin nanofibers containing silver nanoparticles In vitro. *Macromolecular Research*, 22(7):796–803, 2014.
- [81] P. V. AshaRani et al. Cytotoxicity and Genotoxicity of Silver Nanoparticles in Human Cells. *ASC Nano*, 3(2):279–290, 2009.
- [82] B. Halliwell and J. M. C. Gutteridge. *Free Radicals in Biology and Medicine*. Oxford University Press, 5th edition, 2015.
- [83] D. Hülsenberg, A. Harnisch, and A. Bismarck. *Microstructuring of Glasses*. Springer Series in Materiala Science. Springer-Verlag Berlin Heidelberg, 2008.
- [84] S. Torquato. Hard knock for thermodynamics. *Nature*, 405:521–523, 2000.
- [85] W. v. Munch. *Werkstoffe der Elektrotechnik*. Teubner Studienskripten, 6. edition, 1989.
- [86] S. Mrotzek. *Kristallisation eines UV-strukturierbaren Glases im System $Li_2O-Al_2O_3-SiO_3$* . PhD thesis, Technische Universität Ilmenau, 2005.
- [87] S. D. Stookey. Photosensitive Glass - A New Photographic Medium. *Industrial and Engineering Chemistry*, 41(4):856–861, 1949.
- [88] W. Nachtigall et al. *Bionik - Grundlagen und Beispiele für Ingenieure und Naturwissenschaftler*, chapter Anthropo- und biomedizinische Technik, pages 209–223. Springer-Verlag Berlin Heidelberg, 1998.
- [89] M. Masuda et al. Direct fabrication of freely movable microplate inside photosensitive glass by femtosecond laser for lab-on-chip application. *Applied Physics A*, 78(7):1029–1032, 2004.
- [90] K. Peter, C. Vollhard, and N. E. Schore. *Organische Chemie*, volume 2. VCH Verlagsgesellschaft mbH, Weinheim, 1995.
- [91] T. M. Alam and J. E. Jenkins. *Advanced Aspects of Spectroscopy*, chapter HR-MAS NMR Spectroscopy in Material Science, pages 279–306. InTech, Rijeka, Croatia, 2012.

- [92] G. Gauglitz and T. Vo-Dinh. *Handbook of Spectroscopy*. WILEY-VCH GmbH & Co. KGaA, Weinheim, 2003.
- [93] P. K. Mitra. *Characterization of Materials*. PHI Learning Private Limited, Delhi, 2014.
- [94] S. J. Oldenburg. Silver nanoparticles: Properties and applications. nanoComposix, Inc. www.sigmaaldrich.com/materials-science/nanomaterials/silver-nanoparticles.html (retrieved on 21. Sep. 2015).
- [95] C. M. Simonescu. *Advanced Aspects of Spectroscopy*, chapter Application of FTIR Spectroscopy in Environmental Studies, pages 49–84. InTech, Rijeka, Croatia, 2012.
- [96] J. I. Goldstein et al. *Scanning Electron Microscopy and X-ray Microanalysis*. Springer Science & Business Media New York, 3rd edition, 2003.
- [97] M. Mulisch and U. Welsch. *Romeis - Mikroskopische Technik*. Springer-Verlag Berlin Heidelberg, 19th edition, 2015.
- [98] Yang Leng. *Materials Characterization: Introduction to Microscopic and Spectroscopic Methods*. Wiley-VCH Verlag GmbH & Co., Weinheim, 2nd edition, 2013.
- [99] J. W. Robinson, E. M. Skelly Frame, and G. M. Frame II. *Undergraduate Instrumental Analysis*. CRC Press LLC, Boca Raton, 7th edition, 2014.
- [100] Molecular Probes Inc. *LIVE/DEAD BacLight Bacterial Viability Kits*, July 2004.
- [101] C. Obermair. *Nanostrukturierung mittels Rasterkraftmikroskopie und Elektrochemie*. Cuvillier Verlag Göttingen, 1st edition, 2005.
- [102] H. Wang and P. K. Chu. *Characterization of Biomaterials*, chapter Surface Characterization of Biomaterials, pages 105–174. Elsevier, Waltham, 2013.
- [103] B. Bhushan. *Modern Tribology Handbook*, chapter Surface Roughness Analysis and Measurement Techniques, pages 49–119. CRC Press LLC, Boca Raton, 2001.
- [104] DIN EN ISO 4287:2010-07. Geometrische Produktspezifikation (GPS) - Oberflächenbeschaffenheit: Tastschnittverfahren - Benennungen, Definitionen und Kenngrößen der Oberflächenbeschaffenheit. Norm, July 2010.
- [105] O. Nuyken et al. Systematic investigation on the reactivity of oxazolinium salts. *Macromolecular Chemistry and Physics*, 197:83–95, 1996.
- [106] J. Rueda et al. Synthesis of new hydrogels by copolymerization of poly(2-methyl-2-oxazoline), bis(macromonomers) and N-vinylpyrrolidone. *Macromolecular Chemistry and Physics*, 204:947–953, 2003.
- [107] X. D. Feng et al. Study of initiation mechanism of the vinyl polymerization with the system persulfate/ N,N,N', N'-tetramethylenediamine. *Makromolekulare Chemie*, 189:77–83, 1988.
- [108] I. Dimitrov et al. Thermosensitive water-soluble copolymers with doubly responsive reversibly interacting entities. *Progress in Polymer Science*, 32:1275–1343, 2007.
- [109] K. Fussgaenger et al. UV Absorption of Ag⁺ Doped Alkali Halide Crystals. *Physica Status Solidi B: Basic Solid State Physics*, 12(1):383–397, 1965.
- [110] M. Richter et al. Proof of reversible Ag⁺/Ag⁰ redox transformation on mesoporous alumina by in situ UV-Vis spectroscopy. *Journal of Applied Spectroscopy*, 71(3):400–403, 2004.

- [111] B. Stuart. *Infrared Spectroscopy: Fundamentals and Applications*. John Wiley & Sons, Ltd, 2004.
- [112] R. Devika et al. Biosynthesis of silver nanoparticles using the fungus *pleurotus ostreatus* and their antibacterial activity. *Open Access Scientific Reports*, 1:1–5, 2012.
- [113] P. Kumar Singh et al. UV-assisted size sampling and antibacterial screening of *Lantana camara* leaf extract synthesized silver nanoparticles. *RSC Advances*, 5:24513–24520, 2015.
- [114] R. Müller, E. D. Zanotto, and V. M. Fokin. Surface crystallization of silicate glasses: nucleation sites and kinetics. *Journal of Non-Crystalline Solids*, 274:208–231, 2000.
- [115] L. Feng et al. Super-Hydrophobic Surface: From Natural to Artificial. *Advanced Materials*, 14(24):1857–1860, 2002.
- [116] N. Kaiser. Review of the fundamentals of thin-film growth. *Applied Optics*, 41(16):3053–3060, 2002.
- [117] A. Bal et al. Synthesis and characterization of copolymeric and terpolymeric hydrogel-silver nanocomposites based on acrylic acid, acrylamide and itaconic acid: Investigation of their antibacterial activity against gram-negative bacteria. *Brazilian Journal of Chemical Engineering*, 32(2):50–518, 2015.
- [118] S. D. Stookey. Chemical Machining of Photosensitive Glass. *Industrial and Engineering Chemistry*, 45(1):115–118, 1953.
- [119] A. Nykänen et al. Phase Behavior and Temperature-Responsive Molecular Filters Based on Self-Assembly of Polystyrene-block-poly(N-isopropylacrylamide)-block-polystyrene. *Macromolecules*, 40:5827–5834, 2007.
- [120] C. M. Nolan et al. Thermally Modulated Insulin Release from Microgel Thin Films. *Biomacromolecules*, 5:1940–1946, 2004.
- [121] M. J. Serpe et al. Doxorubicin Uptake and Release from Microgel Thin Films. *Biomacromolecules*, 6:408–413, 2005.
- [122] A. Richter et al. Characterization of a microgravimetric sensor based on pH sensitive hydrogels. *Sensors and Actuators B*, 99:579–585, 2004.
- [123] R. de Lima et al. Silver nanoparticles: a brief review of cytotoxicity and genotoxicity of chemically and biogenically synthesized nanoparticles. *Journal of Applied Toxicology*, 32:867–879, 2012.
- [124] T. Wu et al. Fabrication of Thermoresponsive Cross-Linked Poly(N-isopropylacrylamide) Nanocapsules and Silver Nanoparticle-Embedded Hybrid Capsules with Controlled Shell Thickness. *Chemistry of Materials*, 23:2370–2380, 2011.
- [125] I. B. Malham and L. Bureau. Density effects on collapse, compression and adhesion of thermoresponsive polymer brushes. *Langmuir*, 26(7):4762–4768, 2010.

A Appendix

A.1 Calculations

A.1.1 Calculations for macromonomer synthesis

Approximately 10 g of MM with 21 monomer units (20 mol% 2-methoxycarbonylethyl-2-oxazoline (FOxa) and 80 mol% MeOxa) are to synthesize. The resulting molar weight (M) and amount ratio (n) are:

$$M(MM) = (117 + 0.80 \cdot 21 \cdot 85.11 + 0.20 \cdot 21 \cdot 157.11 + 17) \frac{g}{mol} = 2224 \frac{g}{mol}$$
$$n(MM) = \frac{10 g}{2224 \frac{g}{mol}} = 4.50 mmol$$

To synthesize 1 mol MM 1 mol CMS, $0.8 \cdot 21$ mol MeOxa, $0.2 \cdot 21$ mol FOxa and 1 mol KOH are needed. Volume of CMS (density $\rho = 1.083$ g/mL) can be calculated as follows:

$$m(CMS) = 4.5 mmol \cdot 152.62 \frac{g}{mol} = 0.686 g$$
$$V(CMS) = \frac{0.686 g}{1.083 \frac{g}{mL}} = 0.633 mL$$

To fill in an exact volume of CMS, 0.7 mL were taken that corresponds to 0.758 g and 4.97 mmol. From this follow amounts and volumes of MeOxa (density $\rho = 1.005$ g/mL) and FOxa (density $\rho = 1.15$ g/mL):

$$n(MeOxa) = 4.97 mmol \cdot 0.8 \cdot 21 = 83.50 mmol$$
$$m(MeOxa) = 83.50 mmol \cdot 85 \frac{g}{mol} = 7.098 g$$
$$V(MeOxa) = \frac{7.098 g}{1.005 \frac{g}{mL}} = 7.06 mL$$

$$n(FOxa) = 4.97 mmol \cdot 0.2 \cdot 21 = 20.87 mmol$$
$$m(FOxa) = 20.87 mmol \cdot 157 \frac{g}{mol} = 3.277 g$$
$$V(FOxa) = \frac{3.277 g}{1.15 \frac{g}{mL}} = 2.85 mL$$

To terminate the polymerization KOH methanol solution was used:

$$m(KOH) = 4.97 \text{ mmol} \cdot 56.11 \frac{\text{g}}{\text{mol}} = 0.279 \text{ g}$$

Considering the minimal purity of 85 % of KOH, the needed amount is:

$$m(KOH) = \frac{4.97 \text{ mmol} \cdot 56.11 \frac{\text{g}}{\text{mol}}}{0.85} = 0.328 \text{ g}$$

To obtain a good solution a tenfold amount (exact mass = 3.258 g) was dissolved in 20 mL methanol, from there 2 mL were used.

A.1.2 Calculation of water absorption

Water absorption can be calculated by weight measuring of hydrogels in swollen and dry state. Therefore, water absorption can be calculated in g of H₂O absorbed by 1 g of dry HG.

$$Abs_{H_2O}(HG) = \frac{m_{sHG,p} - m_{dHG,p}}{m_{dHG,p}}$$

with

$Abs_{H_2O}(HG)$ = Relativ absorption of a hydrogel

$m_{sHG,p}$ = Mass of a swollen piece of hydrogel

$m_{dHG,p}$ = Mass of a dried piece of hydrogel

The following calculation should serve as an example:

$$Abs_{H_2O}(S0) = \frac{0.482 \text{ g} - 0.046 \text{ g}}{0.046 \text{ g}} = 9.48 \frac{\text{g } H_2O}{\text{g } HG}$$

The obtained values were for hydrogels with and without silver nanoparticles can be found in Table 4.1 and Table 4.2

A.1.3 Calculation of reaction yield

To describe the reaction yield, the mass of dried hydrogel and the sum of educts (NiPAAm, MM, MBA, TEMED and APS) were compared:

$$Abs_{H_2O}(HG) = \frac{m_{sHG,p} - m_{dHG,p}}{m_{dHG,p}}$$

with

$Abs_{H_2O}(HG)$ = Relativ absorption of a hydrogel

$m_{sHG,p}$ = Mass of a swollen piece of hydrogel

$m_{dHG,p}$ = Mass of a dried piece of hydrogel

The total mass of dried hydrogel was calculated by means of dry to swollen HG ratio:

$$m_{dHG,t} = \frac{m_{dHG,p}}{m_{sHG,p}} \cdot m_{sHG,t}$$

with

$m_{dHG,t}$ = Total mass of dried hydrogel

$m_{dHG,p}$ = Mass of a dried piece of hydrogel

$m_{sHG,p}$ = Mass of a swollen piece hydrogel

$m_{sHG,t}$ = Total mass of swollen hydrogel

Mass of dried hydrogel (e.g.):

$$m(dry\ S0)_t = \frac{0.046\ g}{0.482\ g} \cdot 5.374\ g = 0.513\ g$$

Calculated reaction yield (e.g.):

$$RY = \frac{0.513\ g}{(0.5006 + 0 + 0.0347 + 0.0336 + 0.0197)\ g} = \frac{0.513\ g}{0.5886\ g} = 87\%$$

A.2 Photographic images



Figure A.1: Purification of 2-methoxycarbonylethyl-2-oxazoline (FOxa) by vacuum assisted distillation



Figure A.2: Purification of 2-methyl-2-oxazoline (MeOxa) by distillation

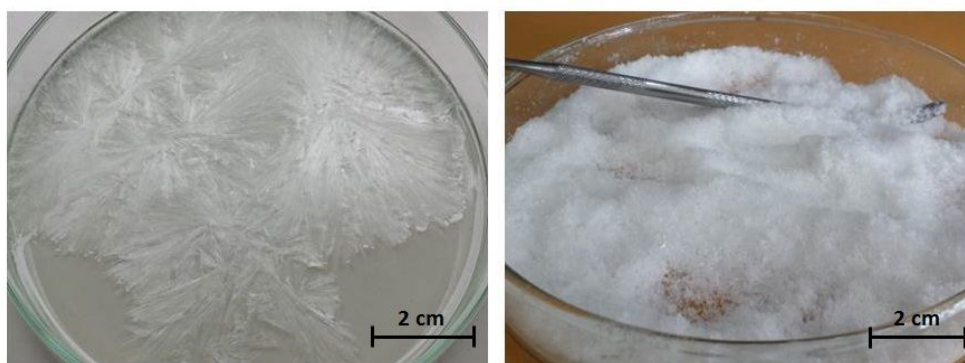


Figure A.3: Purification of N-isopropylacrylamide (NIPAM) by recrystallizing in ethanol

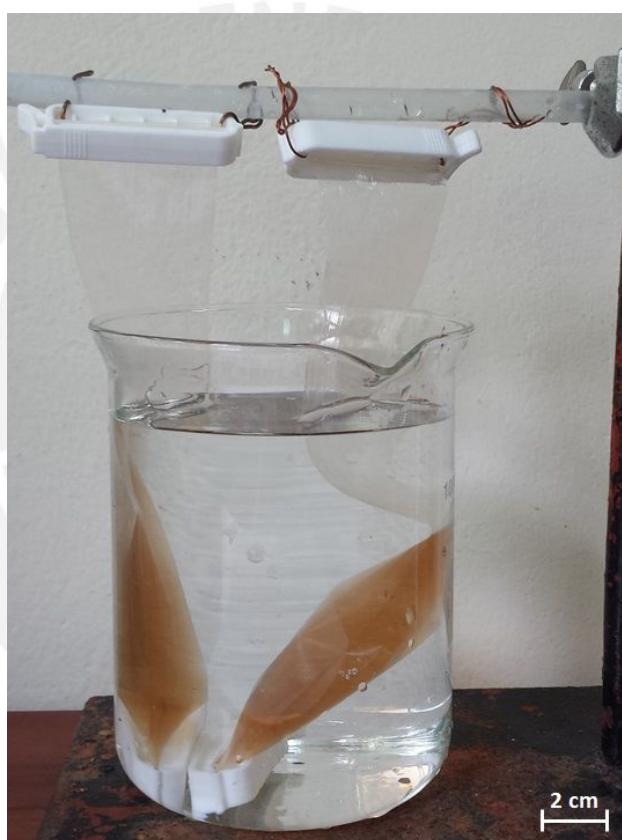


Figure A.4: Purification of the hydrolyzed macromonomer (MM) by dialysis in deionized water

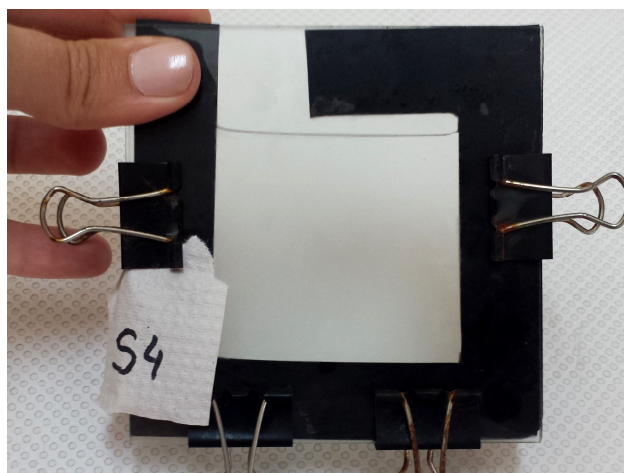


Figure A.5: Reaction vessel for hydrogel formation

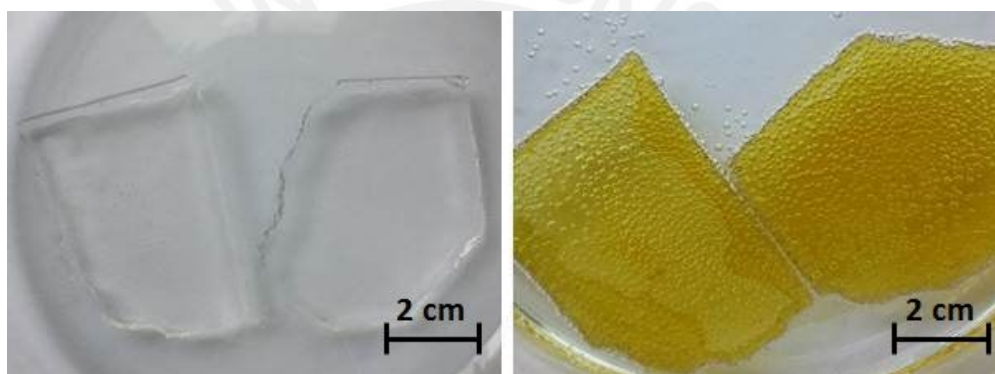


Figure A.6: S0 after complexation with Ag^+ ions (left) and after reduction to Ag-NPs (right)

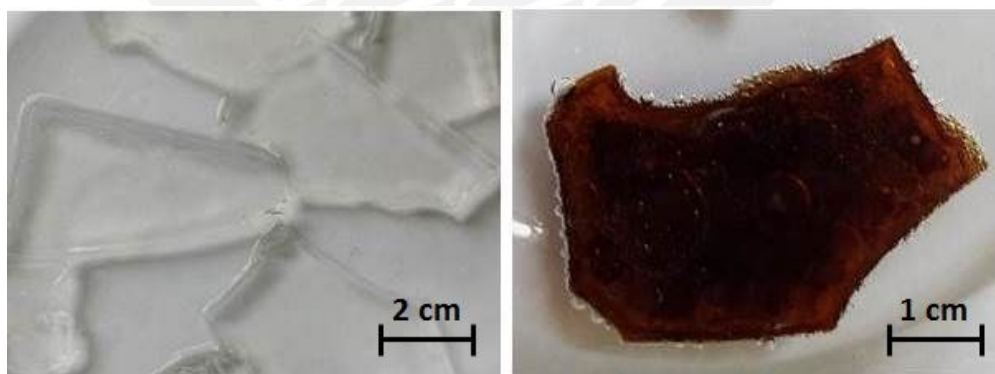


Figure A.7: S1 after complexation with Ag^+ ions (left) and after reduction to Ag-NPs (right)

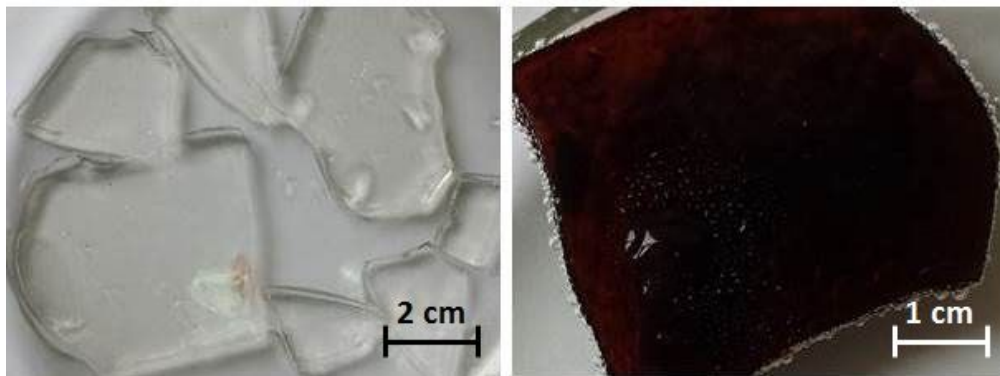


Figure A.8: S2 after complexation with Ag^+ ions (left) and after reduction to Ag-NPs (right)

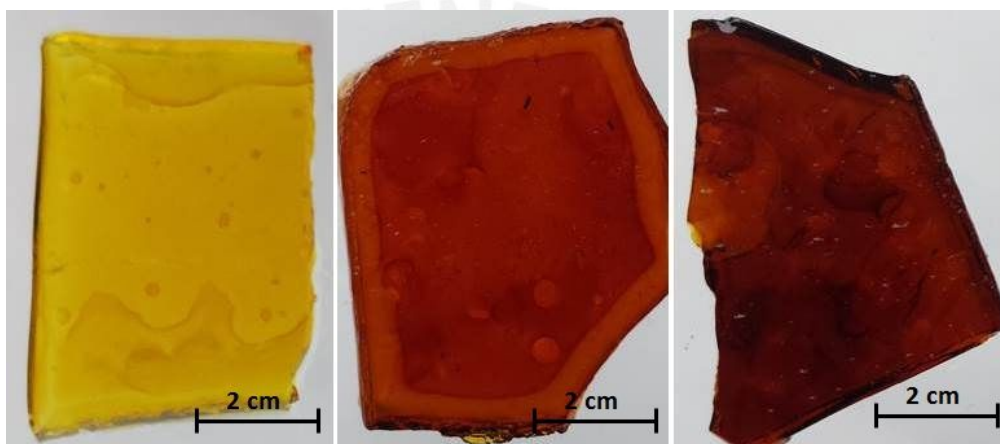


Figure A.9: Swollen HGs S0, S1 and S2 (from left to right) containing Ag-NPs

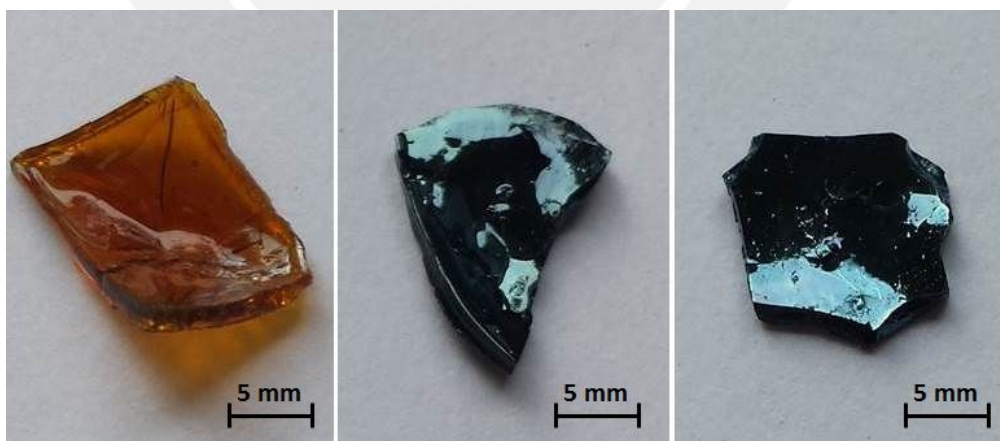


Figure A.10: Dry HGs S0, S1 and S2 (from left to right) containing Ag-NPs



Figure A.11: Measurement setup for determination of transition temperature T_{tr}

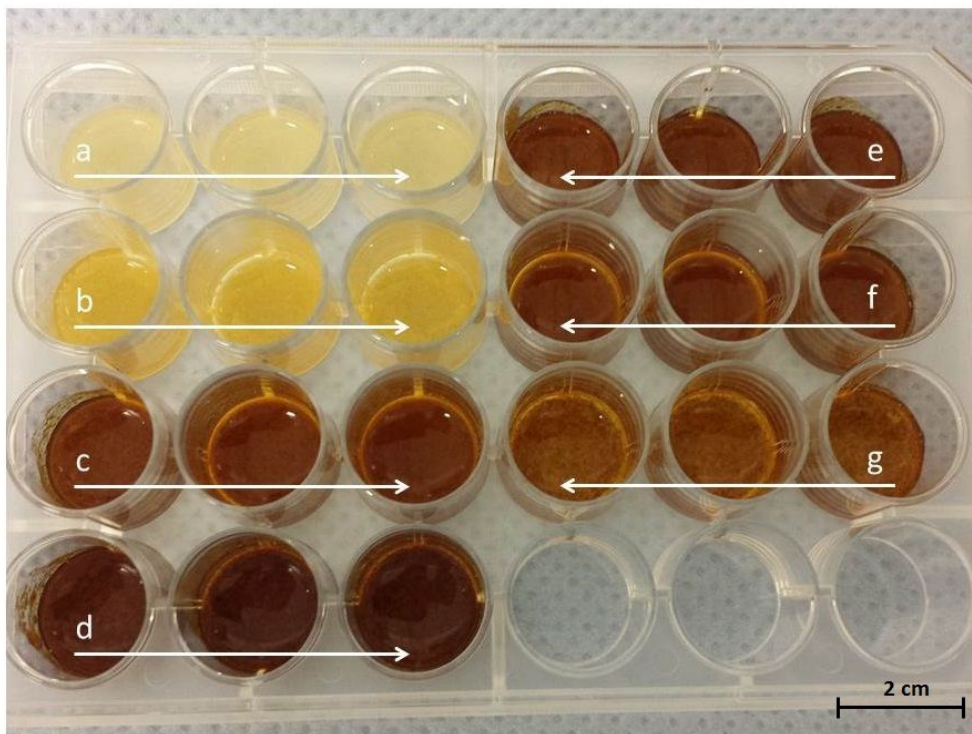


Figure A.12: 24-well cell culture plate containing hydrogel powder added to tryptic soy broth (TSB) with *Staphylococcus aureus*: (a) S0 without Ag nanoparticles (NPs) as a reference, (b) S0 with Ag-NPs, (c) S1 with Ag-NPs, (d) S2 with Ag-NPs, (e) S3 with Ag-NPs, (f) S4 with Ag-NPs and (g) S5 with Ag-NPs

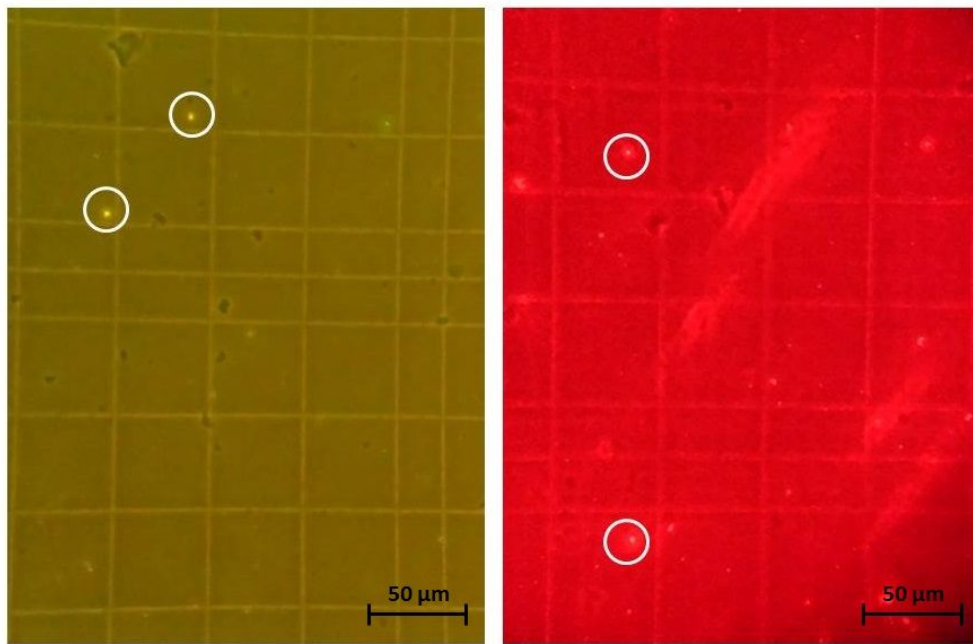
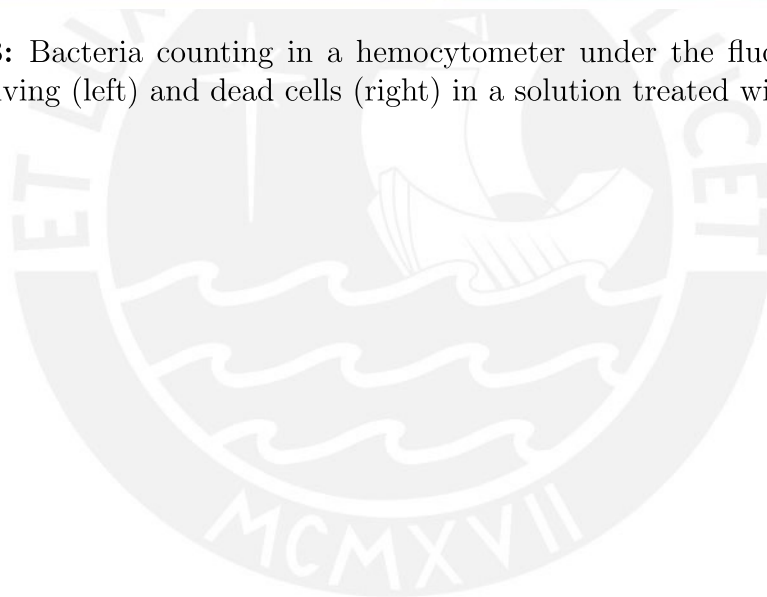


Figure A.13: Bacteria counting in a hemocytometer under the fluorescence microscope: Counting of living (left) and dead cells (right) in a solution treated with hydrogel S1



Declaration of Authorship

I hereby certify that the work presented here is entirely the result of my own work except where otherwise indicated. No other person's work has been used without due acknowledgment in this thesis. All sources of information and materials used here, have been quoted.

Ilmenau, September 9, 2016

.....
Kristina Schelestow

